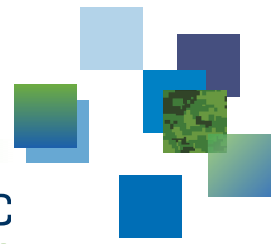




CAN UNCLASSIFIED



DRDC | RDDC
technologysciencetechnologie

Validation of ShipMo3D Version 4.2 User Applications for Simulation of Ship Motions

Kevin McTaggart
DRDC – Atlantic Research Centre

The body of this CAN UNCLASSIFIED document does not contain the required security banners according to DND security standards. However, it must be treated as CAN UNCLASSIFIED and protected appropriately based on the terms and conditions specified on the covering page.

Defence Research and Development Canada
Scientific Report
DRDC-RDDC-2021-R008
January 2021

CAN UNCLASSIFIED

IMPORTANT INFORMATIVE STATEMENTS

This document was reviewed for Controlled Goods by DRDC using the Schedule to the *Defence Production Act*.

Disclaimer: This publication was prepared by Defence Research and Development Canada an agency of the Department of National Defence. The information contained in this publication has been derived and determined through best practice and adherence to the highest standards of responsible conduct of scientific research. This information is intended for the use of the Department of National Defence, the Canadian Armed Forces ("Canada") and Public Safety partners and, as permitted, may be shared with academia, industry, Canada's allies, and the public ("Third Parties"). Any use by, or any reliance on or decisions made based on this publication by Third Parties, are done at their own risk and responsibility. Canada does not assume any liability for any damages or losses which may arise from any use of, or reliance on, the publication.

Endorsement statement: This publication has been peer-reviewed and published by the Editorial Office of Defence Research and Development Canada, an agency of the Department of National Defence of Canada. Inquiries can be sent to: Publications.DRDC-RDDC@drdc-rddc.gc.ca.

© Her Majesty the Queen in Right of Canada, Department of National Defence, 2021

© Sa Majesté la Reine en droit du Canada, Ministère de la Défense nationale, 2021

Abstract

ShipMo3D is an object-oriented library with associated user applications for predicting ship motions in calm water and in waves. This Scientific Report describes the validation of ShipMo3D Version 4.2 user applications with data from model tests and full-scale trials. Version 4.2 of ShipMo3D introduces several new capabilities developed since Version 3. Irregular frequencies for hull radiation and diffraction computations are eliminated using a lid method. Autopilot modelling now includes a track keeping capability. A new tracking spring capability can be used to model forces from various stationary or translating entities, including a mooring system, a towing tank carriage, or a ship replenishment system. New wave excitation maneuvering forces significantly influence lateral plane motions at lower encounter frequencies. Seakeeping predictions were validated using model tests and sea trials for a steered warship, a frigate, a destroyer, and a research vessel with azimuthing propellers. Predicted root-mean-squared (RMS) heave, roll, and pitch motions in random seas are typically within 10 to 30 percent of measured values, with heave motions being the most accurate and roll motions being the least accurate. Manoeuvring validation was performed for the tanker Esso Osaka performing turning circles. Validation of sloshing predictions was performed using data for a barge model with two sloshing tanks. In the absence of validation data, verification studies were performed for seakeeping for vessels with active stabilizer fins and U-tube tanks.

Significance for Defence and Security

The completed validation indicates that ShipMo3D applications give reliable predictions of ship motions within the intended capabilities of the software. The evaluation of ship hull hydrodynamic forces using the frequency domain Green function for zero forward speed is suitable for forward speed Froude numbers up to 0.4. The linear modelling of radiation and diffraction forces gives good motion predictions for frigates and destroyers in conditions up to and including Sea State 7. Manoeuvring validation has been limited to turning circles for the tanker Esso Osaka. Future work should examine manoeuvring of naval ships in greater detail.

Résumé

ShipMo3D est une bibliothèque orientée objet avec applications utilisateur connexes pour la prévision des mouvements de navires en eaux calmes et dans les vagues. Le présent rapport scientifique fournit une description de la validation des applications utilisateur de la version 4.2 de ShipMo3D avec des données provenant d'essais de modèles et d'essais à grand déploiement. La version 4.2 de ShipMo3D présente plusieurs nouvelles capacités mises au point depuis la version 3. Les fréquences irrégulières pour le calcul du rayonnement et de la diffraction de la coque sont éliminées grâce à une méthode dite « lid ». La modélisation du pilote automatique comporte à présent une capacité de suivi. On peut utiliser une nouvelle capacité de suivi pour la modélisation des forces de diverses entités stationnaires ou en translation, notamment un système d'amarrage, un réservoir de remorquage ou un système de ravitaillement de navire. Les nouvelles forces de manœuvre d'excitation des vagues influencent de manière significative les mouvements sur le plan latéral à des fréquences de rencontre plus basses. Les prévisions de la tenue en mer ont été validées à l'aide des essais sur modèle et en mer d'un navire de guerre commandé, d'une frégate, d'un destroyer et d'un navire de recherche à hélices orientables en azimut. Les mouvements de tangage, de roulis et de houle prévus dans des mers aléatoires sont généralement compris entre 10 et 30 % des valeurs mesurées, les mouvements de tangage étant les plus précis et ceux de roulis les moins précis. On a procédé à la validation des manœuvres du pétrolier Esso Osaka effectuant des cercles de giration. La validation des prévisions du ballonnement a été effectuée à l'aide des données d'un modèle de barge avec deux citernes antiroulis. En l'absence de données de validation, on a mené des études de vérification de la tenue en mer de navires à ailerons stabilisateurs actifs et de citernes à tube en U.

Importance pour la défense et la sécurité

La fin de la validation indique que les applications ShipMo3D fournissent des prévisions fiables sur les mouvements de navires dans les limites des capacités attendues du logiciel. L'évaluation des forces hydrodynamiques de la coque du navire à l'aide de la fonction de Green du domaine fréquentiel pour une vitesse avant nulle convient pour un nombre de Froude jusqu'à 0,4. La modélisation linéaire des forces de rayonnement et de diffraction permet d'obtenir de bonnes prévisions du mouvement des frégates et des destroyers dans des conditions allant jusqu'à l'état de mer 7, inclusivement. La validation des manœuvres a été limitée aux cercles de giration du pétrolier Esso Osaka. Des travaux futurs devraient permettre d'explorer plus en détail les manœuvres des navires militaires.

Table of Contents

Abstract	i
Significance for Defence and Security	i
Résumé	ii
Importance pour la défense et la sécurité	ii
Table of Contents	iii
List of Figures	vi
List of Tables	x
1 Introduction	1
2 Changes in ShipMo3D Version 4.2 Affecting Motion Predictions	2
2.1 Initial Panelling of Entire Hull Followed by Wet and Dry Panel Hull Models with SM3DPanelHull	2
2.2 Wet Hull Lid for Suppression of Irregular Frequencies with SM3DPanelLid and SM3DRadDif	2
2.3 Default Drag Coefficient of 2.0 for Bilge Keels and Skegs with SM3DBuildShip	2
2.4 Oscillating Plate Model for Bilge Keel and Skeg Roll Damping with SM3DBuildShip	3
2.5 Hull Wave Excitation Manoeuvring Forces	3
2.6 Default Vertical Location of Lateral Manoeuvring Forces Based on Centroid of Underwater Profile with SM3DBuildShip	3
3 Wave-induced Motions of the Haslar Steered Warship from Model Tests in Regular Waves	4
3.1 Haslar Steered Warship Model	4
3.2 ShipMo3D Model of Haslar Steered Warship Model	7
3.3 Comparisons of Numerical Predictions and Experimental Results for Haslar Steered Warship Model in Regular Waves	8
DRDC-RDDC-2021-R008	iii

3.4	Motions of the Haslar Steered Warship Model in Random Waves for Sea State 6	26
4	Wave-induced Motions of the Canadian Patrol Frigate Hydroelastic Model in Regular Head Seas	32
4.1	Canadian Patrol Frigate Hydroelastic Model	32
4.2	ShipMo3D Model of CPF Hydroelastic Model	33
4.3	Comparisons of Numerical Predictions and Experimental Results for the CPF Hydroelastic Model in Regular Head Seas	33
5	Wave-induced Motions of the Naval Destroyer HMCS NIPIGON from Sea Trials	41
5.1	HMCS NIPIGON	41
5.2	Conditions for HMCS NIPIGON Sea Trial	44
5.3	ShipMo3D Model of HMCS NIPIGON	45
5.4	Comparisons of Numerical Predictions and Experimental Results for HMCS NIPIGON Sea Trials	46
6	Wave-induced Motions of the Research Vessel R/V Melville from Model Tests . .	59
6.1	Scale Model of R/V Melville	59
6.2	ShipMo3D Model of R/V Melville	59
6.3	R/V Melville Motions in Regular Seas	61
6.4	R/V Melville Motions in Random Seas	68
7	Comparisons of Numerical Predictions and Experimental Results for Esso Osaka Turning Circles	75
7.1	ShipMo3D Model of Esso Osaka	75
7.2	Comparisons of Numerical Predictions and Experimental Results for Esso Osaka Turning Circles	76
8	Wave-induced Roll Motions of a Barge with Sloshing Tanks	82
8.1	ShipMo3D Model of Barge and Sloshing Tanks	83
8.2	Validation Results for Barge with Sloshing Tanks	83

9	Verification for a Frigate with Stabilizer Fins for Roll Stabilization	86
10	Verification for a Frigate with a U-tube Tank for Roll Stabilization	90
11	Verification of SM3DSeakeepSeawayFromRaos Motions in Random Seas Determined using Precomputed RAOs	95
12	Verification of SM3DTimeSeriesFromRaos Motions in Random Seas	97
13	Conclusions	99
	References	101
	List of Symbols/Abbreviations/Acronyms/Initialisms	105

List of Figures

Figure 1:	Body plan for Haslar steered warship model.	5
Figure 2:	ShipMo3D model for Haslar steered warship model.	8
Figure 3:	Steered warship RAOs, following seas at 0 degrees, Froude number 0.28.	10
Figure 4:	Steered warship RAOs, following seas at 0 degrees, Froude number 0.37.	10
Figure 5:	Steered warship RAOs, stern quartering seas at 30 degrees, Froude number 0.18.	11
Figure 6:	Steered warship RAOs, stern quartering seas at 30 degrees, Froude number 0.27.	12
Figure 7:	Steered warship RAOs, stern quartering seas at 30 degrees, Froude number 0.37.	13
Figure 8:	Steered warship RAOs, stern quartering seas at 60 degrees, Froude number 0.18.	14
Figure 9:	Steered warship RAOs, stern quartering seas at 60 degrees, Froude number 0.27.	15
Figure 10:	Steered warship RAOs, stern quartering seas at 60 degrees, Froude number 0.36.	16
Figure 11:	Steered warship RAOs, stern quartering seas at 75 degrees, Froude number 0.18.	17
Figure 12:	Steered warship RAOs, stern quartering seas at 75 degrees, Froude number 0.28.	18
Figure 13:	Steered warship RAOs, stern quartering seas at 75 degrees, Froude number 0.36.	19
Figure 14:	Steered warship RAOs, beam seas at 90 degrees, Froude number 0.18.	20
Figure 15:	Steered warship RAOs, stern quartering seas at 90 degrees, Froude number 0.28.	21
Figure 16:	Steered warship RAOs, beam seas at 90 degrees, Froude number 0.36.	22
Figure 17:	Steered warship RAOs, bow quartering seas at 120 degrees, Froude number 0.27.	23

Figure 18: Steered warship RAOs, bow quartering seas at 150 degrees, Froude number 0.26.	24
Figure 19: Steered warship RAOs, head seas at 180 degrees, Froude number 0.26.	25
Figure 20: Body plan for CPF hydroelastic model.	33
Figure 21: Profile of CPF hydroelastic model.	33
Figure 22: ShipMo3D model for CPF hydroelastic model.	34
Figure 23: Heave and pitch RAOs for Canadian Patrol Frigate hydroelastic model, head seas at 180 degrees, Froude number 0.06.	36
Figure 24: Heave and pitch RAOs for Canadian Patrol Frigate hydroelastic model, head seas at 180 degrees, Froude number 0.12.	37
Figure 25: Heave and pitch RAOs for Canadian Patrol Frigate hydroelastic model, head seas at 180 degrees, Froude number 0.20.	38
Figure 26: Heave and pitch RAOs for Canadian Patrol Frigate hydroelastic model, head seas at 180 degrees, Froude number 0.25.	39
Figure 27: Heave and pitch RAOs using different seaway models for Canadian Patrol Frigate hydroelastic model, head seas at 180 degrees, Froude number 0.12.	40
Figure 28: HMCS NIPIGON.	42
Figure 29: Body plan for HMCS NIPIGON.	43
Figure 30: ShipMo3D Model for HMCS NIPIGON.	46
Figure 31: Predicted versus observed RMS and zero-crossing period for heave, HMCS NIPIGON Trials and ShipMo3D time domain predictions with linear incident wave and buoyancy forces.	48
Figure 32: Predicted versus observed RMS and zero-crossing period for roll, HMCS NIPIGON Trials and ShipMo3D time domain predictions with linear incident wave and buoyancy forces.	49
Figure 33: Predicted versus observed RMS and zero-crossing period for pitch, HMCS NIPIGON trials and ShipMo3D time domain predictions with linear incident wave and buoyancy forces.	50
Figure 34: Oceanographic research ship R/V Melville.	59

Figure 35:	ShipMo3D model of research ship R/V Melville.	60
Figure 36:	R/V Melville motions in regular seas, wave steepness $H/\lambda = 1/60$, ship speed $U = 8$ knots, following seas (relative sea direction $\beta_s = 0$ degrees).	62
Figure 37:	R/V Melville motions in regular seas, wave steepness $H/\lambda = 1/60$, ship speed $U = 8$ knots, beam seas (relative sea direction $\beta_s = 90$ degrees).	63
Figure 38:	RV Melville motions in regular seas, wave steepness $H/\lambda = 1/60$, ship speed $U = 8$ knots, head seas (relative sea direction $\beta_s = 180$ degrees).	64
Figure 39:	R/V Melville motions in regular seas, wave steepness $H/\lambda = 1/60$, ship speed $U = 12$ knots, following seas (relative sea direction $\beta_s = 0$ degrees).	65
Figure 40:	R/V Melville motions in regular seas, wave steepness $H/\lambda = 1/60$, ship speed $U = 12$ knots, beam seas (relative sea direction $\beta_s = 90$ degrees).	66
Figure 41:	R/V Melville motions in regular seas, wave steepness $H/\lambda = 1/60$, ship speed $U = 12$ knots, head seas (relative sea direction $\beta_s = 180$ degrees).	67
Figure 42:	R/V Melville motions in random seas, Sea State 3, ship speed $U = 8$ knots.	69
Figure 43:	R/V Melville motions in random seas, Sea State 3, ship speed $U = 12$ knots.	70
Figure 44:	R/V Melville motions in random seas, Sea State 4, ship speed $U = 8$ knots.	71
Figure 45:	R/V Melville motions in random seas, Sea State 4, ship speed $U = 12$ knots.	72
Figure 46:	R/V Melville motions in random seas, Sea State 5, ship speed $U = 8$ knots.	73
Figure 47:	R/V Melville motions in random seas, Sea State 5, ship speed $U = 12$ knots.	74
Figure 48:	ShipMo3D model for Esso Osaka.	76
Figure 49:	Esso Osaka trajectory during turning circle, initial speed of 10 knots.	77
Figure 50:	Esso Osaka total speed during turning circle, initial speed of 10 knots.	78
Figure 51:	Esso Osaka heading rate during turning circle, initial speed of 10 knots.	79
Figure 52:	Esso Osaka trajectory during turning circle, initial speed of 7.7 knots.	80
Figure 53:	Esso Osaka total speed during turning circle, initial speed of 7.7 knots.	81

Figure 54:	Esso Osaka heading rate during turning circle, initial speed of 7.7 knots.	81
Figure 55:	Barge with sloshing tanks roll RAOs in beam seas with JONSWAP spectrum, $H_s = 0.066$ m, $T_p = 1.6$ s, $\gamma = 2.0$.	85
Figure 56:	Barge with sloshing tanks roll RAOs in regular beam seas, wave steepness $H/\lambda = 0.0165$.	85
Figure 57:	ShipMo3D model of generic frigate with stabilizer fins.	87
Figure 58:	Roll amplitude versus wave frequency, generic frigate at 10 knots in regular waves, beam seas with steepness H/λ of 0.01.	88
Figure 59:	Stabilizer fin deflection RAO versus wave frequency, generic frigate at 10 knots in regular waves, beam seas with steepness H/λ of 0.01.	88
Figure 60:	RMS roll versus relative sea direction, generic frigate at 10 knots in Sea State 5.	89
Figure 61:	RMS stabilizer fin deflection versus sea direction, generic frigate at 10 knots in Sea State 5.	89
Figure 62:	Example U-tube tank for generic frigate.	91
Figure 63:	Roll amplitude versus wave frequency, generic frigate at 10 knots in regular waves, beam seas with steepness H/λ of 0.01.	92
Figure 64:	U-tube tank fluid displacement amplitude versus wave frequency, generic frigate at 10 knots in regular waves, beam seas with steepness H/λ of 0.01.	92
Figure 65:	RMS roll versus relative sea direction, generic frigate at 10 knots in Sea State 5.	94
Figure 66:	RMS U-tube tank fluid displacement angle versus sea direction, generic frigate at 10 knots in Sea State 5.	94
Figure 67:	Frequency domain predictions of RMS heave and roll for generic frigate at 10 knots in Sea State 5, short-crested Bretschneider spectrum, mean wave heading 30 degrees, cosine-squared spreading angle 90 degrees.	96
Figure 68:	Heave and roll time series for generic frigate at 20 knots in Sea State 5, ship heading 30 degrees, unidirectional Bretschneider spectrum with waves from 0 degrees.	98

List of Tables

Table 1:	Main particulars for Haslar steered warship model.	4
Table 2:	Bilge keel dimensions for Haslar steered warship model.	5
Table 3:	Propeller shaft bracket dimensions for Haslar steered warship model. . .	5
Table 4:	Stabilizer fin dimensions for Haslar steered warship model.	6
Table 5:	Rudder dimensions for Haslar steered warship model.	6
Table 6:	Rudder control properties for Haslar steered warship model.	7
Table 7:	Sway of full-scale steered warship in Sea State 6 based on experimental RAOs and ShipMo3D frequency domain predictions.	27
Table 8:	Heave of full-scale steered warship in Sea State 6 based on experimental RAOs and ShipMo3D frequency domain predictions.	28
Table 9:	Roll of full-scale steered warship in Sea State 6 based on experimental RAOs and ShipMo3D frequency domain predictions.	29
Table 10:	Pitch of full-scale steered warship in Sea State 6 based on experimental RAOs and ShipMo3D frequency domain predictions.	30
Table 11:	Yaw of full-scale steered warship in Sea State 6 based on experimental RAOs and ShipMo3D frequency domain predictions.	31
Table 12:	Full scale dimensions for Canadian Patrol Frigate hydroelastic model in fresh water, deep departure condition.	32
Table 13:	Main particulars for HMCS NIPIGON.	41
Table 14:	Bilge keel dimensions for HMCS NIPIGON.	42
Table 15:	Skeg dimensions for HMCS NIPIGON.	42
Table 16:	Propeller shaft bracket dimensions for HMCS NIPIGON.	43
Table 17:	Rudder dimensions for HMCS NIPIGON.	44
Table 18:	HMCS NIPIGON trial runs for ShipMo3D validation.	45
Table 19:	Assumed rudder control properties for HMCS NIPIGON during sea trial.	46

Table 20:	Measured and predicted RMS heave (m) for HMCS NIPIGON.	51
Table 21:	Measured and predicted heave zero-crossing period (s) for HMCS NIPIGON.	52
Table 22:	Measured and predicted RMS roll (deg) for HMCS NIPIGON.	53
Table 23:	Measured and predicted roll zero-crossing period (s) for HMCS NIPIGON.	54
Table 24:	Measured and predicted RMS pitch (deg) for HMCS NIPIGON.	55
Table 25:	Measured and predicted pitch zero-crossing period (s) for HMCS NIPIGON.	56
Table 26:	Predicted RMS yaw (deg) for HMCS NIPIGON.	57
Table 27:	Predicted yaw zero-crossing period (s) for HMCS NIPIGON.	58
Table 28:	Properties for 1/23 scale model of R/V Melville.	60
Table 29:	Modelled autopilot properties for R/V Melville (full-scale).	60
Table 30:	Irregular wave sea states and full scale wave parameters.	68
Table 31:	Main particulars for the Esso Osaka during manoeuvring trials.	75
Table 32:	Turning circle parameters for Esso Osaka.	78
Table 33:	Barge dimensions.	82
Table 34:	Barge sloshing tank dimensions.	82
Table 35:	Inertial properties of barge with two sloshing tanks with fluid height of 0.19 m.	83
Table 36:	Main particulars for generic frigate.	86
Table 37:	Stabilizer fin properties for generic frigate.	86
Table 38:	Properties of example U-tube tank for generic frigate.	90

This page intentionally left blank.

1 Introduction

ShipMo3D is an object-oriented library with associated user applications for predicting ship motions in both the frequency domain and time domain. This report gives validation results for comparisons of ShipMo3D Version 4.2 with experimental data from model tests and sea trials. In cases where suitable experimental data were unavailable, verification was performed using other numerical predictions.

References [1–6] describe much of the underlying theory for ShipMo3D. References [7–9] give validation results for ShipMo3D Versions 1.0, 2.0, and 3.0. This report gives validation results for ShipMo3D Version 4.2, the current release version of the software. References [10, 11] are the user manuals for ShipMo3D Version 4.2.

Section 2 of this report describes changes between ShipMo3D Versions 3.0 and 4.2. Section 3 gives validation results for the steered warship model of Lloyd and Crossland [12] in regular head and oblique waves of low steepness. Section 4 gives results for the Canadian Patrol Frigate hydroelastic model [13] in regular head seas of higher steepness. Validation with full-scale sea trials for HMCS NIPIGON [14] is given in Section 5. Modelling of azimuthing propellers is validated in Section 6 using model tests data for the United States research ship R/V Melville [15, 16]. Section 7 gives results for turning circles from sea trials for the tanker Esso Osaka [17]. Validation of sloshing computations is given in Section 8 using experimental data for a barge with 2 sloshing tanks. Section 9 gives verification of frequency domain and time domain computations for a generic frigate with active fins for roll stabilization. Section 10 gives verification of frequency domain and time domain computations for a generic frigate with a U-tube tank for roll stabilization. Sections 11 and 12 give verification results for the programs SM3DSeakeepSeawayFromRaos and SM3DTimeSeriesFromRaos, which provide seakeeping computations and time series based on previously computed response amplitude operators. Final conclusions are given in Section 13.

2 Changes in ShipMo3D Version 4.2 Affecting Motion Predictions

ShipMo3D Version 4.2 introduces several changes intended to improve the accuracy, robustness, and efficiency of the software. Changes described here consider differences between Versions 3.0 and 4.2, which both have formal reporting of validation results. The present commentary focusses on changes influencing motion predictions. Other software changes having no significant influence on motion predictions are described in the user manuals [10, 11]. ShipMo3D applications SM3DPanelHull, SM3DPanelLid, SM3DRadDif, and SM3DBuildShip, which are mentioned below, are used to build ship models which can be used for subsequent motion predictions [10].

2.1 Initial Panelling of Entire Hull Followed by Wet and Dry Panel Hull Models with SM3DPanelHull

ShipMo3D Version 4 initially develops or reads a panelled model of the entire hull. The panels for the entire hull are then used to develop panels for the wet hull, and optionally for the dry hull as well. In contrast, ShipMo3D Version 3 and earlier panel the wet hull and dry hull using patch models of the wet hull and dry hull. The new approach provides improved fidelity of the panelled hull models, especially in the vicinity of the waterline. The new panelling method will have only very minor influence on predicted motions in most cases.

2.2 Wet Hull Lid for Suppression of Irregular Frequencies with SM3DPanelLid and SM3DRadDif

Radiation and diffraction computations with SM3DRadDif can now use a panelled lid over the hull waterplane to suppress poor numerical results arising from irregular frequencies [18]. The panelled lid is generated using the new application SM3DPanelLid. Suppression of irregular frequencies using a hull lid will have only very minor influence on predicted motions in most cases.

2.3 Default Drag Coefficient of 2.0 for Bilge Keels and Skegs with SM3DBuildShip

The application SM3DBuildShip now uses a default value of 2.0 for the drag coefficient of a bilge keel or skeg. This value is based on experimental data for a plate of low aspect ratio normal to flow [19]. This change will have only a minor influence on ship motion predictions in most cases because the drag coefficient is not used by the Ikeda method for predicting roll damping of bilge keels and skegs, which was the default roll damping method for ShipMo3D Versions 1, 2, and 3.

2.4 Oscillating Plate Model for Bilge Keel and Skeg Roll Damping with SM3DBuildShip

A new roll damping method has been developed based on experimental data from Sarkpaya and O’Keefe [20] for plates of low aspect ratio in oscillatory flow:

$$C_d^{osc}(\overline{KC}) = 2.0 + 16.0 \exp\{-0.2 \overline{KC}\} \quad (1)$$

The local Keulegan-Carpenter number is evaluated as follows:

$$\overline{KC} = \frac{\pi r_{BK}(x) \hat{\phi}}{s(x)} \quad (2)$$

where r_{BK} is the local radius of the bilge keel from the ship centre of gravity, $\hat{\phi}$ is the ship roll amplitude (rad), and $s(x)$ is the local bilge keel span. The above drag coefficient has an upper limit of 18.0. In contrast, the widely used bilge keel damping method of Ikeda, Himeno, and Tanaka [21] has infinite drag as the Keulegan-Carpenter number \overline{KC} goes to zero.

The oscillating plate model replaces the method of Ikeda, Himeno, and Tanaka as the default roll damping method for bilge keels and skegs in ShipMo3D Version 4.2. This change moderately influences predicted roll motions, with a corresponding very minor influence on sway and yaw motions. All validation results presented in this report use the oscillating plate model for bilge keel and skeg roll damping.

2.5 Hull Wave Excitation Manoeuvring Forces

When evaluating wave excitation forces, the influence of hull manoeuvring force coefficients is now modelled based on the effective sway and yaw velocities of water induced by waves [22]. The inclusion of hull manoeuvring wave excitation forces significantly influences sway and yaw motions at low wave encounter frequencies, producing the expected result of the ship following water particle motions at low wave frequencies in beam seas. All validation results presented in this report include hull manoeuvring wave excitation forces.

2.6 Default Vertical Location of Lateral Manoeuvring Forces Based on Centroid of Underwater Profile with SM3DBuildShip

When evaluating the vertical location of lateral manoeuvring forces acting on the ship hull, SM3DBuildShip now uses a default location based on the centroid of the wet hull profile. Bertram [23] and Söder, Rosén, and Huss [24] give experimental data indicating that the effective vertical centre of lateral force will be in the vicinity of the lateral profile centroid. This revised location of the default lateral force centroid will have a minor influence on roll motions, with a related very small influence on sway and yaw motions. All validation results presented in this report include the revised vertical location of lateral manoeuvring forces.

3 Wave-induced Motions of the Haslar Steered Warship from Model Tests in Regular Waves

Lloyd and Crossland [12] published results of model tests for a steered warship model travelling in regular waves of small steepness. The model was tested in the seakeeping basin of the Admiralty Marine Technology Establishment (Haslar), which is now part of QinetiQ Limited in the United Kingdom. The experimental program included comprehensive ranges of ship speeds, relative sea directions, and wave frequencies. The model was self-propelled and was steered using an autopilot. Due to the wide range of test conditions, the control of the experimental conditions, and the range of data collected, this an excellent set of experimental data for validating ship motion predictions at moderate speeds in moderate seaways.

3.1 Haslar Steered Warship Model

The steered warship model can be considered to be a nominally 1/20 scale model of a naval frigate or destroyer. Table 1 gives the main particulars for the steered warship model, and Figure 1 shows the body plan. Tables 2 to 5 give dimensions for the bilge keels, propeller shaft brackets, stabilizer fins, and rudders. Some of the longitudinal locations of appendages in Tables 2 to 5 have corrections from Reference [12], which were provided by Paul Crossland, one of the original authors.

Table 1: Main particulars for Haslar steered warship model.

Length L	5580 mm
Beam B	671 mm
Midships draft T_{mid}	196 mm
Trim by stern t_{stern}	0 mm
Displacement Δ	345 kg
Vertical centre of gravity \overline{KG}	276 mm
Metacentric height \overline{GM}	76 mm
Roll radius of gyration r_{xx}	257 mm
Pitch radius of gyration r_{yy}	1293 mm
Yaw radius of gyration r_{zz}	1265 mm

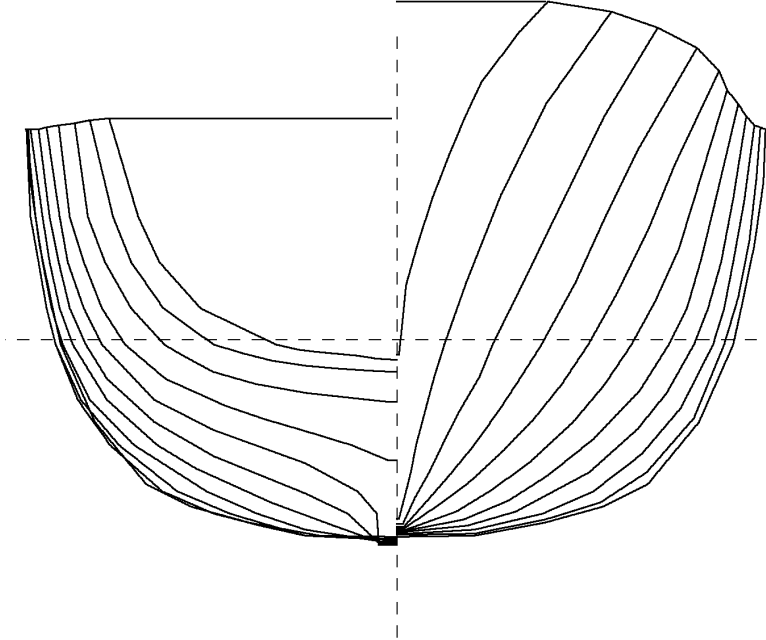


Figure 1: Body plan for Haslar steered warship model.

Table 2: Bilge keel dimensions for Haslar steered warship model.

Station (20 at AP)	6.79	7	8	9	9.69
Span (mm)	68	68	68	68	68
Root lateral offset (mm)	239	239	243	248	248
Root above baseline (mm)	107	107	82	64	64
Dihedral angle (deg, port side)	-45	-45	-45	-45	-45

Table 3: Propeller shaft bracket dimensions for Haslar steered warship model.

	Aft inner bracket	Aft outer bracket	Fore inner bracket	Fore outer bracket
Station (20 at AP)	18.40	18.40	17.97	17.97
Span (mm)	165	127	81	68
Root chord (mm)	30	30	12	12
Tip chord (mm)	30	30	12	12
Root lateral offset (mm)	21	132	72	157
Root above baseline (mm)	148	163	103	125
Dihedral angle (deg, port side)	-47.5	-99.5	-42	-90

Table 4: Stabilizer fin dimensions for Haslar steered warship model.

Station (20 at AP)	10.38
Span (mm)	83
Root chord (mm)	174
Tip chord (mm)	92
Root lateral offset (mm)	273
Root above baseline (mm)	75
Dihedral angle (deg, port side)	-46

Table 5: Rudder dimensions for Haslar steered warship model.

Station (20 at AP)	19.46
Span (mm)	153
Root chord (mm)	124
Tip chord (mm)	88
Root lateral offset (mm)	79
Root above baseline (mm)	178
Dihedral angle (deg, port side)	-83

ShipMo3D models a proportional-integral-derivative (PID) autopilot [6], with the command rudder angle determined as follows:

$$\delta_C^{rudder} = \sum_{j=1}^6 \left[k_{\delta j}^P (\eta_j^f - \eta_{Cj}^f) + k_{\delta j}^I \int_0^{\tau_{max}^{rudder}} (\eta_j^f(t - \tau) - \eta_{Cj}^f) d\tau + k_{\delta j}^D \dot{\eta}_j^f \right] \quad (3)$$

where δ_C^{rudder} is the command rudder angle, $k_{\delta j}^P$ is the proportional gain for mode j , η_j^f is the motion displacement in earth-fixed axes for mode j , η_{Cj}^f is the command motion displacement for mode j , $k_{\delta j}^I$ is the integral gain for mode j , τ_{max}^{rudder} is the integration duration, t is the current time, τ is the time delay for integration, $k_{\delta j}^D$ is the derivative gain for mode j , and $\dot{\eta}_j^f$ is the motion velocity in earth-fixed axes for mode j . For a given command rudder angle δ_C^{rudder} , which can be provided by the autopilot or by a helmsman, the rudder response is modelled as follows:

$$\ddot{\delta}^{rudder} + 2 \zeta_{\delta} \omega_{\delta} \dot{\delta}^{rudder} + \omega_{\delta}^2 \delta^{rudder} = \omega_{\delta}^2 \delta_C^{rudder} \quad (4)$$

where ζ_{δ} is the nondimensional damping response constant, and ω_{δ} is the rudder frequency response constant.

The steered warship model included an autopilot with control parameters as given in Table 6. The heading autopilot gains are based on the ShipMo3D convention of earth-fixed heading being positive clockwise when viewed from above, and rudder deflection being positive counter-clockwise when viewed from inside the ship (i.e., positive counter-clockwise when viewed from above for a typical downward rudder stock).

Table 6: Rudder control properties for Haslar steered warship model.

Maximum deflection angle δ_{max}^{rudder}	35 deg
Maximum deflection rate $\dot{\delta}_{max}^{rudder}$	35 deg/s
Deflection natural frequency ω_{δ}	25.8 rad/s
Deflection damping ratio ζ_{δ}	0.85
Heading displacement gain $k_{\delta 6}^P$	-3.8
Heading velocity gain $k_{\delta 6}^D$	-1.7 s

3.2 ShipMo3D Model of Haslar Steered Warship Model

The model of the steered warship model was built using the applications SM3DPanelHull, SM3DPanelLid, SM3DRadDif, and SM3DBuildShip. Figure 2 shows the model produced by SM3DBuildShip.

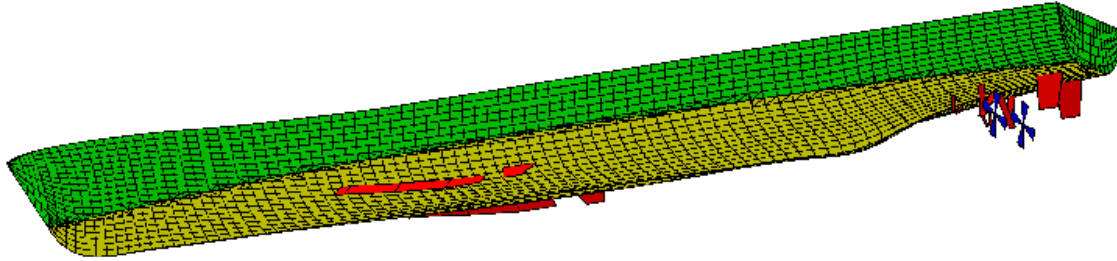


Figure 2: *ShipMo3D model for Haslar steered warship model.*

Due to lack of available data, some of the input parameters for the steered warship model had to be estimated. Hull resistance was estimated using the method of Holtrop and Mennen [25], which is available as an option in SM3DBuildShip. The variation of propeller thrust coefficient with advance ratio was based on a representative curve from Reference [26]. For each rudder, the rudder-propeller interaction coefficient associated with the propeller on the same side of the ship was given a value of 0.9, based on the assumption that 90 percent of the rudder area was within the propeller slipstream. The flow straightening coefficient for each rudder was estimated to be 0.7 based on the following equation from Lewandowski [27]:

$$\gamma_r \approx \frac{1}{1 + C_B} \quad (5)$$

where C_B is the ship block coefficient.

For each ship speed used for model tests, the associated propeller RPM (revolutions per minute) settings for calm water were determined using SM3DBuildShip, which uses an iterative process.

3.3 Comparisons of Numerical Predictions and Experimental Results for Haslar Steered Warship Model in Regular Waves

Figures 3 to 19 show comparisons of ShipMo3D frequency and time domain predictions with experimental response amplitude operators (RAOs) for the steered warship model. The experimental data include additional results provided directly by QiniteQ that were not published in Reference [12].

Comparisons between experimental results and predictions are generally good, and time domain predictions give very good agreement with frequency domain predictions. As expected, vertical plane predictions are generally better than lateral plane predictions. For some of the plots (e.g., Figure 7), there are gaps in predictions for certain wave frequency ranges because predictions weren't made at encounter frequencies below 0.41 rad/s.

Pitch predictions are generally good, with somewhat poorer agreement with experiments at headings of 60 and 75 degrees (stern quartering seas). Low encounter frequencies occur at these headings, violating assumptions made when predicting hull hydrodynamic forces.

The lateral plane motion predictions from ShipMo3D Version 4.2 are somewhat different from those for Version 3 [9] due to changes discussed in Section 2. The inclusion of wave excitation manoeuvring forces appears to give improved yaw predictions at forward speed in bow quartering seas.

There is noticeable underprediction of roll in several cases, including stern quartering seas at 30 degrees for Froude number 0.37 (Figure 7), bow quartering seas at 120 degrees for Froude number 0.27 (Figure 17), and bow quartering seas at 150 degrees for Froude number 0.26 (Figure 18). These differences could possibly be due to the influence of forward speed on appendage forces, which could be an area of improvement in force predictions.

Differences between time domain and frequency domain predictions, which are generally small, are likely due to neglecting the influence of the propeller slipstream on rudder forces during frequency domain computations.

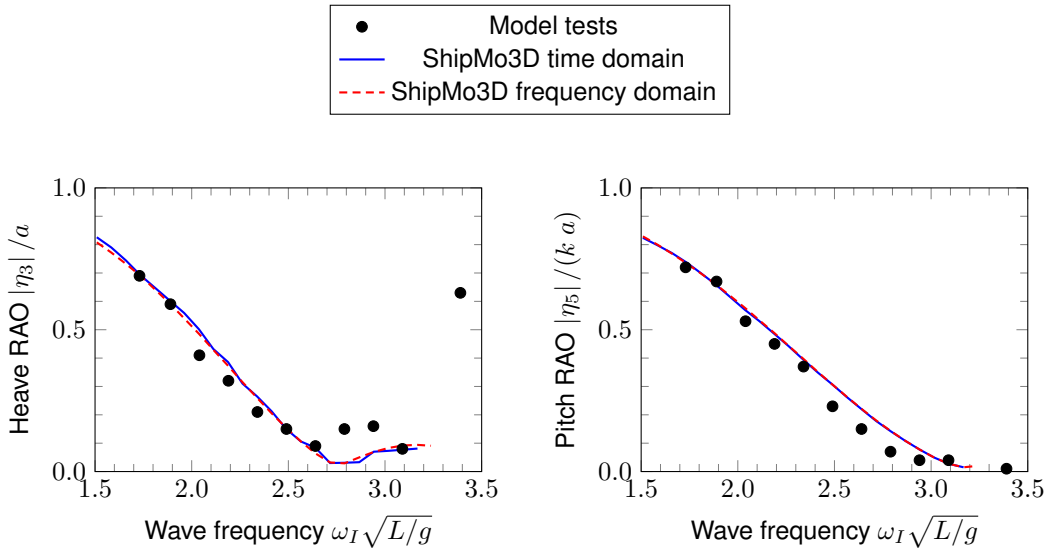


Figure 3: Steered warship RAOs, following seas at 0 degrees, Froude number 0.28.

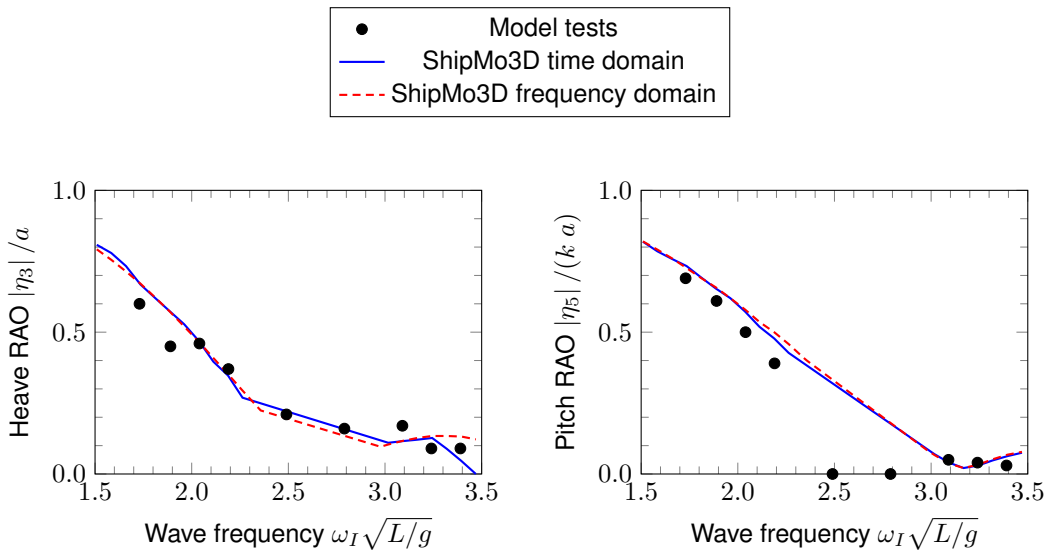


Figure 4: Steered warship RAOs, following seas at 0 degrees, Froude number 0.37.

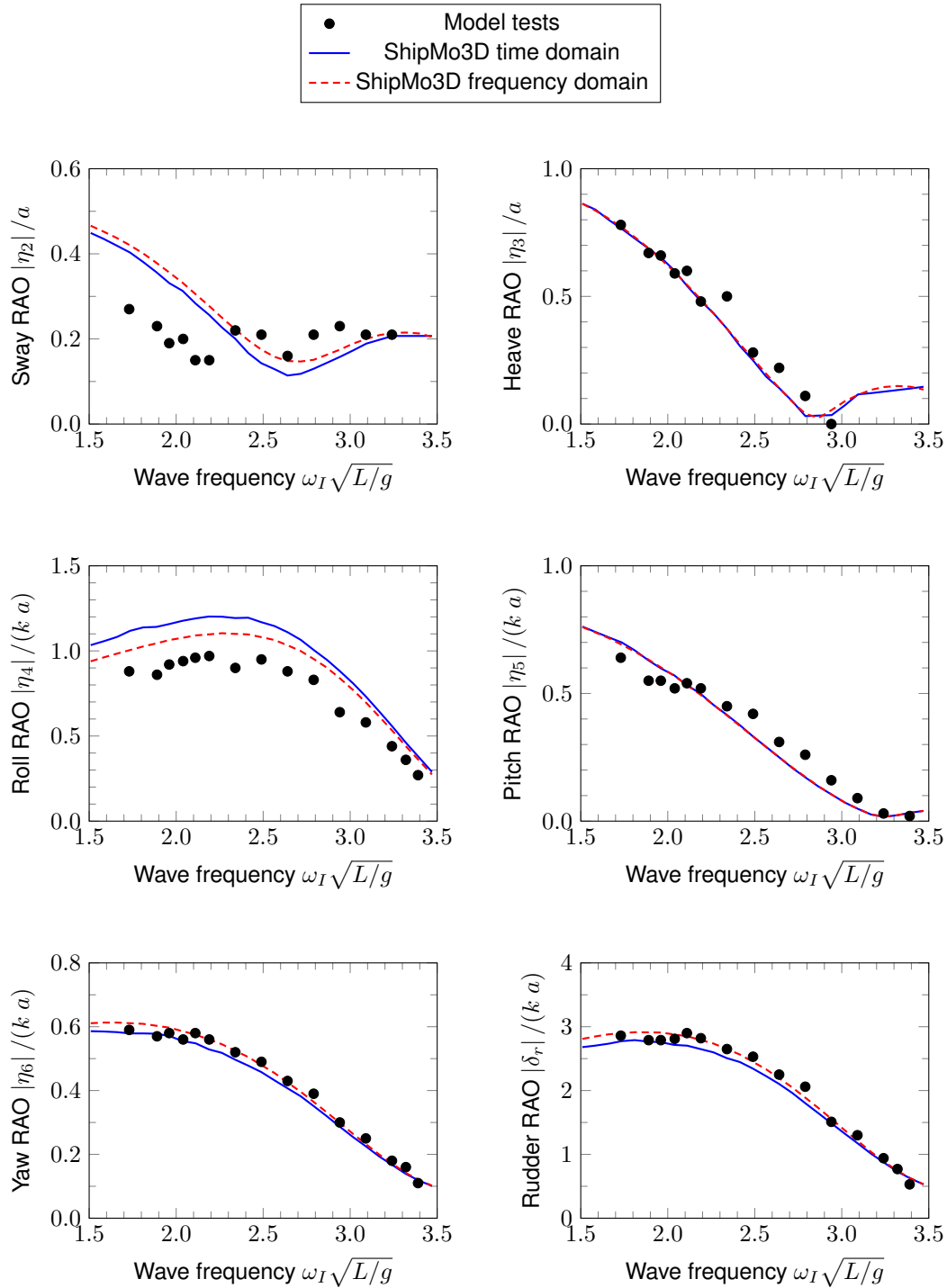


Figure 5: Steered warship RAOs, stern quartering seas at 30 degrees, Froude number 0.18.

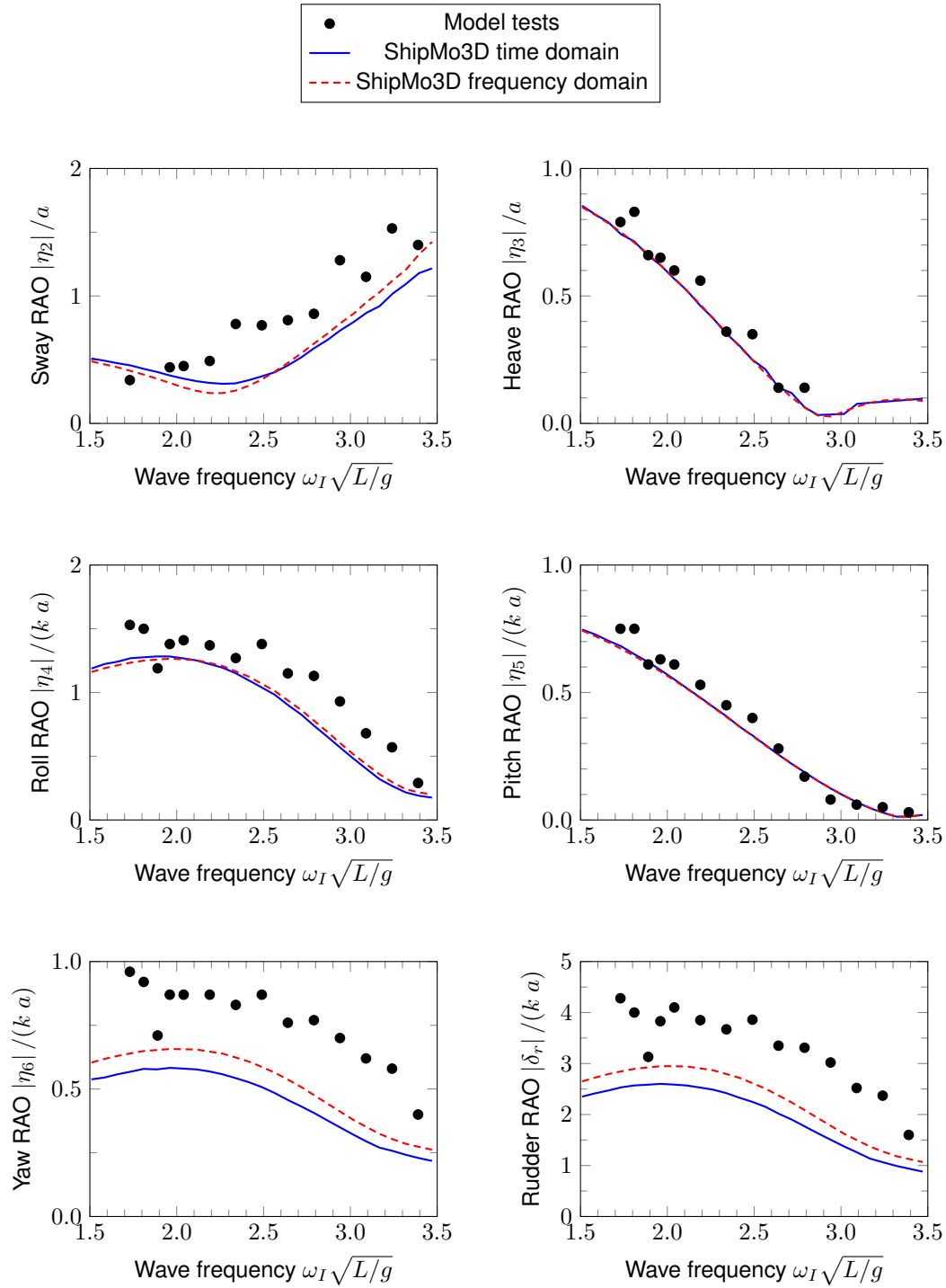


Figure 6: Steered warship RAOs, stern quartering seas at 30 degrees, Froude number 0.27.

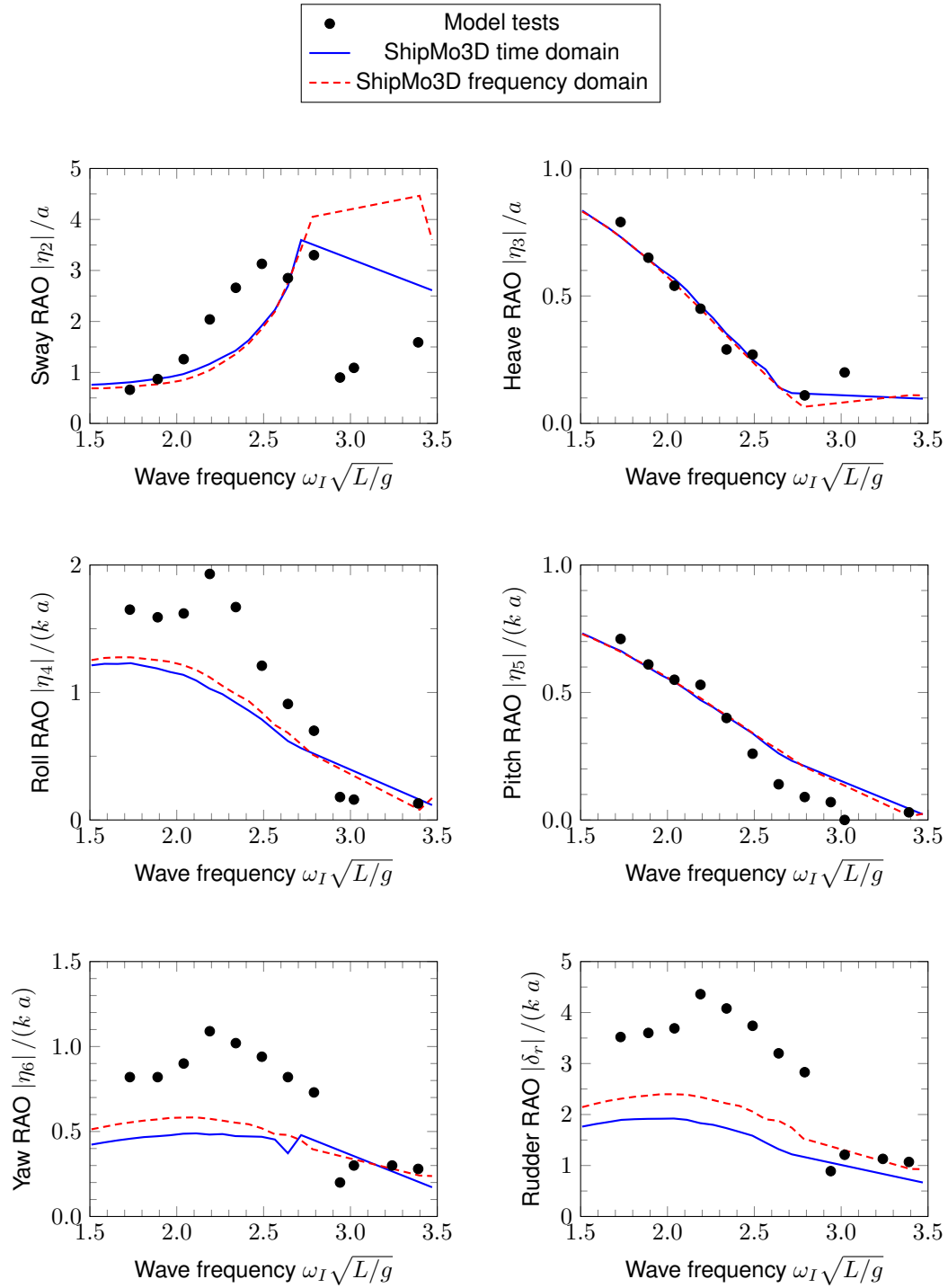


Figure 7: Steered warship RAOs, stern quartering seas at 30 degrees, Froude number 0.37.

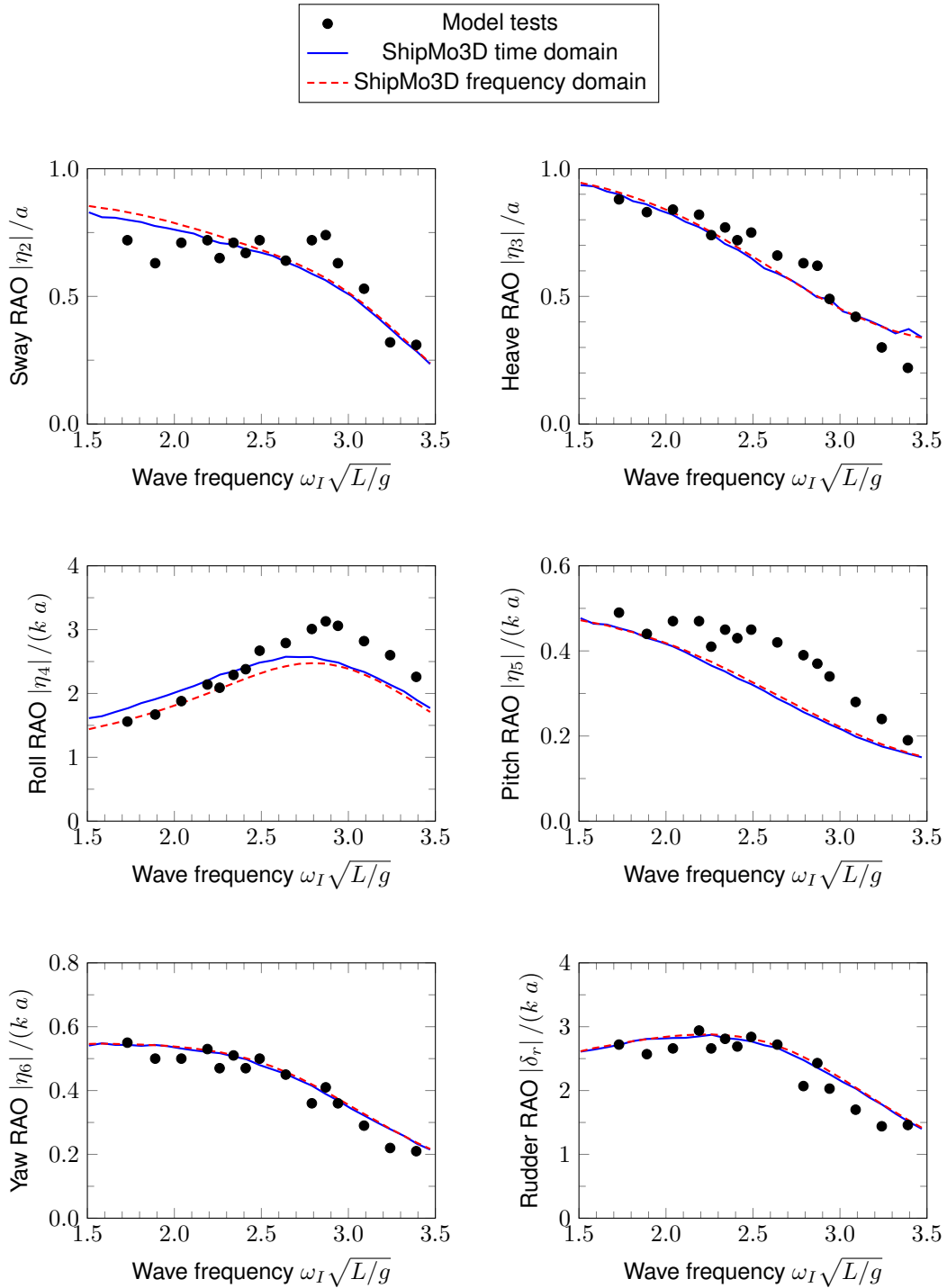


Figure 8: Steered warship RAOs, stern quartering seas at 60 degrees, Froude number 0.18.

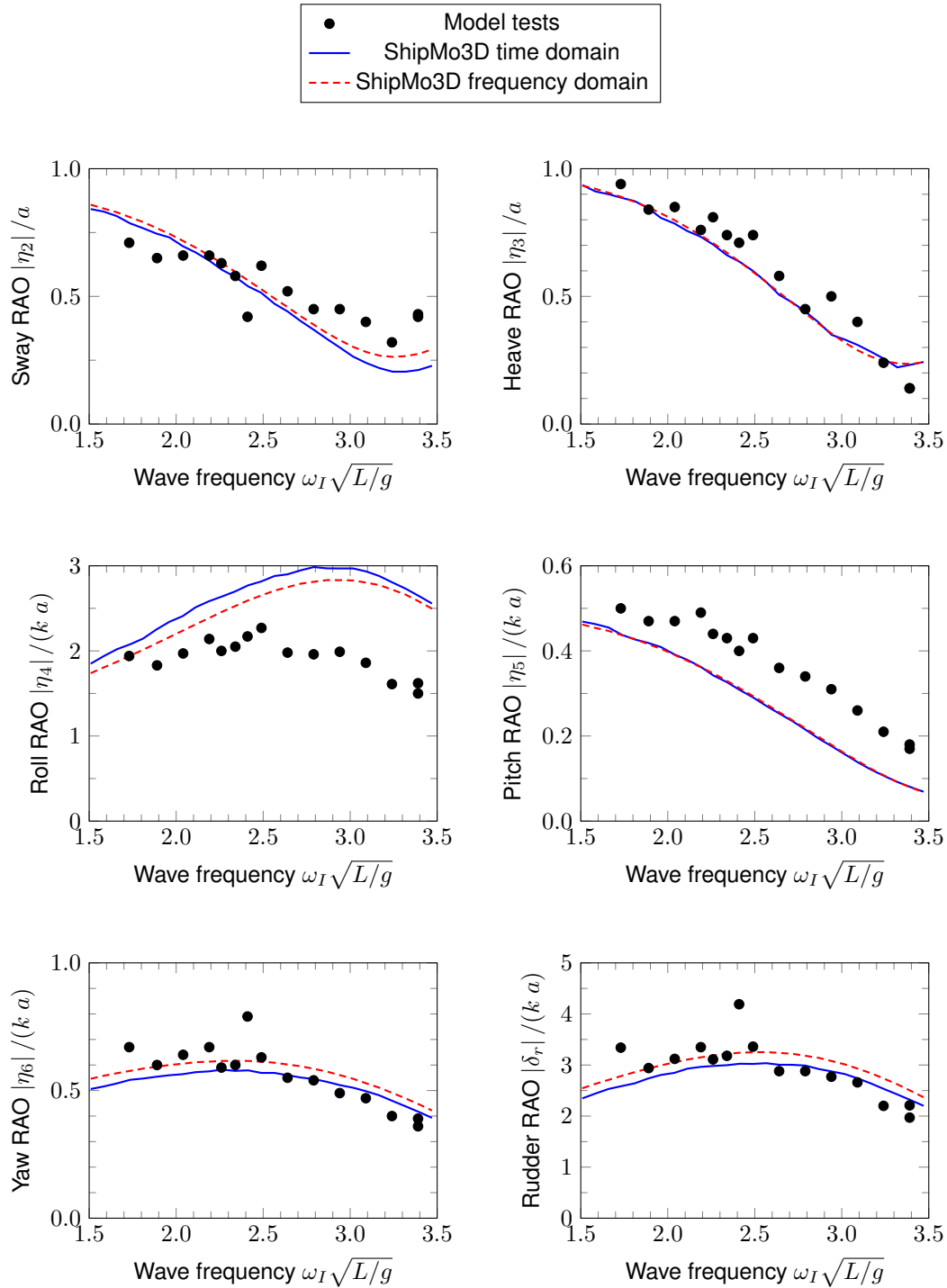


Figure 9: Steered warship RAOs, stern quartering seas at 60 degrees, Froude number 0.27.

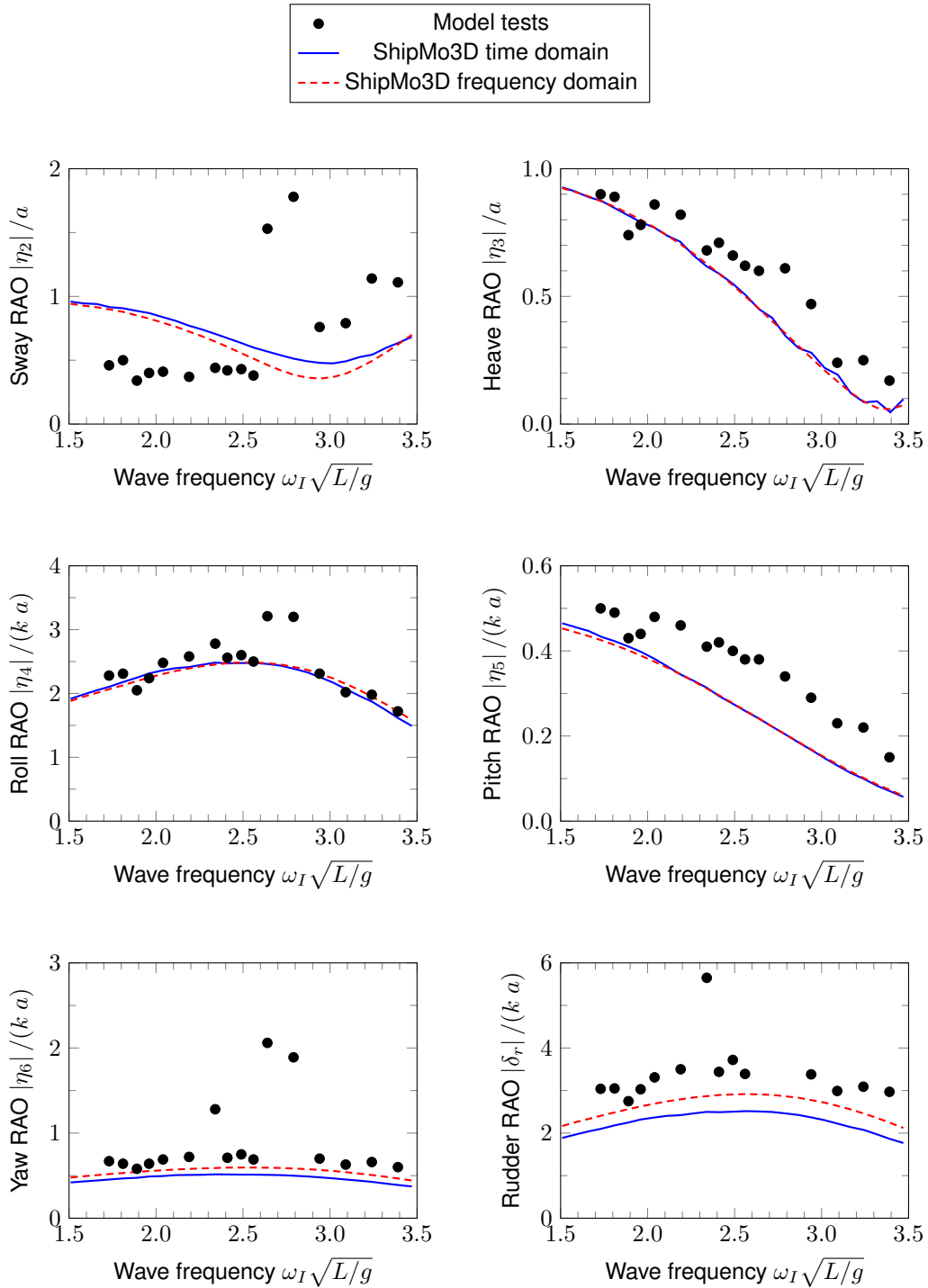


Figure 10: Steered warship RAOs, stern quartering seas at 60 degrees, Froude number 0.36.

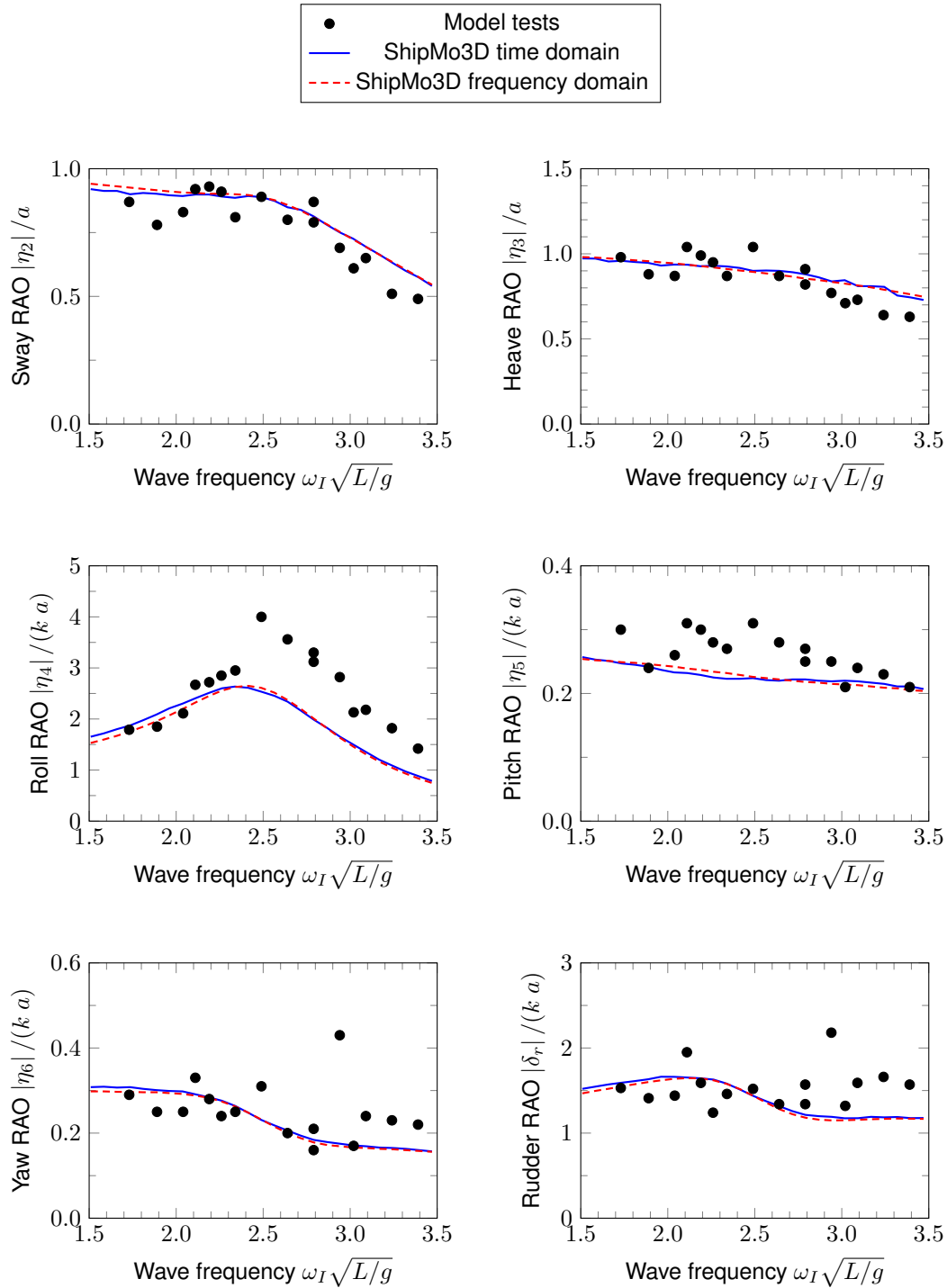


Figure 11: Steered warship RAOs, stern quartering seas at 75 degrees, Froude number 0.18.

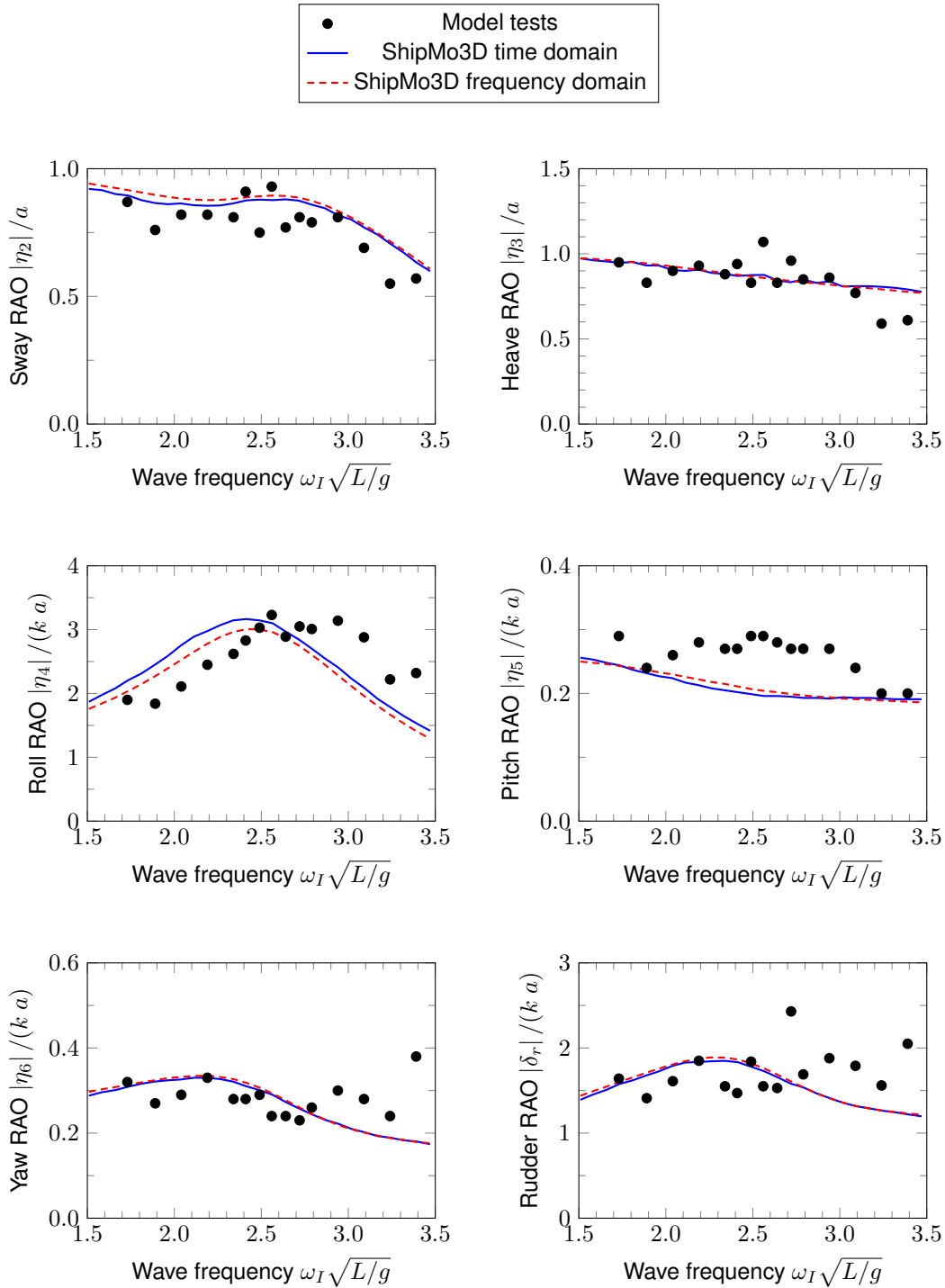


Figure 12: Steered warship RAOs, stern quartering seas at 75 degrees, Froude number 0.28.

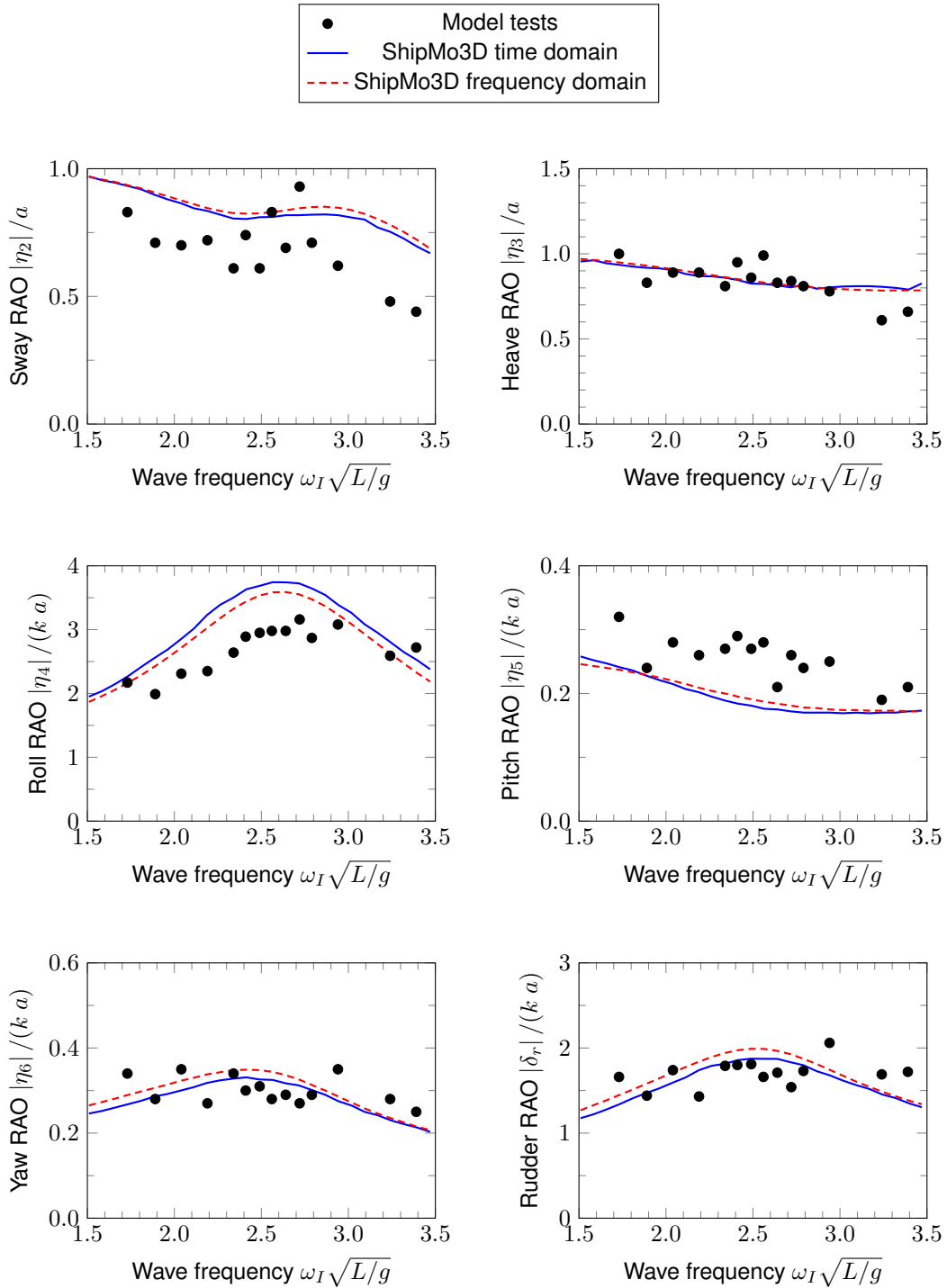


Figure 13: Steered warship RAOs, stern quartering seas at 75 degrees, Froude number 0.36.

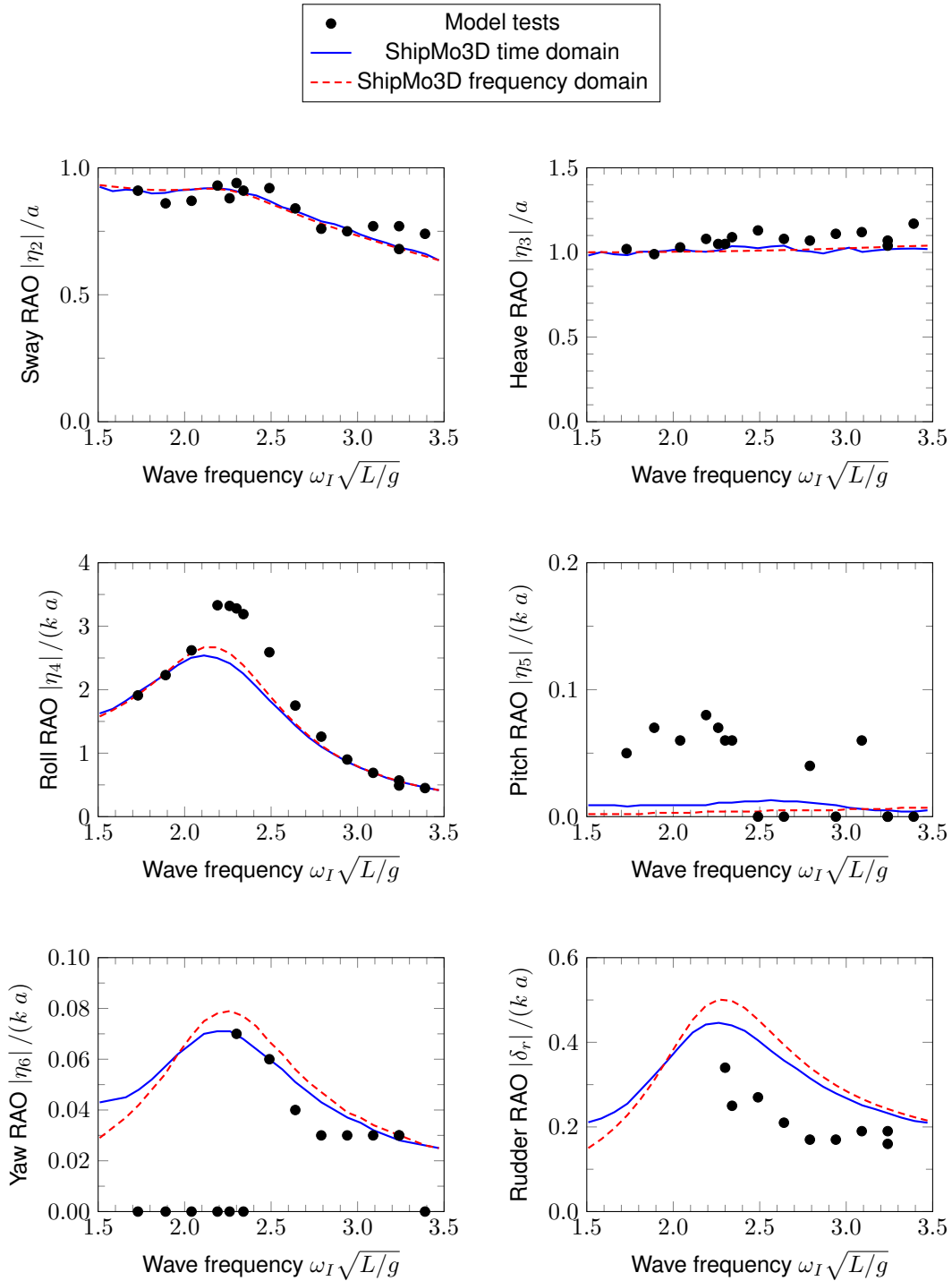


Figure 14: Steered warship RAOs, beam seas at 90 degrees,
 Froude number 0.18.

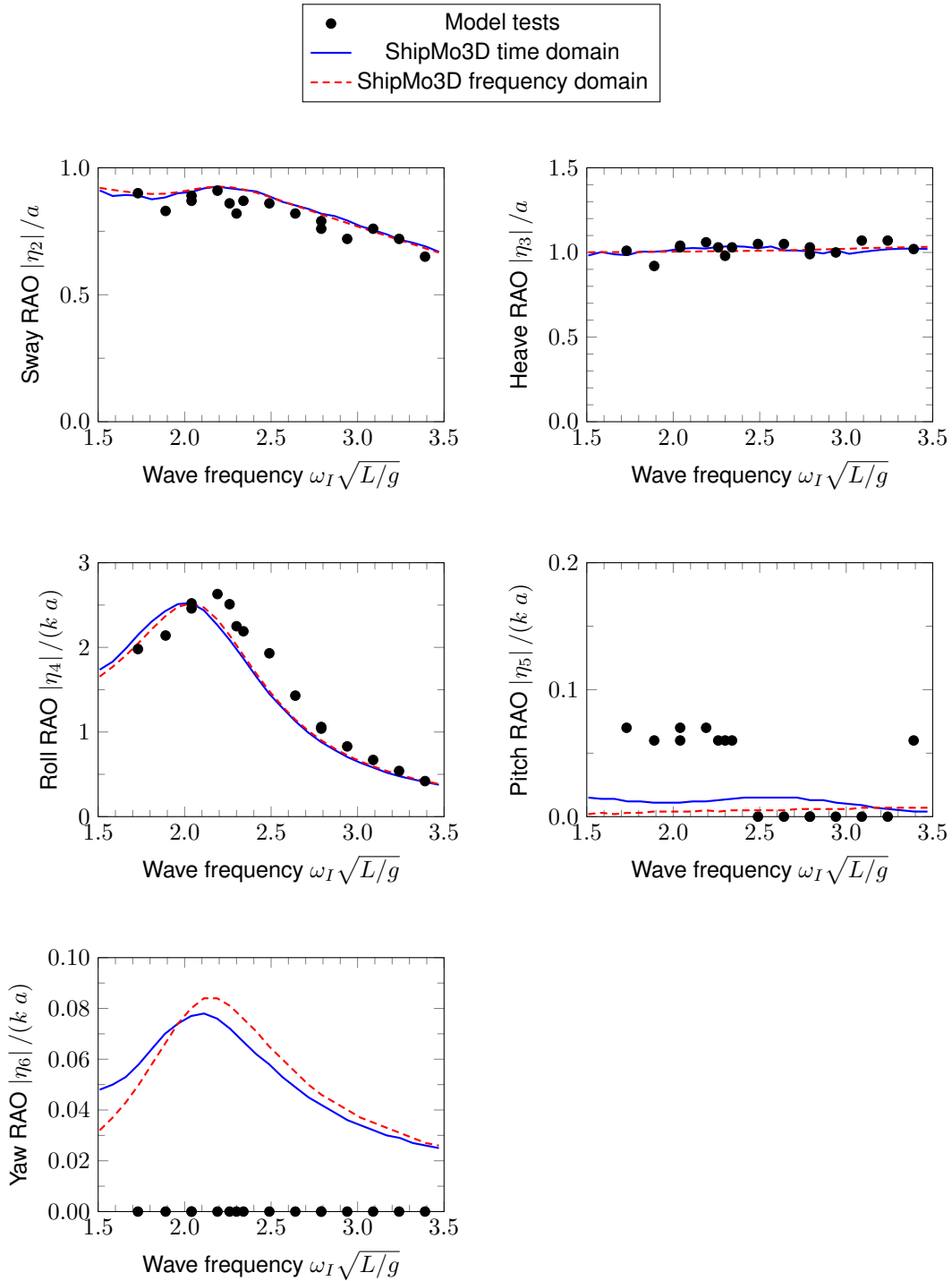


Figure 15: Steered warship RAOs, stern quartering seas at 90 degrees, Froude number 0.28.

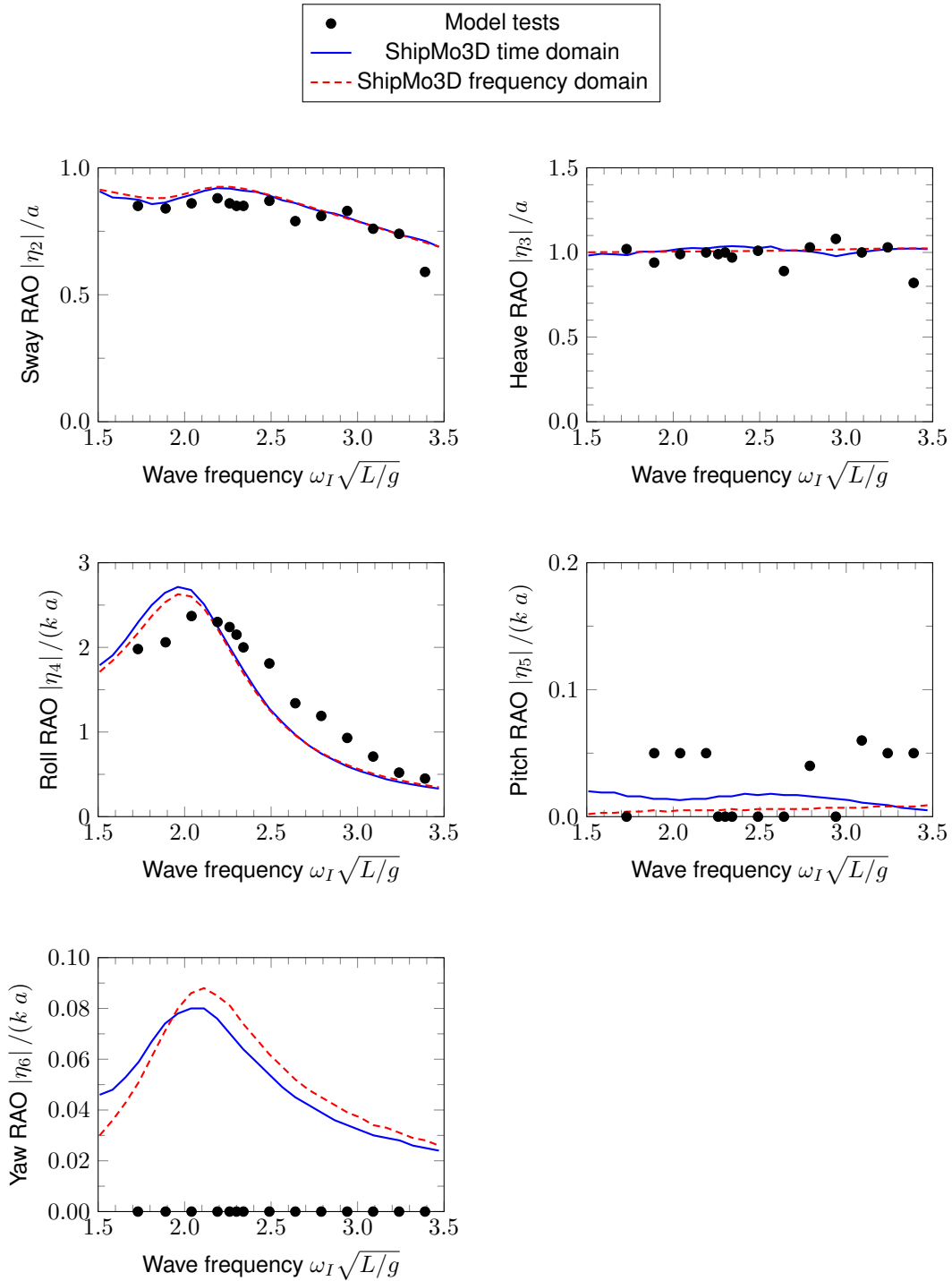


Figure 16: Steered warship RAOs, beam seas at 90 degrees,
 Froude number 0.36.

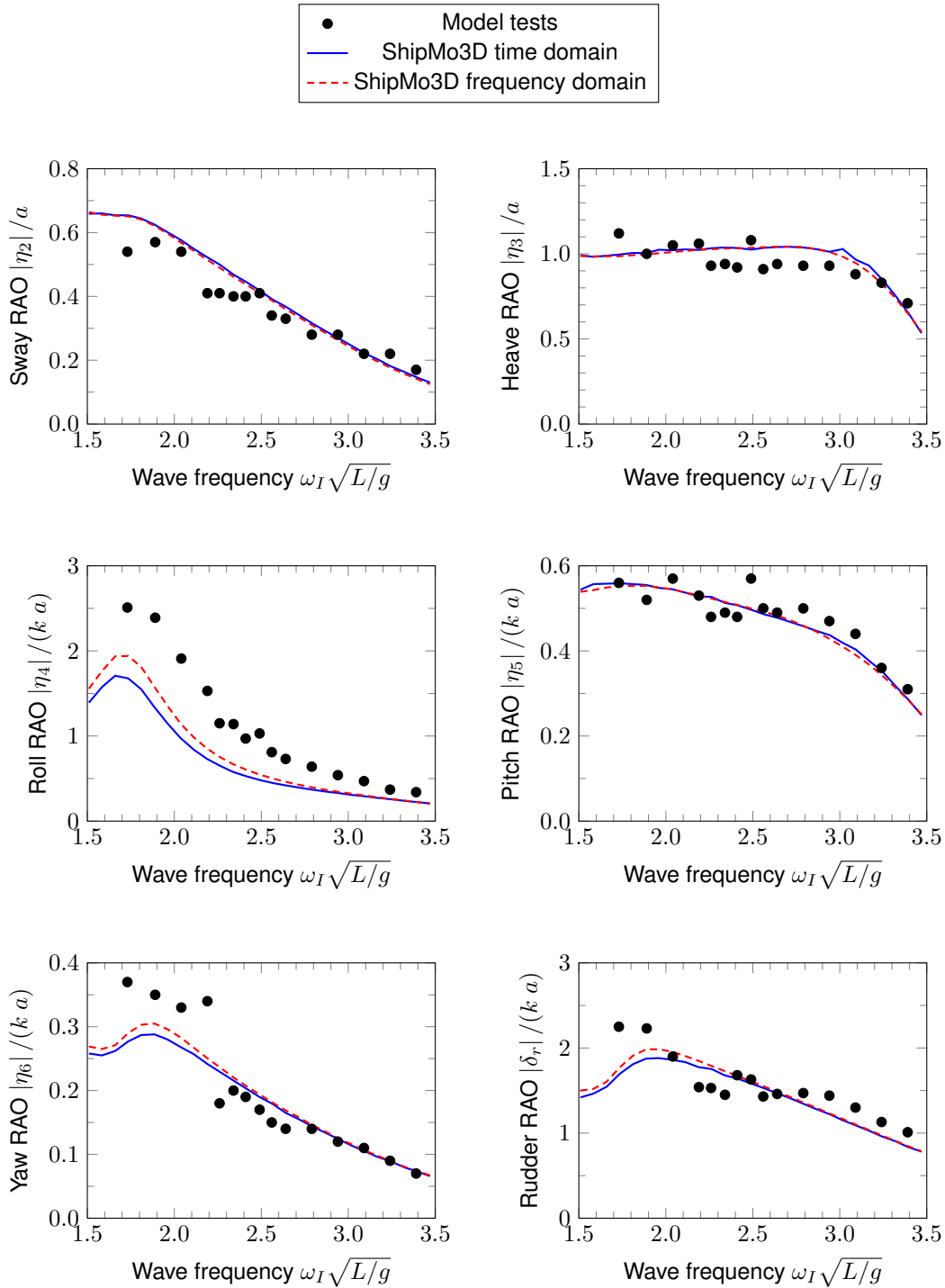


Figure 17: Steered warship RAOs, bow quartering seas at 120 degrees, Froude number 0.27.

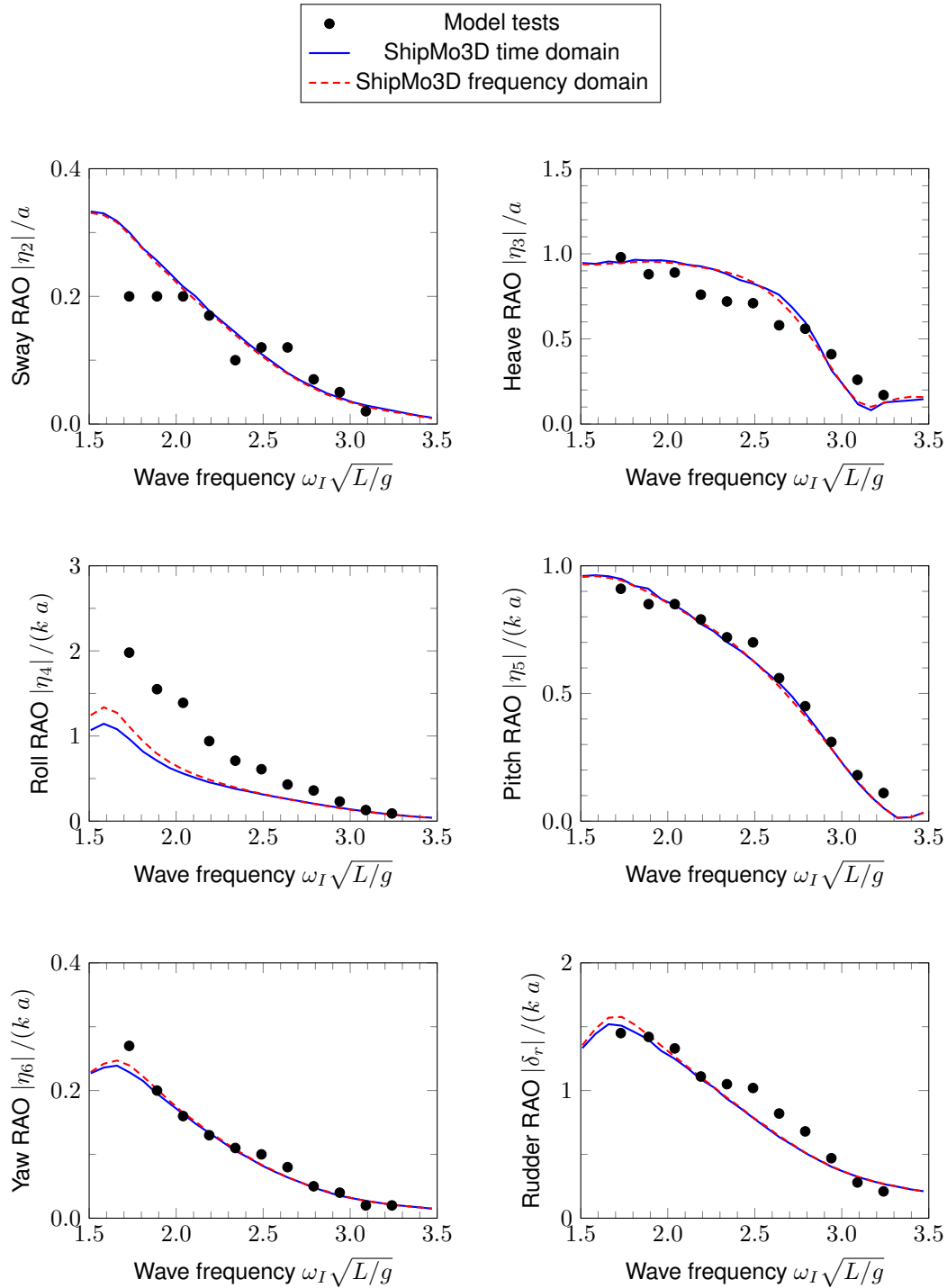


Figure 18: Steered warship RAOs, bow quartering seas at 150 degrees, Froude number 0.26.

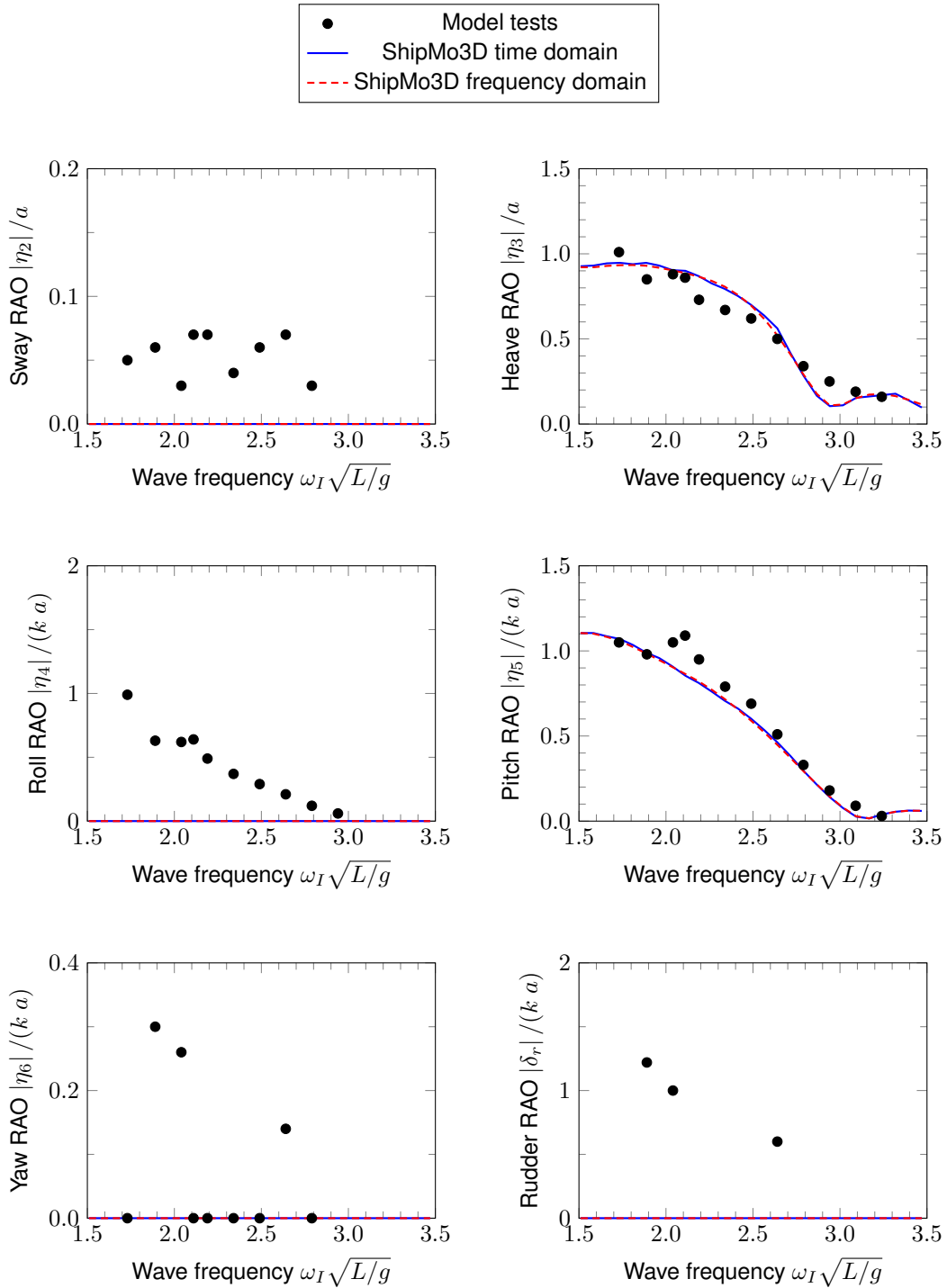


Figure 19: Steered warship RAOs, head seas at 180 degrees, Froude number 0.26.

3.4 Motions of the Haslar Steered Warship Model in Random Waves for Sea State 6

In practice, ship motion predictions are most commonly used to examine motions in random seaways. Consequently, it is useful to examine motions for the Haslar steered warship in random waves based on experimental RAOs and ShipMo3D predictions. Tables 7 to 11 give motions for the Haslar steered warship at full-scale in Sea State 6, consisting of a long-crested seaway with significant wave height of 5.0 m and peak wave period of 12.4 s. Assuming a model scale of 1/20, the full-scale ship has a length L of 111.6 m.

The results in Tables 7 to 11 indicate that predicted zero-crossing periods for all modes (except surge, for which no data are available) are typically within 10 percent of values based on experimental RAOs. RMS values based on experimental RAOs and predictions show generally good agreement. Predicted RMS sway and heave are typically within 10 percent of values based on experimental RAOs. The ratio of predicted to experimental RMS roll has an average of 89 percent (11 percent underprediction) and standard deviation of 20 percent, reflecting challenges with prediction of viscous damping forces. Pitch is under-predicted by 10 percent on average, with predicted/experimental pitch having a moderately high standard deviation of 13 percent. Yaw is under-predicted by 14 percent on average, with predicted/experimental yaw having a higher standard deviation of 17 percent. Challenges in predicting yaw motions could be caused by difficulties in accurately predicting yaw-yaw manoeuvring force coefficients, which were estimated using the regression method of Inoue et al. [28] for the present study.

Table 7: Sway of full-scale steered warship in Sea State 6 based on experimental RAOs and ShipMo3D frequency domain predictions.

Speed (knots)	Rel sea dir. (deg)	RMS (m)		T_z (s)	
		Experiments	ShipMo3D	Experiments	ShipMo3D
11.6	30	0.25	0.37	10.12	11.04
17.3	30	0.73	0.53	7.96	8.12
23.8	30	2.13	2.12	8.45	7.58
11.6	60	0.76	0.84	10.01	10.38
17.3	60	0.70	0.77	10.38	10.81
23.1	60	0.74	0.85	8.19	10.69
11.6	75	0.93	0.99	10.00	10.04
18.0	75	0.91	0.99	9.94	9.92
23.1	75	0.82	0.99	10.11	9.96
11.6	90	0.98	0.99	9.92	10.03
18.0	90	0.96	0.99	9.95	9.94
23.1	90	0.94	0.99	9.86	9.88
17.3	120	0.53	0.61	10.68	10.84
16.7	150	0.19	0.25	10.99	11.57

Statistics for ratios of predicted/experimental

	RMS	T_z
Mean	1.11	1.03
Deviation	0.17	0.09

Table 8: Heave of full-scale steered warship in Sea State 6 based on experimental RAOs and ShipMo3D frequency domain predictions.

Speed (knots)	Rel sea dir. (deg)	RMS (m)		T_z (s)	
		Experiments	ShipMo3D	Experiments	ShipMo3D
18.0	0	0.54	0.57	11.67	11.77
23.8	0	0.50	0.56	11.26	11.67
11.6	30	0.66	0.66	11.36	11.52
17.3	30	0.67	0.64	11.37	11.56
23.8	30	0.63	0.62	11.50	11.57
11.6	60	0.88	0.89	10.43	10.59
17.3	60	0.89	0.85	10.65	10.80
23.1	60	0.86	0.81	10.60	10.97
11.6	75	1.03	1.04	10.00	9.96
18.0	75	1.00	1.02	9.94	9.97
23.1	75	1.00	1.00	10.08	10.00
11.6	90	1.17	1.13	9.57	9.68
18.0	90	1.13	1.13	9.64	9.69
23.1	90	1.11	1.12	9.75	9.69
17.3	120	1.14	1.12	10.06	9.79
16.7	150	0.91	0.97	10.76	10.54
16.7	180	0.90	0.91	11.00	10.79

Statistics for ratios of predicted/experimental

	RMS	T_z
Mean	1.00	1.00
Deviation	0.05	0.02

Table 9: Roll of full-scale steered warship in Sea State 6 based on experimental RAOs and ShipMo3D frequency domain predictions.

Speed (knots)	Rel sea dir. (deg)	RMS (deg)		T_z (s)	
		Experiments	ShipMo3D	Experiments	ShipMo3D
11.6	30	2.41	2.80	8.82	8.71
17.3	30	3.49	2.84	9.09	9.30
23.8	30	3.70	2.54	9.71	9.76
11.6	60	7.41	6.39	7.74	7.91
17.3	60	5.87	7.67	8.30	7.83
23.1	60	7.46	6.78	8.28	8.22
11.6	75	8.08	5.98	8.22	8.65
18.0	75	7.86	7.28	7.92	8.40
23.1	75	8.07	9.02	7.89	8.04
11.6	90	6.16	5.22	9.30	9.38
18.0	90	5.15	4.71	9.48	9.65
23.1	90	4.89	4.59	9.44	9.90
17.3	120	4.05	2.61	10.44	10.56
16.7	150	2.84	1.50	10.91	10.91

Statistics for ratios of predicted/experimental

	RMS	T_z
Mean	0.89	1.01
Deviation	0.20	0.03

Table 10: Pitch of full-scale steered warship in Sea State 6 based on experimental RAOs and ShipMo3D frequency domain predictions.

Speed (knots)	Rel sea dir. (deg)	RMS (deg)		T_z (s)	
		Experiments	ShipMo3D	Experiments	ShipMo3D
18.0	0	1.13	1.18	10.82	10.53
23.8	0	1.01	1.22	11.12	10.45
11.6	30	1.19	1.16	9.95	10.32
17.3	30	1.28	1.14	10.36	10.26
23.8	30	1.15	1.15	10.63	10.08
11.6	60	1.20	0.97	8.85	9.14
17.3	60	1.16	0.87	9.05	9.51
23.1	60	1.14	0.83	9.08	9.56
11.6	75	0.80	0.68	8.40	8.28
18.0	75	0.79	0.63	8.37	8.36
23.1	75	0.77	0.59	8.52	8.44
17.3	120	1.47	1.42	8.56	8.62
16.7	150	1.87	1.81	9.69	9.79
16.7	180	2.07	1.87	10.07	10.16

Statistics for ratios of predicted/experimental

	RMS	T_z
Mean	0.90	1.00
Deviation	0.13	0.03

Table 11: Yaw of full-scale steered warship in Sea State 6 based on experimental RAOs and ShipMo3D frequency domain predictions.

Speed (knots)	Rel sea dir. (deg)	RMS (deg)		T_z (s)	
		Experiments	ShipMo3D	Experiments	ShipMo3D
11.6	30	1.35	1.34	9.28	9.31
17.3	30	2.33	1.59	8.71	8.90
23.8	30	2.40	1.40	8.95	8.93
11.6	60	1.30	1.35	8.96	8.81
17.3	60	1.72	1.72	8.67	8.30
23.1	60	3.07	1.67	8.03	8.16
11.6	75	0.80	0.69	8.28	8.89
18.0	75	0.88	0.83	8.10	8.72
23.1	75	0.92	0.91	8.26	8.37
17.3	120	0.68	0.60	9.95	9.43
16.7	150	0.38	0.35	10.71	10.55

Statistics for ratios of predicted/experimental

	RMS	T_z
Mean	0.86	1.01
Deviation	0.17	0.04

4 Wave-induced Motions of the Canadian Patrol Frigate Hydroelastic Model in Regular Head Seas

The Canadian Patrol Frigate (CPF) hydroelastic model was the subject of a comprehensive series of model tests for measuring ship motions and sea loads in regular and random seas [13]. Tests were conducted in a towing tank for head seas, and in an offshore basin for both head and oblique seas.

4.1 Canadian Patrol Frigate Hydroelastic Model

The CPF hydroelastic model was constructed at a scale of 1/20, and is described in detail in Reference [13]. Table 12 gives full-scale particulars and Figure 20 gives the body plan. The model was designed such that both motions and sea loads could be measured. The model consists of six rigid segments mounted on a flexible backbone, as shown in Figure 21. The flexible backbone was designed to model the stiffness properties of the full-scale ship for shear and bending in the horizontal and vertical directions. Consequently, the transient structural response to events such as slamming is captured in the model experiments.

Table 12: Full scale dimensions for Canadian Patrol Frigate hydroelastic model in fresh water, deep departure condition.

Length overall, L_{oa}	134.7 m
Length between perpendiculars, L	124.5 m
Beam, B	14.8 m
Midships draft, T	4.97 m
Trim by bow	0.04 m
Displacement, Δ	4655 tonnes
LCG station	10.45
Center of gravity above keel, \overline{KG}	6.26 m
Metacentric height, \overline{GM}	1.08 m
Roll period in water, T_4	12.3 s

The current validation of ShipMo3D predictions only considers model experiments that were conducted in a towing tank for regular head seas. For these experiments, the model was attached to a towing carriage and towed in regular waves for a range of wave frequencies and wave steepnesses of 1/30, 1/20, and 1/15. This data set is especially useful for examining the variation of heave and pitch response with wave steepness, and for validating nonlinear ship motion predictions.

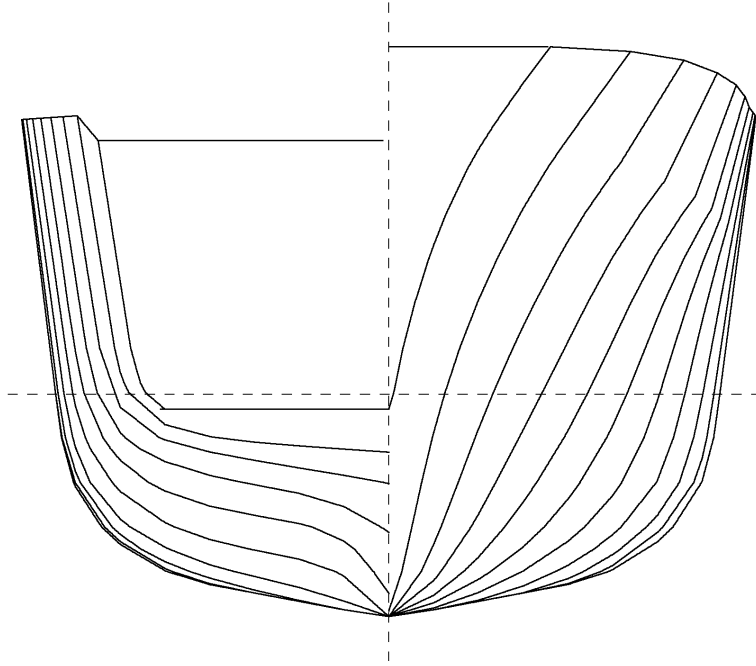


Figure 20: Body plan for CPF hydroelastic model.

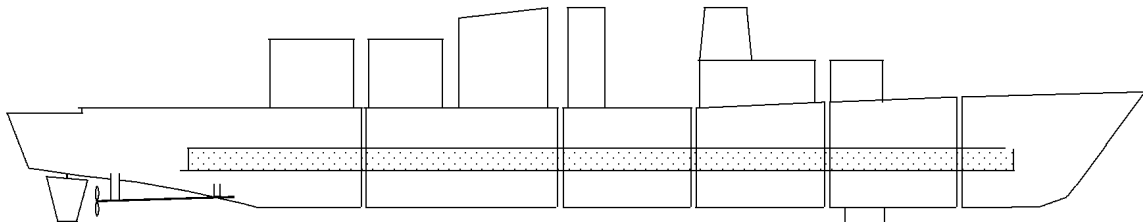


Figure 21: Profile of CPF hydroelastic model.

4.2 ShipMo3D Model of CPF Hydroelastic Model

Figure 22 shows the ShipMo3D model of the CPF hydroelastic model.

4.3 Comparisons of Numerical Predictions and Experimental Results for the CPF Hydroelastic Model in Regular Head Seas

Validation for the CPF hydroelastic model is limited to heave and pitch motions. Changes between Versions 3 and 4.2 of ShipMo3D generally have minimal influence on heave and pitch forces, leading to predictions for Version 3 and 4.2 being almost identical for heave and pitch of the CPF hydroelastic model.

Figures 23 to 26 show heave and pitch in head seas for Froude numbers of 0.06, 0.12,

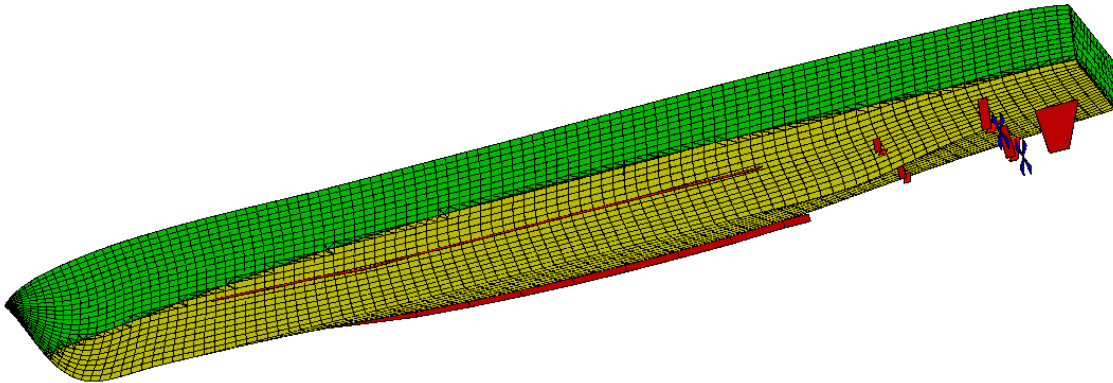


Figure 22: *ShipMo3D model for CPF hydroelastic model.*

0.20, and 0.25. The time domain motion predictions use nonlinear modelling of forces from incident waves and buoyancy, with Stokes' second order theory for modelling the seaway. The numerical predictions are generally good, and the frequency domain predictions give very good agreement with the time domain predictions for the lowest wave steepness of $1/30$. The pitch predictions are generally better than the heave predictions. At the lowest Froude number of 0.06, the heave predictions are noticeably smaller than experimental values in the lower frequency range. At the two highest Froude numbers of 0.20 and 0.25, heave predictions are greater than experimental values at intermediate frequencies. Surprisingly, the usage of nonlinear buoyancy and incident forces in the time domain predictions appears to lead to somewhat poorer agreement with experiments than for the frequency domain predictions.

Figure 27 shows predictions in head seas at a Froude number of 0.12 using different seaway models. The Stokes second order seaway is the most accurate of the 3 seaway models, and adds little computational burden relative to the linear seaway. Wheeler stretching is recommended for seaways modelled using multiple components, which is most commonly done when modelling random seaways. The results in Figure 27 indicate that the motion predictions are insensitive to the 3 approaches used for modelling the seaway.

The results for the CPF hydroelastic model indicate there is potential for improvement of heave and pitch predictions in both lower and higher wave steepnesses. Reference [29] examined inclusion of the steady double body flow potential [30,31] when computing ShipMo3D hull radiation coefficients. These computations indicated that the uniform steady flow potential used for the present computations gives better motion predictions than the more complex double body flow potential. Note that both the uniform steady flow potential and the double body flow potential don't consider the effects of water viscosity and steady waves.

Huijsmans et al. [32] suggest that inclusion of the steady scattered wave potential could especially lead to improvements in heave predictions. Nonlinear bow flare slamming forces could be evaluated using a momentum approach [33], which would have minimal computational penalty and would likely give improved predictions in higher sea states. Nonlinear radiation and radiation forces would also likely give improved force predictions in higher sea states.

The motion predictions for the CPF hydroelastic model from ShipMo3D Version 4.2 are very similar to those for Version 3.0 [9]. This strong similarity in predictions arises because only heave and pitch motion have been used for validation with the CPF hydroelastic model.

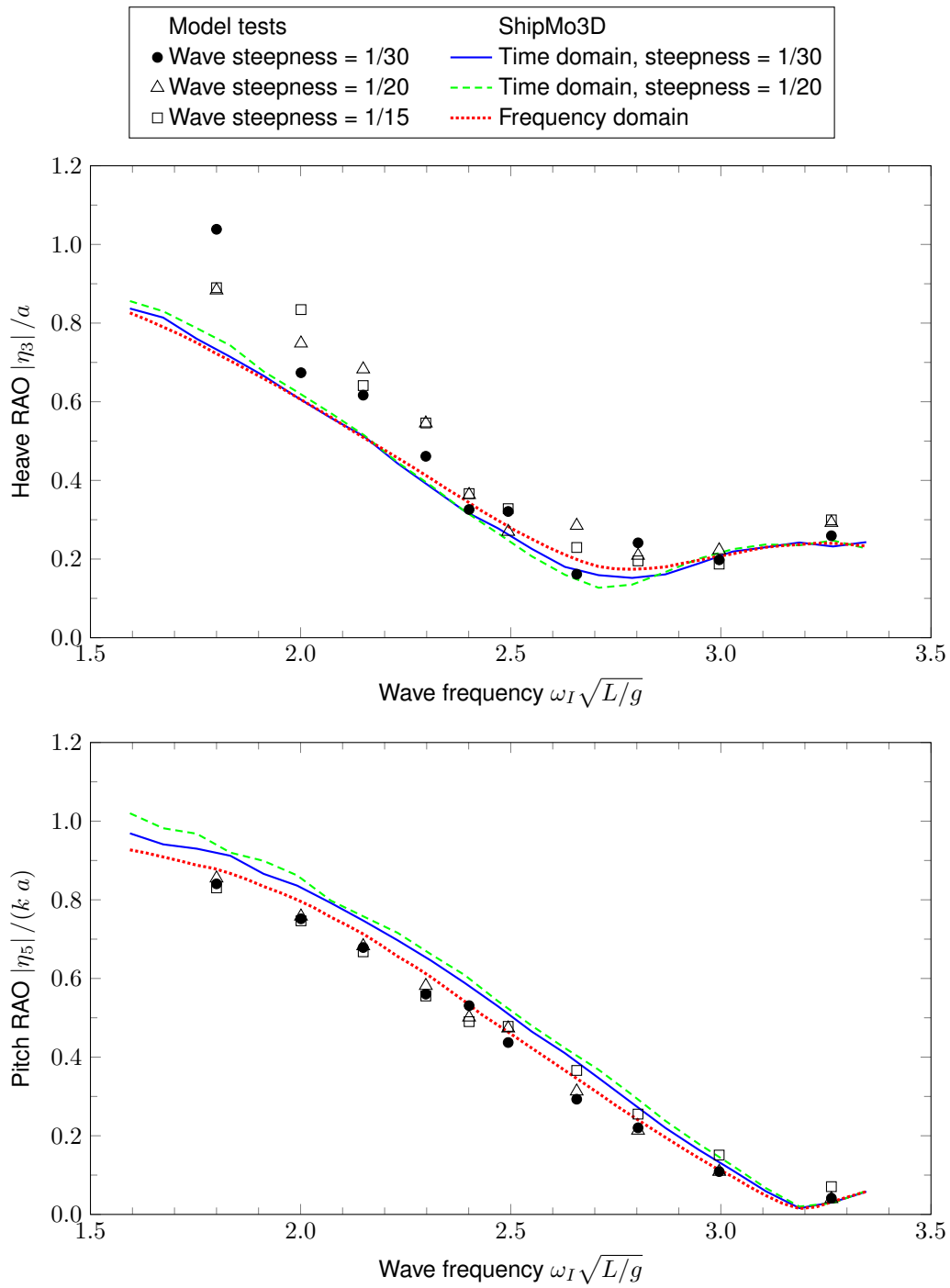


Figure 23: Heave and pitch RAOs for Canadian Patrol Frigate hydroelastic model, head seas at 180 degrees, Froude number 0.06.

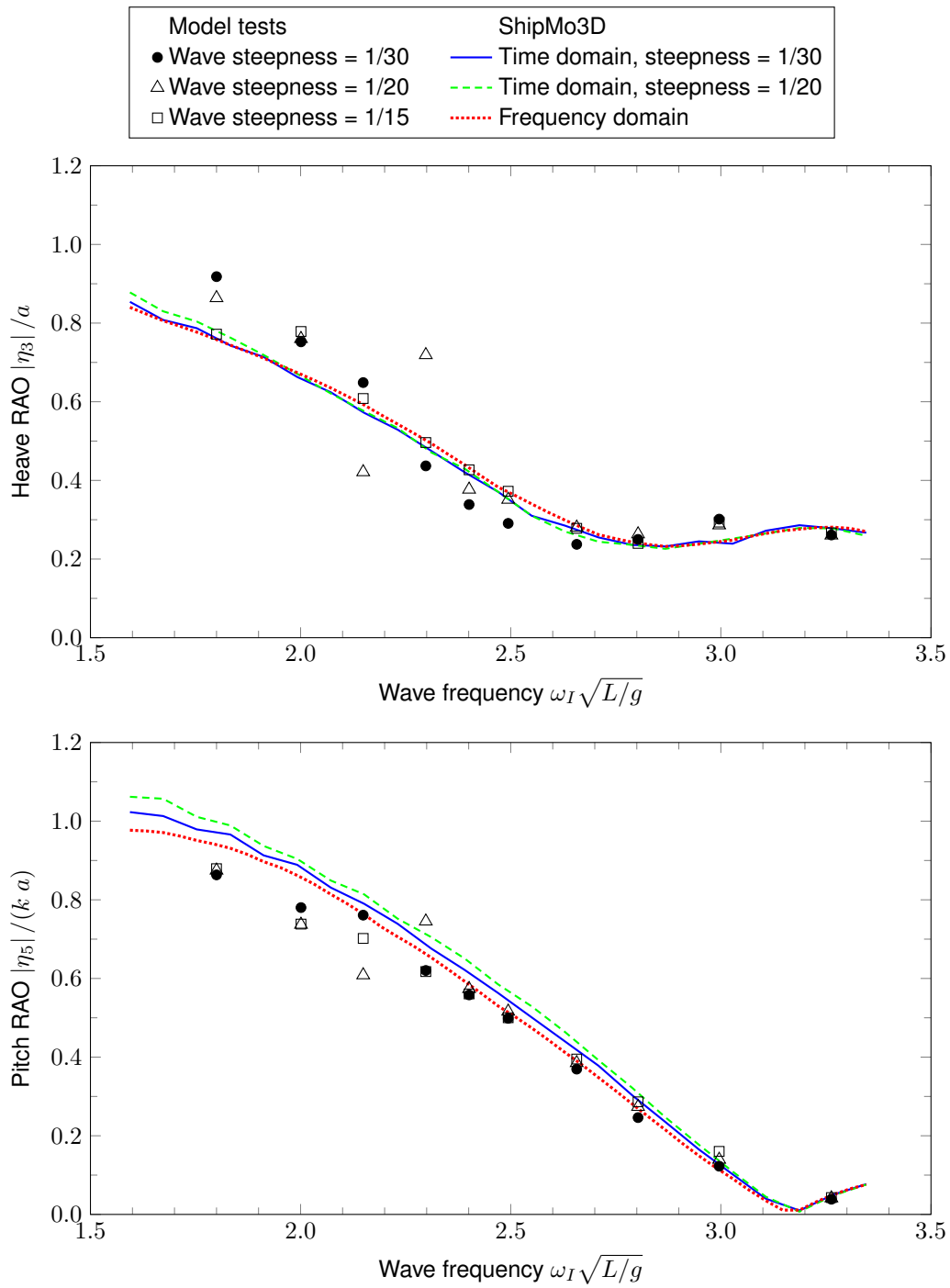


Figure 24: Heave and pitch RAOs for Canadian Patrol Frigate hydroelastic model, head seas at 180 degrees, Froude number 0.12.

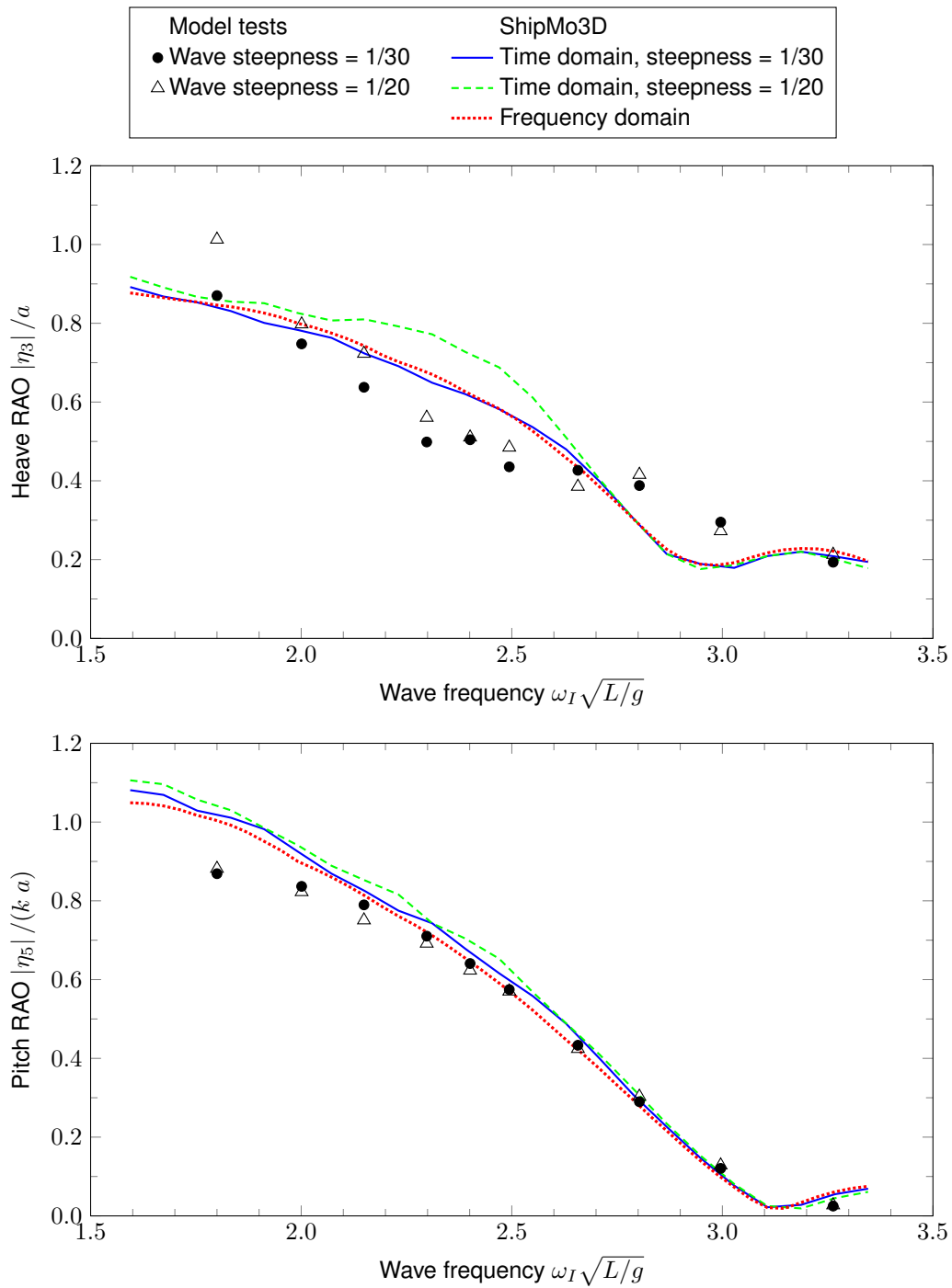


Figure 25: Heave and pitch RAOs for Canadian Patrol Frigate hydroelastic model, head seas at 180 degrees, Froude number 0.20.

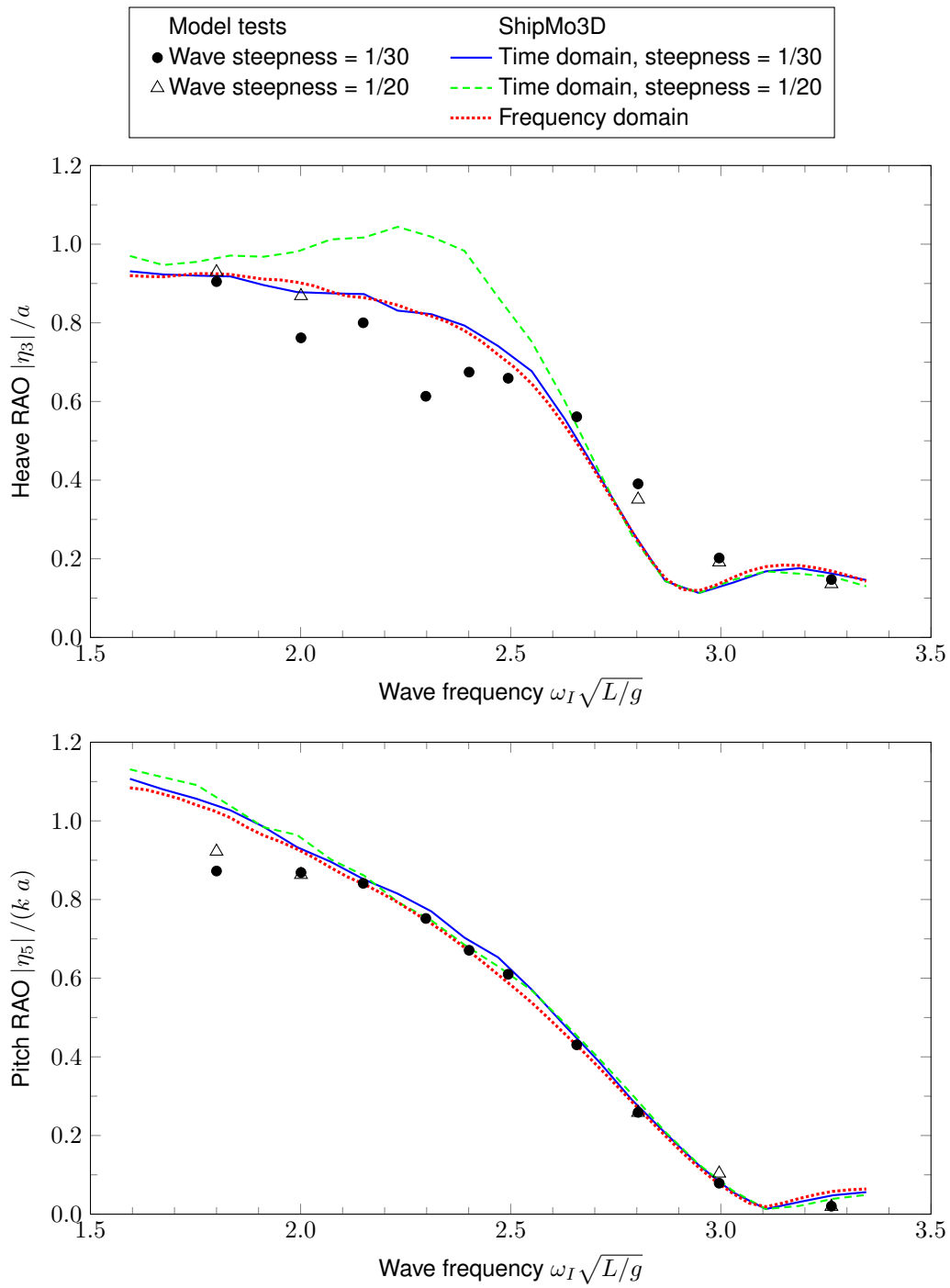


Figure 26: Heave and pitch RAOs for Canadian Patrol Frigate hydroelastic model, head seas at 180 degrees, Froude number 0.25.

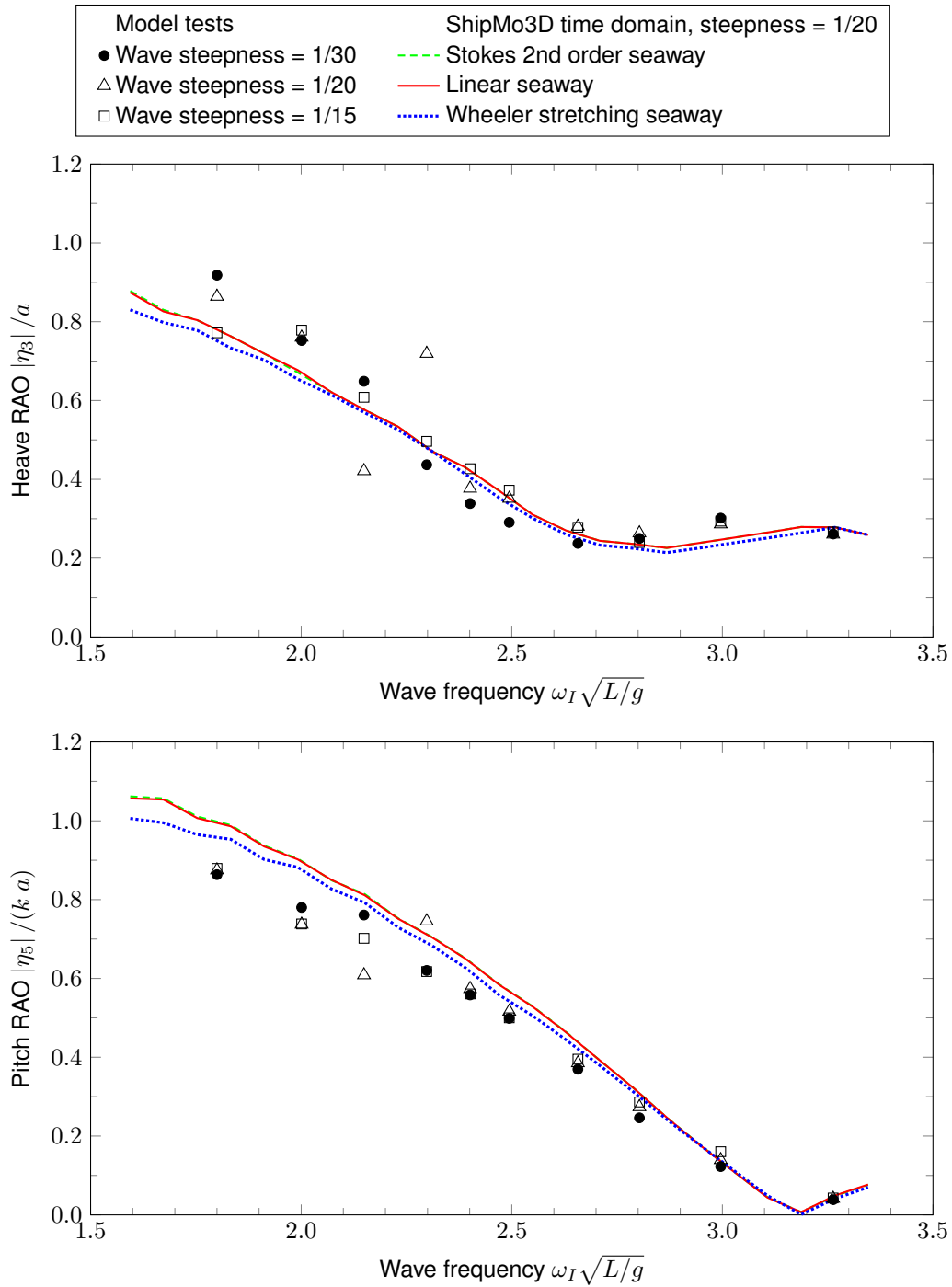


Figure 27: Heave and pitch RAOs using different seaway models for Canadian Patrol Frigate hydroelastic model, head seas at 180 degrees, Froude number 0.12.

5 Wave-induced Motions of the Naval Destroyer HMCS NIPIGON from Sea Trials

Although seakeeping model tests likely experience only minimal scale effects for reasonably sized models (e.g., model scales greater than 1/30 for naval frigates and destroyers), comparisons with full-scale sea trials can provide further confidence in predictions of ship motions. Reliable measurements of both ship motions and wave conditions are essential for sea trial data to be used for validation of ship motion predictions. DRDC – Atlantic Research Centre has conducted many sea trials for measuring ship motions, with structural load measurements often being included in sea trials. A comprehensive sea trial was conducted in December 1997 to measure ship motions and sea loads for HMCS NIPIGON [14]. This section gives comparisons of measured motions with ShipMo3D predictions.

5.1 HMCS NIPIGON

HMCS NIPIGON (Figure 28) was the last steam-driven destroyer in the Canadian Fleet. Table 13 gives particulars for NIPIGON and Figure 29 gives a body plan. NIPIGON appendages include 2 rudders, 2 outer propeller shaft brackets, 2 inner propeller shaft brackets, 2 bilge keels, and a skeg, with dimensions as given in Tables 14 to 17.

Table 13: Main particulars for HMCS NIPIGON.

Length L	108.4 m
Beam B	12.8 m
Midships draft T_{mid}	4.3 m
Trim by stern t_{stern}	0.5 m
Displacement Δ	3027 tonnes
Vertical centre of gravity \overline{KG}	5.1 m
Metacentric height \overline{GM}_{fluid}	1.2 m
Roll radius of gyration r_{xx}	5.6 m
Pitch radius of gyration r_{yy}	27.1 m
Natural roll period T_4	10.6 s



Figure 28: HMCS NIPIGON.

Table 14: Bilge keel dimensions for HMCS NIPIGON.

Station (20 at AP)	8.82	10	11	12	13	13.79
Span (m)	0.610	0.610	0.610	0.610	0.610	0.610
Root lateral offset (m)	5.775	5.734	5.623	5.559	5.553	5.578
Root above baseline (m)	2.207	1.867	1.848	1.959	2.203	2.448
Dihedral angle (deg, port side)	-45	-45	-45	-45	-45	-45

Table 15: Skeg dimensions for HMCS NIPIGON.

Station (20 at AP)	14	15	16	16.5
Span (m)	0.067	0.293	0.823	1.236
Root above baseline (m)	0.067	0.293	0.823	1.236

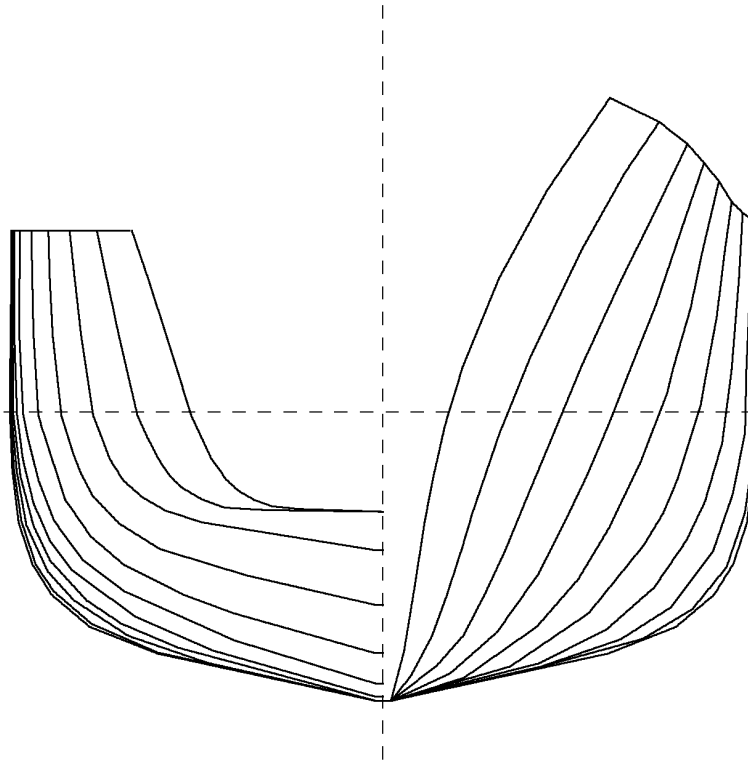


Figure 29: *Body plan for HMCS NIPIGON.*

Table 16: *Propeller shaft bracket dimensions for HMCS NIPIGON.*

	Inner brackets	Outer bracket
Station (20 at AP)	18.3	18.3
Span (m)	2.240	2.256
Root chord (m)	0.800	0.800
Tip chord (m)	0.800	0.800
Root lateral offset (m)	1.158	3.109
Root above baseline (m)	2.957	3.200
Dihedral angle (deg, port side)	-64.2	-99.5

Table 17: Rudder dimensions for HMCS NIPIGON.

Station (20 at AP)	19.3
Span (m)	3.023
Root chord (m)	2.286
Tip chord (m)	1.886
Root lateral offset (m)	1.981
Root above baseline (m)	3.197
Dihedral angle (deg, port side)	-90.0

5.2 Conditions for HMCS NIPIGON Sea Trial

During the December 1997 sea trial, a series of 71 trial runs of 20 to 30 minute duration was undertaken at two nominal ship speeds in head, bow, beam, stern quartering and following seas. Data were collected in higher seas (Sea States 4, 5 and 6) for three days over December 2, 3 and 4th and for four days at lower seas (Sea States 2 and 3) over December 8 to 11th. The “low” ship speed was about 8 knots and “high” ship speed was between 14 and 18 knots depending on what speed the ship could maintain in the given sea state. Speed was limited due to the loss of one of the two propulsion system boilers on the first day of the trial.

Trial instrumentation included a ship motions package, a wave buoy, a TSK over-the-bow wave height meter, an array of 24 pressure transducers outfitted in the hull below the waterline, 15 single strain gauges, and 4 rosette strain gauges. Wave data were collected for 20 minutes out of every hour from the wave buoy. An Endeco type 1156 directional wave buoy was used for the first 3 days of the trial, and an Endeco type 956 buoy was used for the last 4 days. The main data acquisition system was a PC-based LabVIEW system. All sixty instrumentation channels were digitally sampled at 20 Hz. Time histories, statistical distributions and minimum and maximum values were determined and recorded.

For validation of ShipMo3D, runs from the sea trial were selected which satisfy the following criteria:

- the significant wave height H_s was greater than 3 m;
- there was a clear dominant wave direction and minimal directional wave spreading; and
- the nominal relative wave direction was oblique (bow quartering, beam, or stern quartering seas).

Table 18 gives a summary of the runs selected for the present study, with T_z denoting zero-crossing wave period.

Table 18: HMCS NIPIGON trial runs for ShipMo3D validation.

Run	Speed (kt)	H_s (m)	T_z (s)	Wave direction (from, deg)		Ship heading (to, deg)	Relative sea direction
				Mean	Deviation		
203	8	3.73	7.73	218	39	265	Bow quarter
204	8	3.67	7.21	225	39	85	Stern quarter
206	16	3.89	7.39	228	25	355	Stern quarter
209	13	4.75	8.07	224	33	265	Bow quarter
210	15	4.75	8.07	224	33	85	Stern quarter
303	8	5.82	9.45	274	41	310	Bow quarter
304	8	5.57	8.81	272	39	120	Stern quarter
305	8	5.57	8.81	272	39	220	Bow quarter
306	8	5.16	8.66	266	45	50	Stern quarter
309	14	5.39	8.95	279	32	315	Bow quarter
310	14	5.44	8.73	269	43	135	Stern quarter
403	8	5.01	9.34	244	40	290	Bow quarter
404	8	4.90	9.60	238	47	110	Stern quarter
409	16	4.52	8.37	238	50	285	Bow quarter
410	16	4.52	8.37	238	50	105	Stern quarter
413	8	4.98	8.86	245	40	330	Beam

5.3 ShipMo3D Model of HMCS NIPIGON

Figure 30 shows the ShipMo3D Model for HMCS NIPIGON. Due to lack of available data, some of the input parameters for NIPIGON had to be estimated. Hull resistance was estimated using the method of Holtrop and Mennen [25], which is available as an option in SM3DBuildShip4. The variation of propeller thrust coefficient with advance ratio was based on a representative curve from Reference [26]. For each rudder, the rudder-propeller coefficient associated with the propeller on the same side of the ship was given a value of 0.9, based on the assumption that 90 percent of the rudder area was within the propeller slipstream. The flow straightening coefficient for each rudder was estimated to be 0.7 based on Equation (5). For each ship speed used for sea trials, the associated propeller RPM settings for calm water were determined using SM3DBuildShip4, which uses an iterative process. Table 19 gives the assumed rudder autopilot settings that were used for ShipMo3D computations. In the absence of heading gain data from the sea trial, moderate heading gains are used for the numerical predictions.

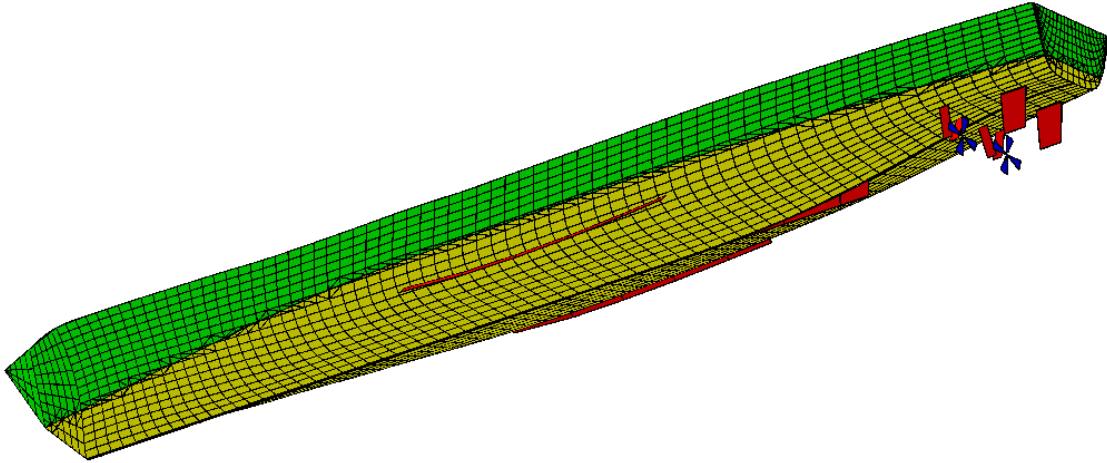


Figure 30: ShipMo3D Model for HMCS NIPIGON.

Table 19: Assumed rudder control properties for HMCS NIPIGON during sea trial.

Maximum deflection angle δ_{max}^{rudder}	35 deg
Maximum deflection rate $\dot{\delta}_{max}^{rudder}$	3 deg/s
Deflection natural frequency ω_{δ}	0.2 rad/s
Deflection damping ratio ζ_{δ}	0.85
Heading displacement gain $k_{\delta\delta}^P$	-2.0
Heading velocity gain $k_{\delta\delta}^D$	-4.0 s

5.4 Comparisons of Numerical Predictions and Experimental Results for HMCS NIPIGON Sea Trials

Predicted and computed motions for HMCS NIPIGON are given in Tables 20 to 27 and Figures 31 to 33. When the directionality of the seaway is modelled (all computations except for frequency domain unidirectional), predicted RMS motions and zero-crossing periods are typically within 10 percent of observed values, with the exception of RMS roll, which is typically within 30 percent of observed values. These results are typical of computations of ship motions in waves (e.g., Reference [34]), which tend to be more accurate for vertical plane motions than for lateral plane motions.

The linear time domain predictions and frequency domain predictions for directional seas have excellent agreement, suggesting the time and frequency domain ShipMo3D implementations are consistent. The frequency domain predictions with directional and unidirectional

seas give similar results, with the directional sea predictions giving better agreement with observed values due to the more accurate modelling of the actual seaways.

Comparisons between linear and nonlinear time domain predictions provide further insight. The heave and pitch predictions show little difference between linear and nonlinear predictions. For roll time domain predictions, ratio of mean predicted to observed RMS value is 1.29 for nonlinear predictions, somewhat greater than the value of 1.20 for linear predictions. This difference prompted further examination of results, including yaw motion predictions. Tables 26 and 27 indicate that predicted yaw motions can be quite sensitive to the inclusion of nonlinear buoyancy and incident wave forces. This sensitivity is likely due to variability of sectional drafts with relative vertical motions. The dependence of predicted yaw on nonlinear effects will influence rudder deflections and roll forces.

In comparison to the Version 3 predictions [9], the most noticeable difference is that roll overprediction is less for Version 4.2, with the mean ratio of predicted to observed RMS roll for linear time domain predictions decreasing from 1.29 to 1.20. Likely causes of changes in roll predictions include a different roll drag model for bilge keels and skegs, inclusion of wave excitation manoeuvring forces in Version 4.2, and the vertical centre of lateral manoeuvring forces changing from the waterplane to the centroid of underwater lateral area.

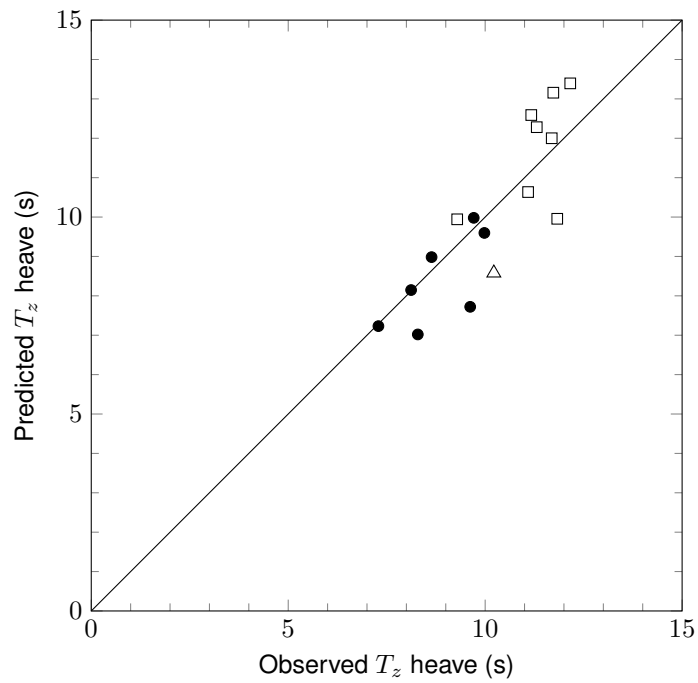
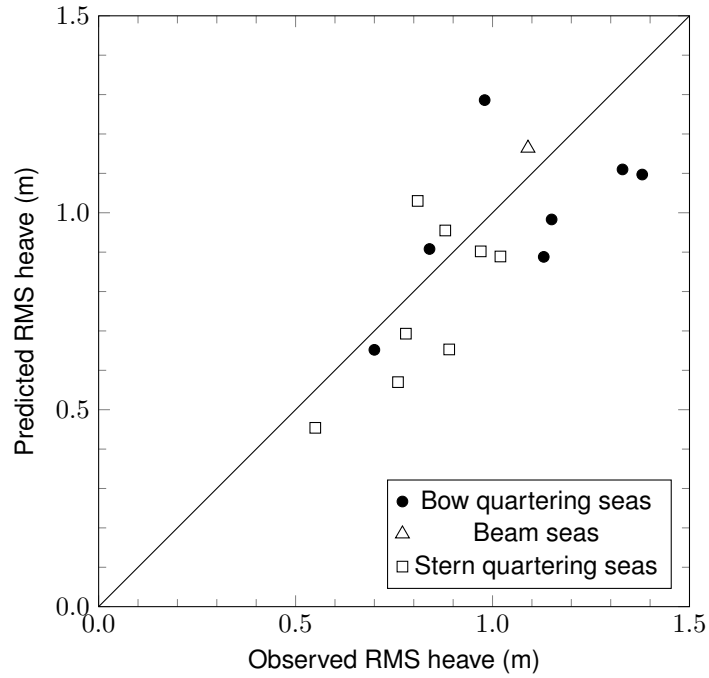


Figure 31: Predicted versus observed RMS and zero-crossing period for heave, HMCS NIPIGON Trials and ShipMo3D time domain predictions with linear incident wave and buoyancy forces.

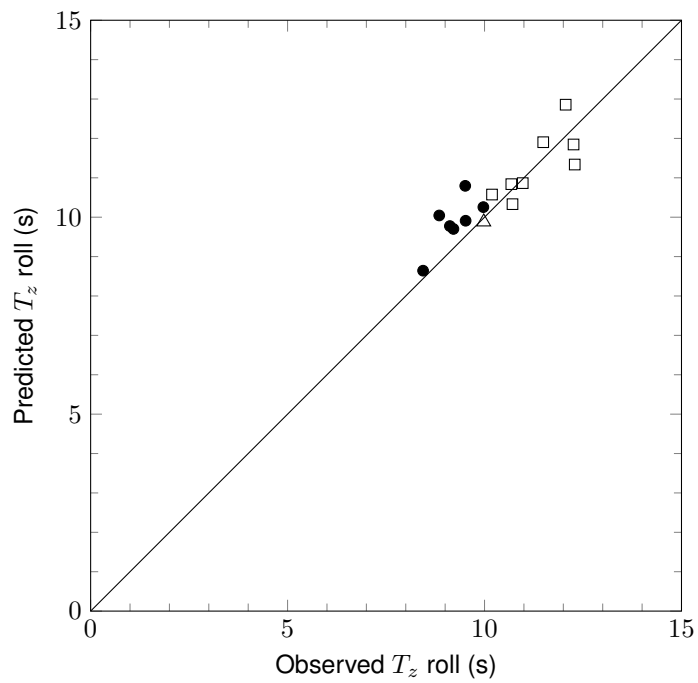
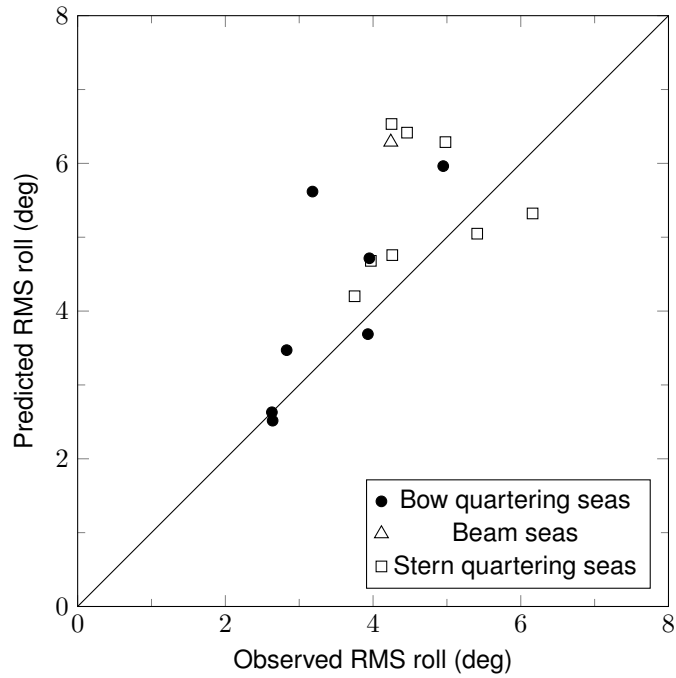


Figure 32: Predicted versus observed RMS and zero-crossing period for roll, HMCS NIPIGON Trials and ShipMo3D time domain predictions with linear incident wave and buoyancy forces.

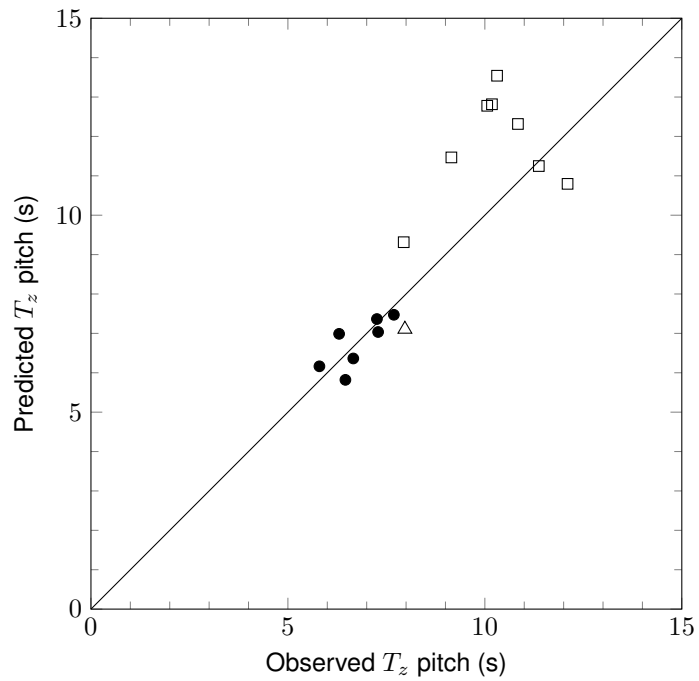
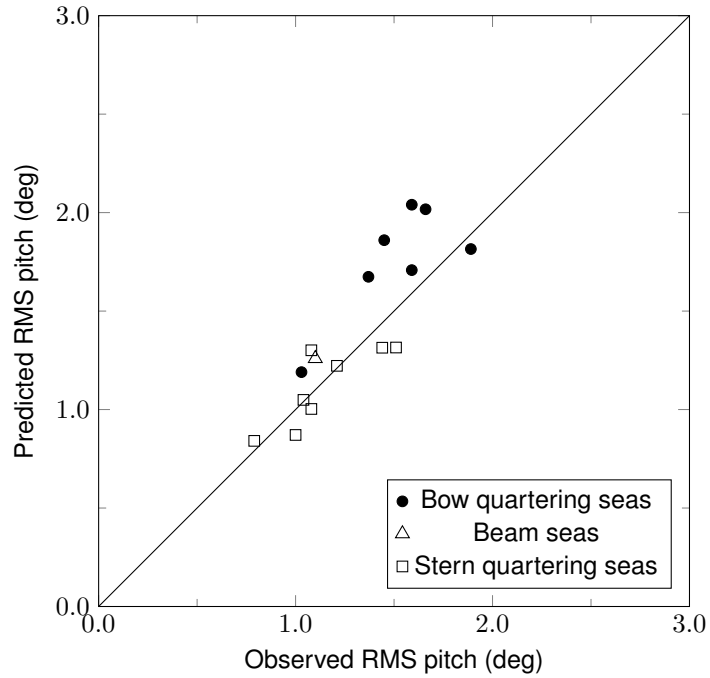


Figure 33: Predicted versus observed RMS and zero-crossing period for pitch, HMCS NIPIGON trials and ShipMo3D time domain predictions with linear incident wave and buoyancy forces.

Table 20: Measured and predicted RMS heave (m)
for HMCS NIPIGON.

Run	Speed (knots)	Relative Sea dir.	Observed	Time domain		Frequency domain		
				Nonlinear	Linear	Direct.	Unidirect.	
203	8	Bow quarter	0.70	0.62	0.65	0.65	0.64	
204	8	Stern quarter	0.55	0.47	0.45	0.48	0.41	
206	16	Stern quarter	0.76	0.55	0.57	0.55	0.45	
209	13	Bow quarter	0.84	0.95	0.91	0.96	0.91	
210	15	Stern quarter	0.89	0.69	0.65	0.67	0.54	
303	8	Bow quarter	1.38	1.15	1.10	1.11	1.12	
304	8	Stern quarter	1.02	0.86	0.89	0.90	0.83	
305	8	Bow quarter	0.98	1.25	1.29	1.21	1.13	
306	8	Stern quarter	0.81	1.06	1.03	0.95	0.77	
309	14	Bow quarter	1.33	1.10	1.11	1.11	1.11	
310	14	Stern quarter	0.97	0.92	0.90	0.89	0.87	
403	8	Bow quarter	1.15	1.01	0.98	1.01	1.02	
404	8	Stern quarter	0.88	0.95	0.95	0.92	0.94	
409	16	Bow quarter	1.13	0.94	0.89	0.94	1.03	
410	16	Stern quarter	0.78	0.73	0.69	0.71	0.69	
413	8	Beam	1.09	1.18	1.16	1.15	1.28	
Predicted/observed								
Mean					0.95	0.94	0.94	0.90
Deviation					0.17	0.17	0.15	0.16

Table 21: Measured and predicted heave zero-crossing period (s)
for HMCS NIPIGON.

Run	Speed (knots)	Relative Sea dir.	Observed	Time domain		Frequency domain		
				Nonlinear	Linear	Direct.	Unidirect.	
203	8	Bow quarter	8.1	8.3	8.1	8.3	8.0	
204	8	Stern quarter	9.3	10.1	9.9	10.1	12.6	
206	16	Stern quarter	11.8	9.8	10.0	10.2	14.4	
209	13	Bow quarter	7.3	7.1	7.2	6.9	6.7	
210	15	Stern quarter	11.7	12.0	12.0	11.7	16.1	
303	8	Bow quarter	9.7	9.9	10.0	9.7	9.3	
304	8	Stern quarter	12.2	13.3	13.4	13.3	15.0	
305	8	Bow quarter	8.6	8.4	9.0	8.5	8.9	
306	8	Stern quarter	11.1	10.1	10.6	10.6	14.2	
309	14	Bow quarter	9.6	8.0	7.7	7.9	7.6	
310	14	Stern quarter	11.7	13.4	13.2	13.2	16.4	
403	8	Bow quarter	10.0	9.3	9.6	9.5	9.3	
404	8	Stern quarter	11.2	12.6	12.6	12.2	13.4	
409	16	Bow quarter	8.3	7.2	7.0	7.2	6.9	
410	16	Stern quarter	11.3	11.8	12.3	11.8	16.8	
413	8	Beam	10.2	8.5	8.6	8.7	8.4	
Predicted/observed								
Mean					0.98	0.99	0.98	1.11
Deviation					0.10	0.10	0.09	0.22

Table 22: Measured and predicted RMS roll (deg)
for HMCS NIPIGON.

Run	Speed (knots)	Relative Sea dir.	Observed	Time domain		Frequency domain		
				Nonlinear	Linear	Direct.	Unidirect.	
203	8	Bow quarter	2.83	3.97	3.47	3.83	3.41	
204	8	Stern quarter	3.97	4.83	4.68	5.27	5.58	
206	16	Stern quarter	4.25	6.35	6.53	6.67	6.75	
209	13	Bow quarter	2.64	3.55	2.52	2.84	1.86	
210	15	Stern quarter	4.98	6.30	6.29	6.31	4.14	
303	8	Bow quarter	4.95	5.98	5.96	6.61	6.77	
304	8	Stern quarter	6.16	5.06	5.32	5.78	5.69	
305	8	Bow quarter	3.18	5.88	5.62	6.43	6.76	
306	8	Stern quarter	4.46	7.10	6.42	7.11	6.48	
309	14	Bow quarter	3.93	4.10	3.69	3.91	3.38	
310	14	Stern quarter	5.41	5.05	5.05	4.97	5.51	
403	8	Bow quarter	3.95	5.07	4.71	5.73	6.41	
404	8	Stern quarter	4.26	4.77	4.76	5.56	6.86	
409	16	Bow quarter	2.63	2.93	2.63	2.91	3.11	
410	16	Stern quarter	3.75	3.96	4.20	4.16	4.59	
413	8	Beam	4.24	7.72	6.29	7.21	8.29	
Predicted/observed								
Mean					1.29	1.20	1.32	1.32
Deviation					0.28	0.24	0.29	0.39

Table 23: Measured and predicted roll zero-crossing period (s)
for HMCS NIPIGON.

Run	Speed (knots)	Relative Sea dir.	Observed	Time domain		Frequency domain		
				Nonlinear	Linear	Direct.	Unidirect.	
203	8	Bow quarter	9.2	9.5	9.7	9.8	9.4	
204	8	Stern quarter	10.2	10.5	10.6	10.5	10.5	
206	16	Stern quarter	12.3	11.3	11.3	11.3	13.1	
209	13	Bow quarter	8.4	8.9	8.6	8.8	7.5	
210	15	Stern quarter	12.3	11.6	11.8	11.7	15.5	
303	8	Bow quarter	9.5	10.4	10.8	10.6	10.3	
304	8	Stern quarter	11.0	10.5	10.9	10.8	10.9	
305	8	Bow quarter	8.8	9.8	10.0	10.2	10.2	
306	8	Stern quarter	10.7	10.4	10.3	10.5	10.9	
309	14	Bow quarter	9.1	9.9	9.8	9.9	9.6	
310	14	Stern quarter	11.5	12.2	11.9	11.8	13.6	
403	8	Bow quarter	10.0	10.1	10.3	10.4	10.3	
404	8	Stern quarter	10.7	10.7	10.8	10.7	10.7	
409	16	Bow quarter	9.5	10.0	9.9	9.9	9.2	
410	16	Stern quarter	12.1	11.9	12.9	12.5	14.8	
413	8	Beam	10.0	10.1	9.9	10.2	10.3	
Predicted/observed								
Mean					1.02	1.03	1.03	1.06
Deviation					0.05	0.06	0.06	0.09

Table 24: Measured and predicted RMS pitch (deg)
for HMCS NIPIGON.

Run	Speed (knots)	Relative Sea dir.	Observed	Time domain		Frequency domain		
				Nonlinear	Linear	Direct.	Unidirect.	
203	8	Bow quarter	1.03	1.13	1.19	1.20	1.44	
204	8	Stern quarter	0.79	0.88	0.84	0.87	0.89	
206	16	Stern quarter	1.00	0.85	0.87	0.90	0.84	
209	13	Bow quarter	1.45	1.90	1.86	1.97	2.16	
210	15	Stern quarter	1.08	1.00	1.00	1.10	1.17	
303	8	Bow quarter	1.66	2.05	2.02	2.05	2.21	
304	8	Stern quarter	1.51	1.35	1.31	1.32	1.43	
305	8	Bow quarter	1.89	1.85	1.81	1.79	2.00	
306	8	Stern quarter	1.44	1.30	1.31	1.30	1.36	
309	14	Bow quarter	1.59	2.04	2.04	2.01	2.20	
310	14	Stern quarter	1.21	1.25	1.22	1.23	1.24	
403	8	Bow quarter	1.37	1.74	1.67	1.71	1.75	
404	8	Stern quarter	1.08	1.30	1.30	1.25	1.21	
409	16	Bow quarter	1.59	1.77	1.71	1.77	1.87	
410	16	Stern quarter	1.04	1.04	1.05	1.10	1.01	
413	8	Beam	1.10	1.24	1.26	1.28	0.43	
Predicted/observed								
Mean					1.08	1.08	1.10	1.10
Deviation					0.15	0.14	0.14	0.26

Table 25: Measured and predicted pitch zero-crossing period (s)
for HMCS NIPIGON.

Run	Speed (knots)	Relative Sea dir.	Observed	Time domain		Frequency domain		
				Nonlinear	Linear	Direct.	Unidirect.	
203	8	Bow quarter	6.3	7.0	7.0	7.2	6.7	
204	8	Stern quarter	7.9	9.6	9.3	9.7	11.4	
206	16	Stern quarter	12.1	11.3	10.8	11.3	13.7	
209	13	Bow quarter	5.8	6.2	6.2	6.2	6.2	
210	15	Stern quarter	10.1	13.1	12.8	13.6	15.7	
303	8	Bow quarter	7.3	7.8	7.4	7.8	7.7	
304	8	Stern quarter	10.8	13.0	12.3	12.7	13.4	
305	8	Bow quarter	7.3	6.9	7.0	6.9	6.8	
306	8	Stern quarter	11.4	10.3	11.2	10.4	12.6	
309	14	Bow quarter	6.7	6.1	6.4	6.3	6.3	
310	14	Stern quarter	10.3	14.4	13.5	13.8	14.8	
403	8	Bow quarter	7.7	7.2	7.5	7.5	7.5	
404	8	Stern quarter	9.2	11.4	11.5	11.3	11.3	
409	16	Bow quarter	6.5	5.9	5.8	6.0	5.9	
410	16	Stern quarter	10.2	13.1	12.8	12.0	15.6	
413	8	Beam	8.0	7.2	7.1	7.1	6.0	
Predicted/observed								
Mean					1.09	1.07	1.08	1.15
Deviation					0.16	0.14	0.15	0.23

Table 26: Predicted RMS yaw (deg) for HMCS NIPIGON.

Run	Speed (knots)	Relative sea dir.	Time domain		Frequency domain	
			Nonlinear	Linear	Direct.	Unidirect.
203	8	Bow	0.93	0.49	0.46	0.49
204	8	Quarter	0.94	0.83	0.61	0.82
206	16	Quarter	1.71	1.63	1.64	1.90
209	13	Bow	1.34	0.55	0.53	0.49
210	15	Quarter	1.72	1.71	1.80	2.10
303	8	Bow	1.22	0.66	0.56	0.67
304	8	Quarter	1.31	1.09	0.80	1.00
305	8	Bow	1.72	0.86	0.70	0.77
306	8	Quarter	1.47	1.43	0.96	1.14
309	14	Bow	1.03	0.50	0.48	0.49
310	14	Quarter	1.72	1.60	1.44	1.98
403	8	Bow	1.36	0.62	0.55	0.67
404	8	Quarter	1.22	1.13	0.86	1.13
409	16	Bow	0.92	0.50	0.49	0.50
410	16	Quarter	1.68	1.75	1.84	2.05
413	8	Beam	1.19	0.96	0.62	0.35

Table 27: Predicted yaw zero-crossing period (s) for HMCS NIPIGON.

Run	Speed (knots)	Relative sea dir.	Time domain		Frequency domain	
			Nonlinear	Linear	Direct.	Unidirect.
203	8	Bow	16.0	9.1	8.5	7.5
204	8	Quarter	15.0	14.4	10.4	11.3
206	16	Quarter	15.0	14.9	14.2	13.3
209	13	Bow	15.8	8.2	7.2	6.6
210	15	Quarter	15.1	15.5	15.4	15.6
303	8	Bow	22.4	11.0	9.5	8.7
304	8	Quarter	20.1	15.8	11.8	12.8
305	8	Bow	18.4	9.4	7.7	7.8
306	8	Quarter	14.4	15.0	10.3	12.2
309	14	Bow	14.8	8.3	7.8	7.3
310	14	Quarter	16.7	16.6	15.7	14.1
403	8	Bow	19.8	9.2	8.4	8.5
404	8	Quarter	14.2	13.4	11.2	11.2
409	16	Bow	14.8	9.1	8.8	6.8
410	16	Quarter	18.7	18.5	19.2	15.6
413	8	Beam	14.9	11.4	8.2	7.7

6 Wave-induced Motions of the Research Vessel R/V Melville from Model Tests

Wave-induced motions were validated using model test data for the research vessel R/V Melville from the United States. Reference [15] describes seakeeping model tests, which were conducted in both regular and random seas. Initial validation of ShipMo3D using the R/V Melville model test data was conducted by McTaggart and Marly [16]. The experimental data for R/V Melville provide a validation case for ship seakeeping with azimuthing propellers.

6.1 Scale Model of R/V Melville

Figure 34 shows the research ship R/V Melville. Table 28 gives the properties for the 1/23 scale model that was used for seakeeping model tests. During the model tests, the azimuthing propellers were steered by a human operator using a remote control.



Figure 34: Oceanographic research ship R/V Melville.

6.2 ShipMo3D Model of R/V Melville

Figure 35 shows the ShipMo3D model of the ship R/V Melville. Forces acting on the azimuthing propellers were estimated using data from Islam, Veitch, Akinturk, Bose and Liu [35]. The steering provided by the human pilot during model tests was modelled using autopilot properties given in Table 29. The heading gain $k_{\delta 6}^P$ and heading velocity gain $k_{\delta 6}^D$ were estimated by analysis of observed RMS yaw and propeller azimuth angles from model tests.

Table 28: Properties for 1/23 scale model of R/V Melville.

Length between perpendiculars L_{pp}	3.366 m
Maximum beam B	0.610 m
Draft at midships T_{mid}	0.216 m
Trim by stern t_{stern}	0.005 m
Height of CG above baseline \overline{KG}	0.256 m
Displacement Δ	234.5 kg
Metacentric height with fluid correction \overline{GM}^{fluid}	0.047 m
Number of ducted azimuthing propellers	2
Ducted propeller diameter D	0.119 m

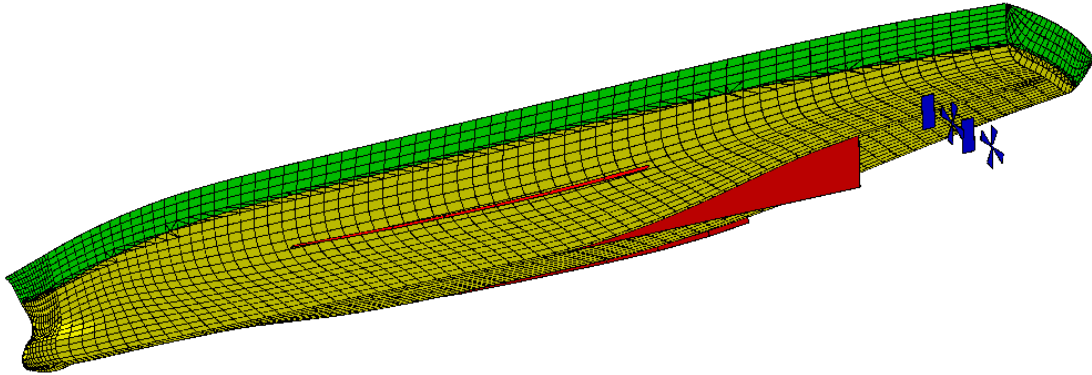


Figure 35: ShipMo3D model of research ship R/V Melville.

Table 29: Modelled autopilot properties for R/V Melville (full-scale).

Maximum deflection δ_{max}	35 deg
Maximum deflection velocity $\dot{\delta}_{max}$	12 deg/s
Response frequency ω_{δ}	3.0 rad/s
Response damping ζ_{δ}	0.85
Heading gain $k_{\delta\delta}^P$	-0.57 deg/deg
Heading velocity gain $k_{\delta\delta}^D$	-1.18 deg/(deg/s)

The numerical predictions presented in this report are somewhat different from the earlier presented results [16] because the presented predictions use the oscillating flat plate model for bilge keel roll drag and include wave excitation manoeuvring forces.

6.3 R/V Melville Motions in Regular Seas

Figures 36 to 41 give motions for the ship in regular waves of steepness 1/60 at speeds of 8 and 12 knots for following, beam, and head seas. The agreement between experiments and predictions is generally good, with notable exceptions. Experimental yaw motions are unexpectedly large, possibly due to challenges with steering the model. These large yaw motions likely contribute significantly to unexpectedly large roll motions in following and head seas.

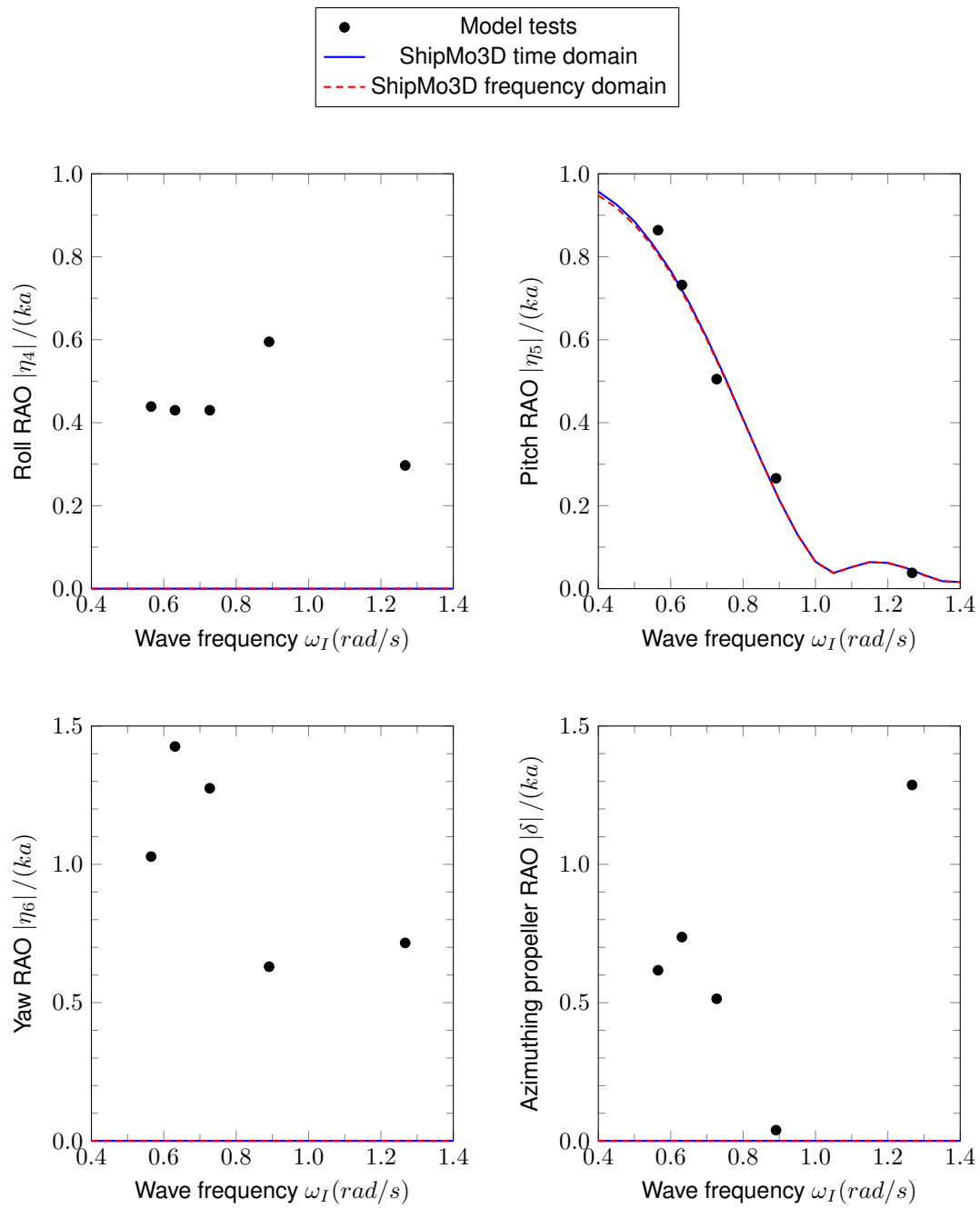


Figure 36: R/V Melville motions in regular seas, wave steepness $H/\lambda = 1/60$, ship speed $U = 8$ knots, following seas (relative sea direction $\beta_s = 0$ degrees).

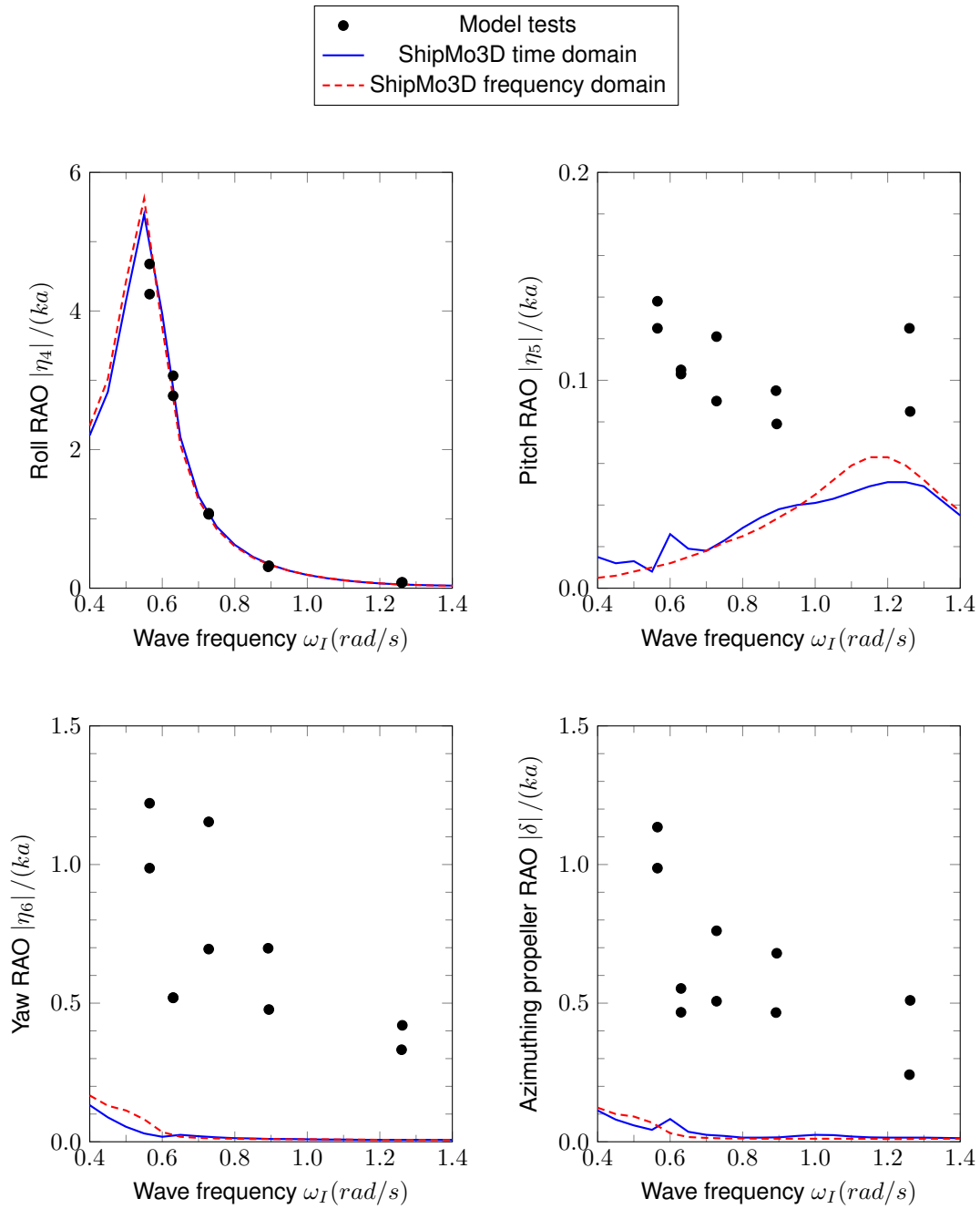


Figure 37: R/V Melville motions in regular seas, wave steepness $H/\lambda = 1/60$, ship speed $U = 8$ knots, beam seas (relative sea direction $\beta_s = 90$ degrees).

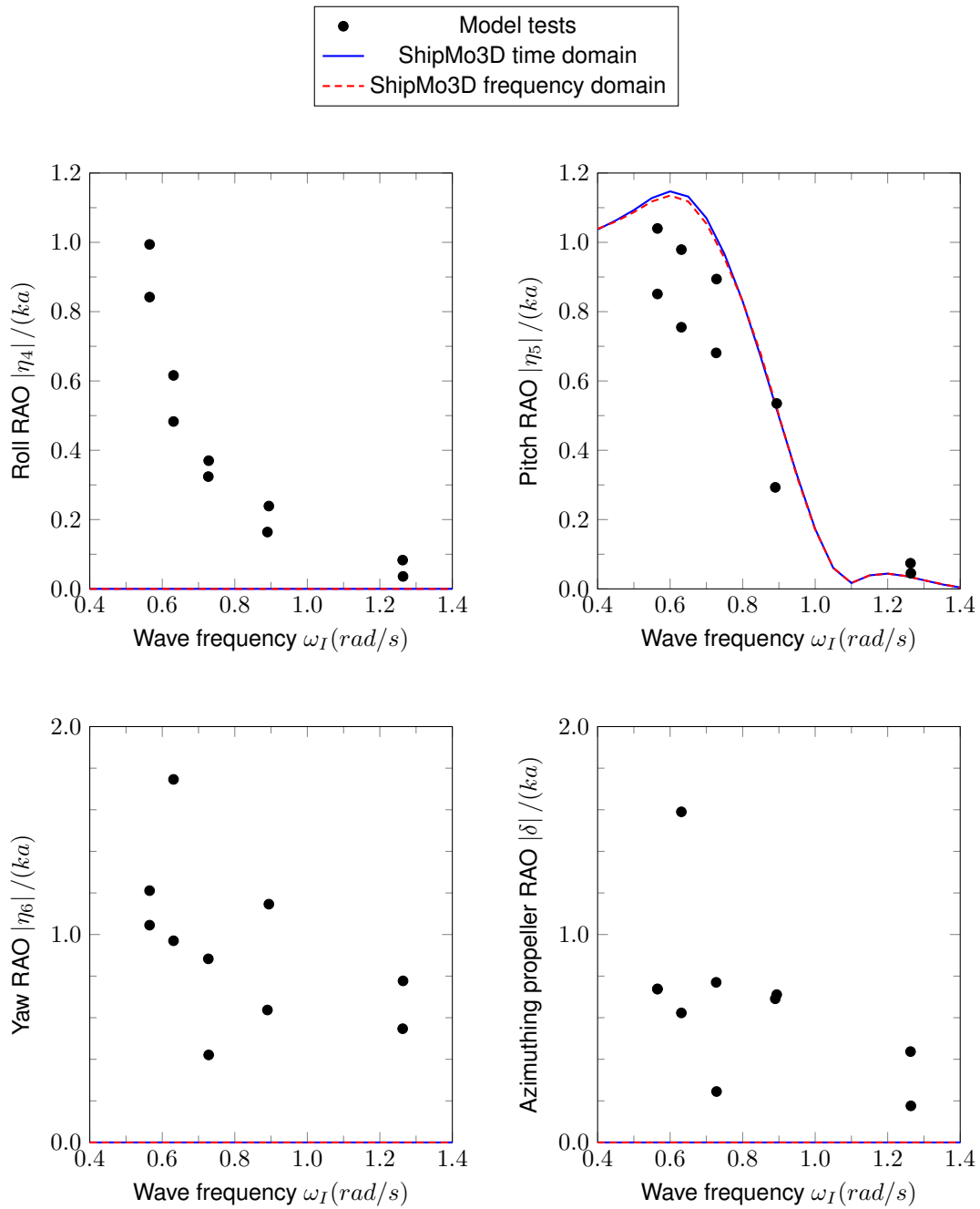


Figure 38: RV Melville motions in regular seas, wave steepness $H/\lambda = 1/60$, ship speed $U = 8$ knots, head seas (relative sea direction $\beta_s = 180$ degrees).

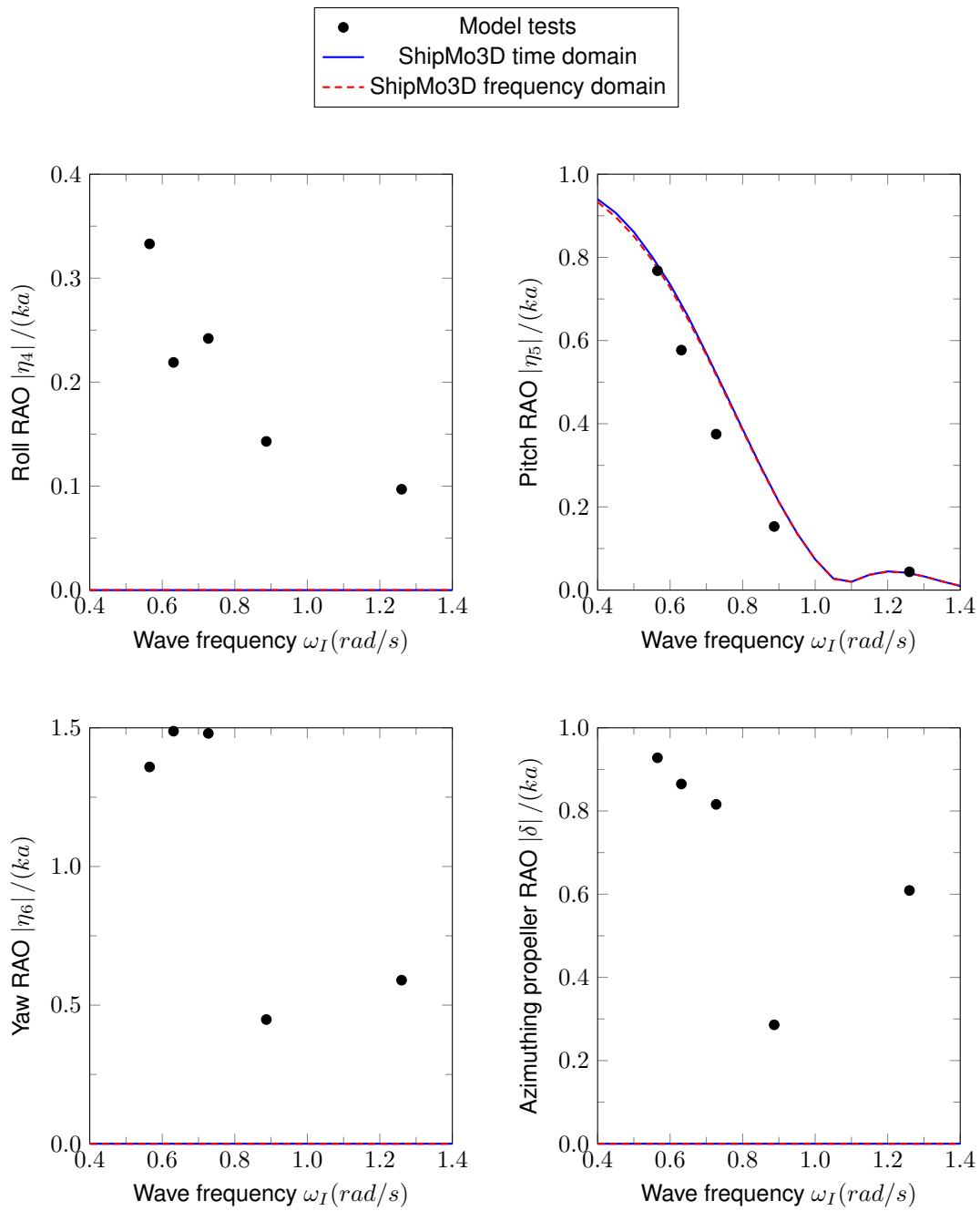


Figure 39: R/V Melville motions in regular seas, wave steepness $H/\lambda = 1/60$, ship speed $U = 12$ knots, following seas (relative sea direction $\beta_s = 0$ degrees).

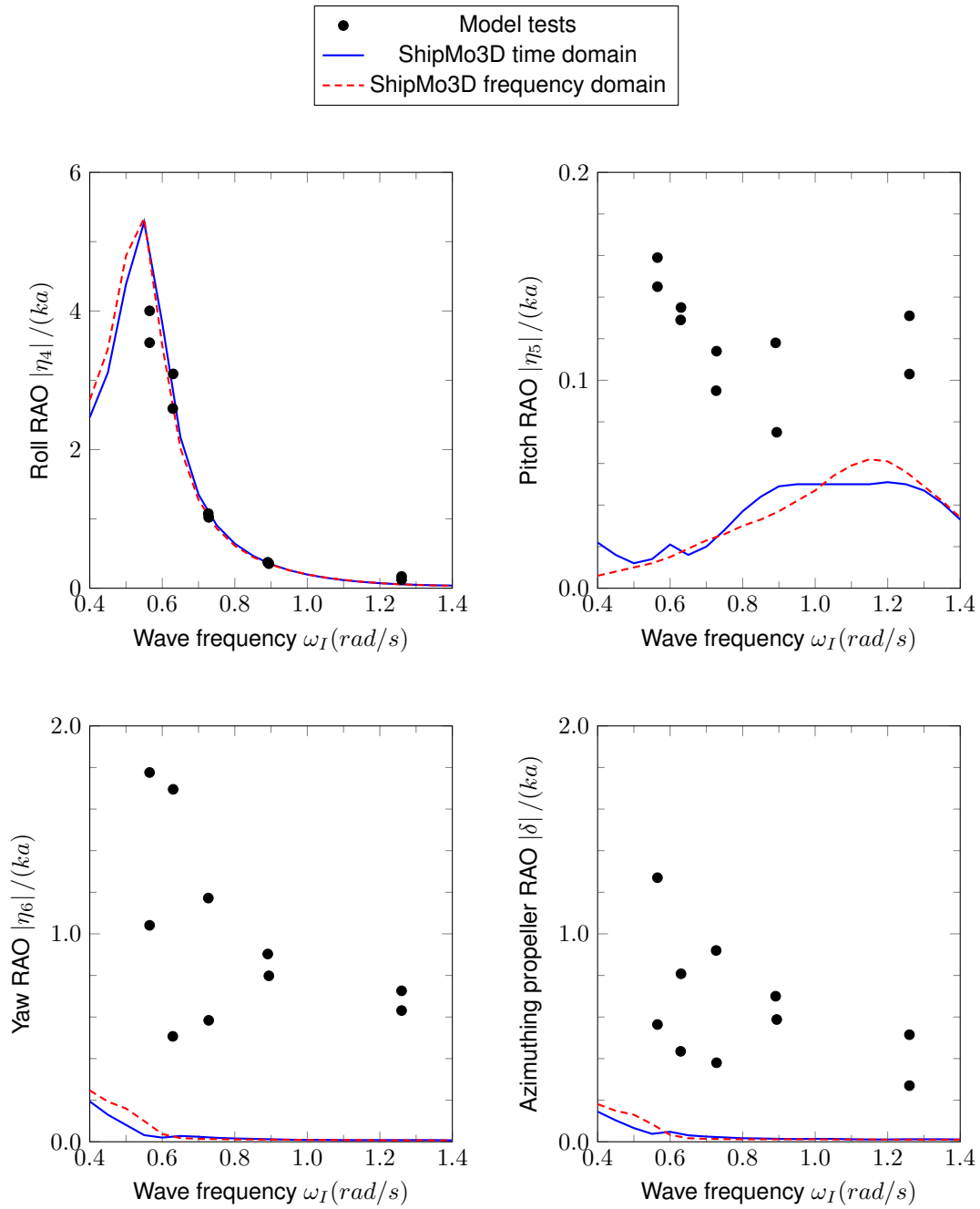


Figure 40: R/V Melville motions in regular seas, wave steepness $H/\lambda = 1/60$, ship speed $U = 12$ knots, beam seas (relative sea direction $\beta_s = 90$ degrees).

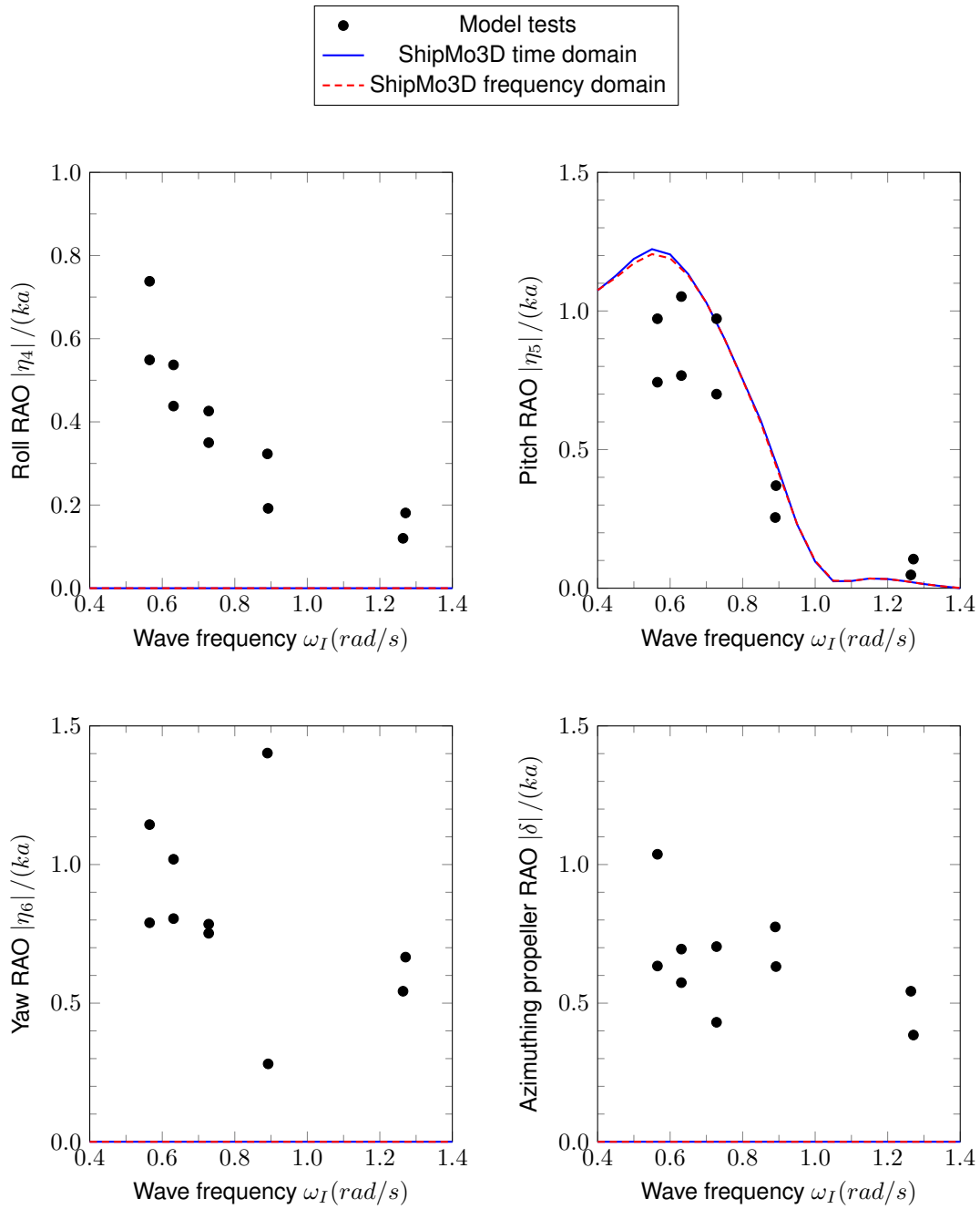


Figure 41: R/V Melville motions in regular seas, wave steepness $H/\lambda = 1/60$, ship speed $U = 12$ knots, head seas (relative sea direction $\beta_s = 180$ degrees).

6.4 R/V Melville Motions in Random Seas

Experiments and numerical predictions were performed for R/V Melville in long-crested random seas with parameters given in Table 30. Figures 42 to 47 show generally good agreement between experimental and predicted motions for roll and pitch. Experimental values for yaw motions and azimuthing propeller steering angles are much greater than predictions, possibly due to high steering angles by the human pilot.

Table 30: *Irregular wave sea states and full scale wave parameters.*

Sea State	Significant wave height	Peak wave period
	H_s	T_p
3	0.9 m	7.5 s
4	1.9 m	8.8 s
5	3.2 m	9.7 s

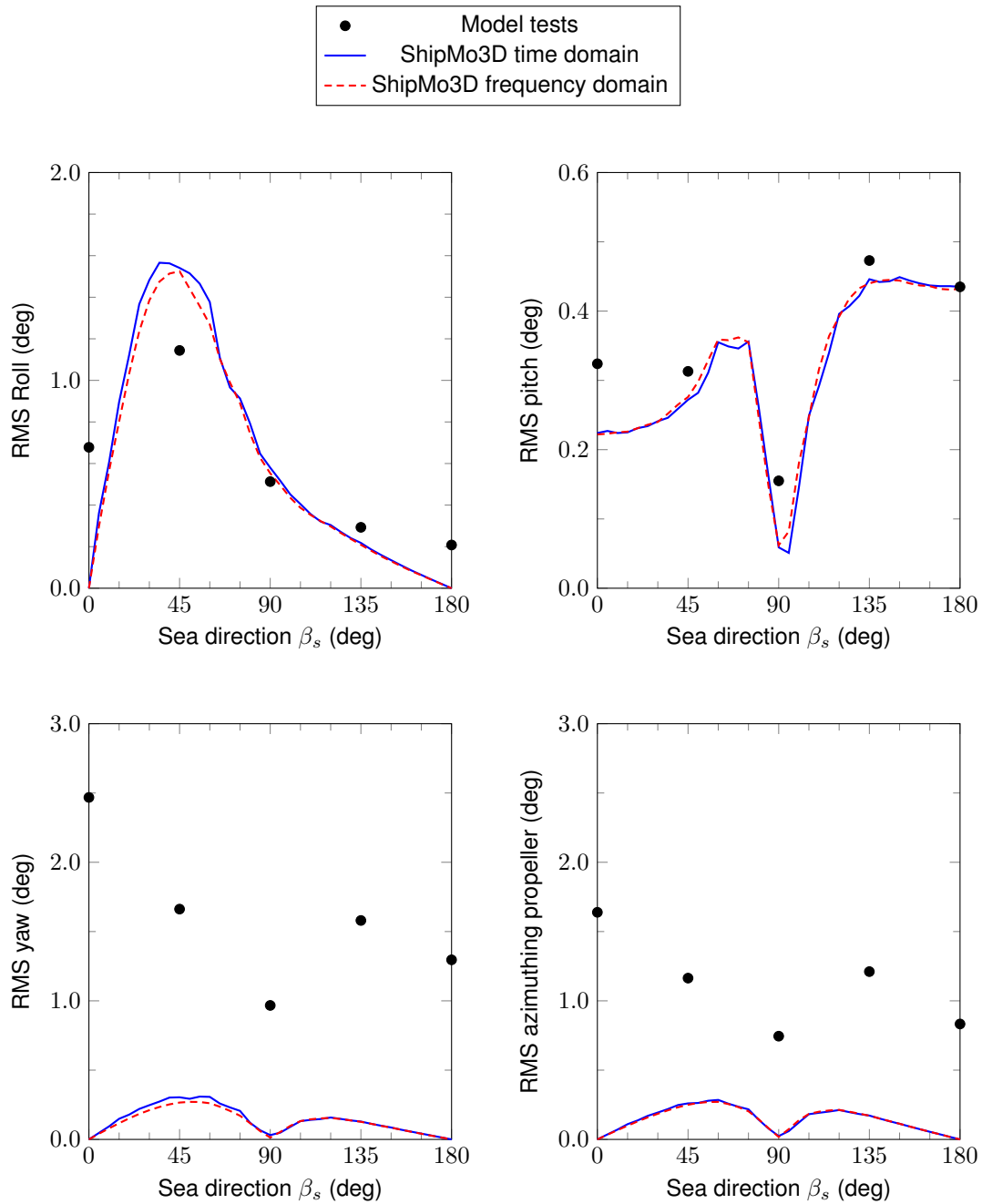


Figure 42: *R/V Melville motions in random seas, Sea State 3, ship speed $U = 8$ knots.*

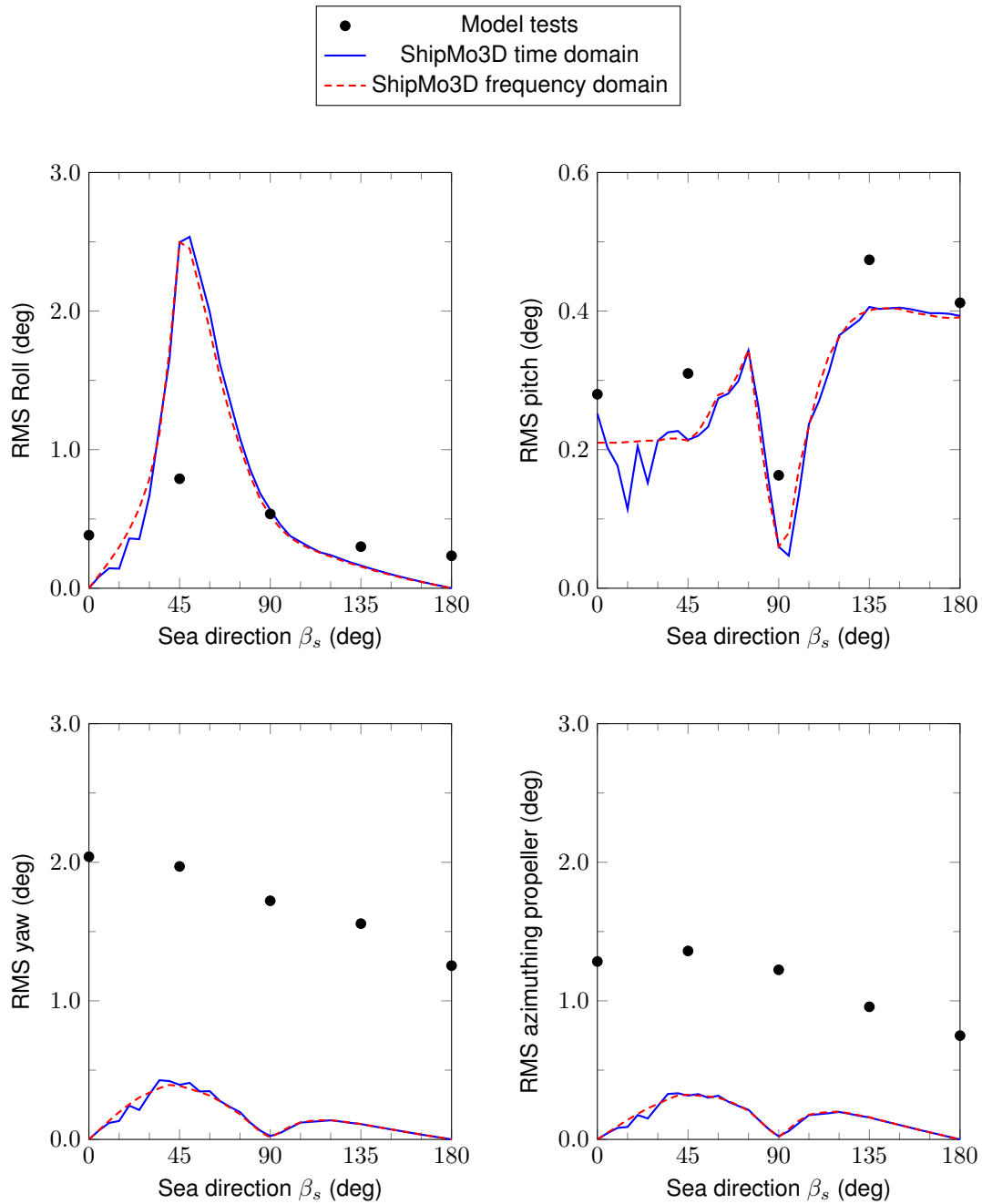


Figure 43: R/V Melville motions in random seas, Sea State 3, ship speed $U = 12$ knots.

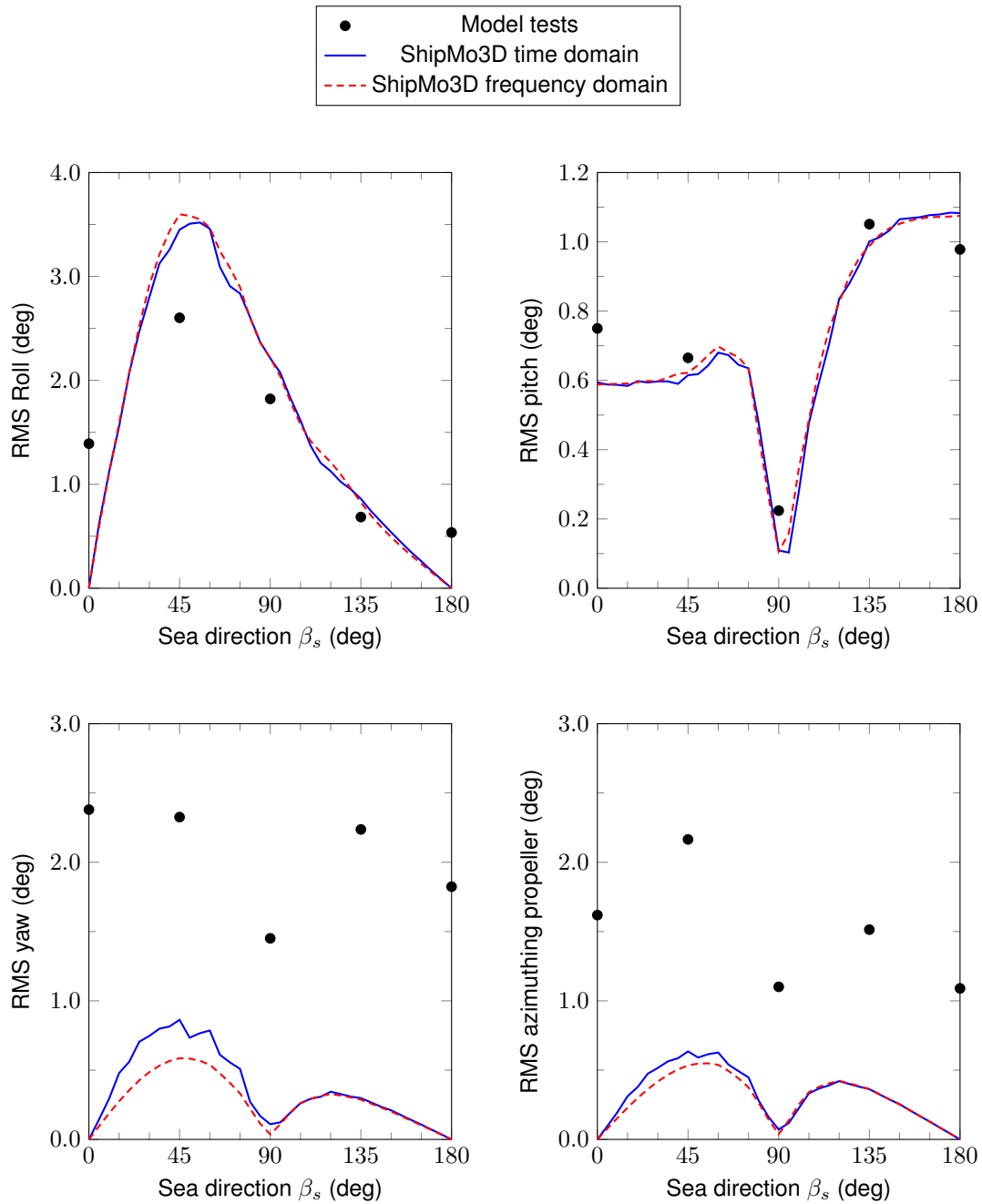


Figure 44: R/V Melville motions in random seas, Sea State 4, ship speed $U = 8$ knots.

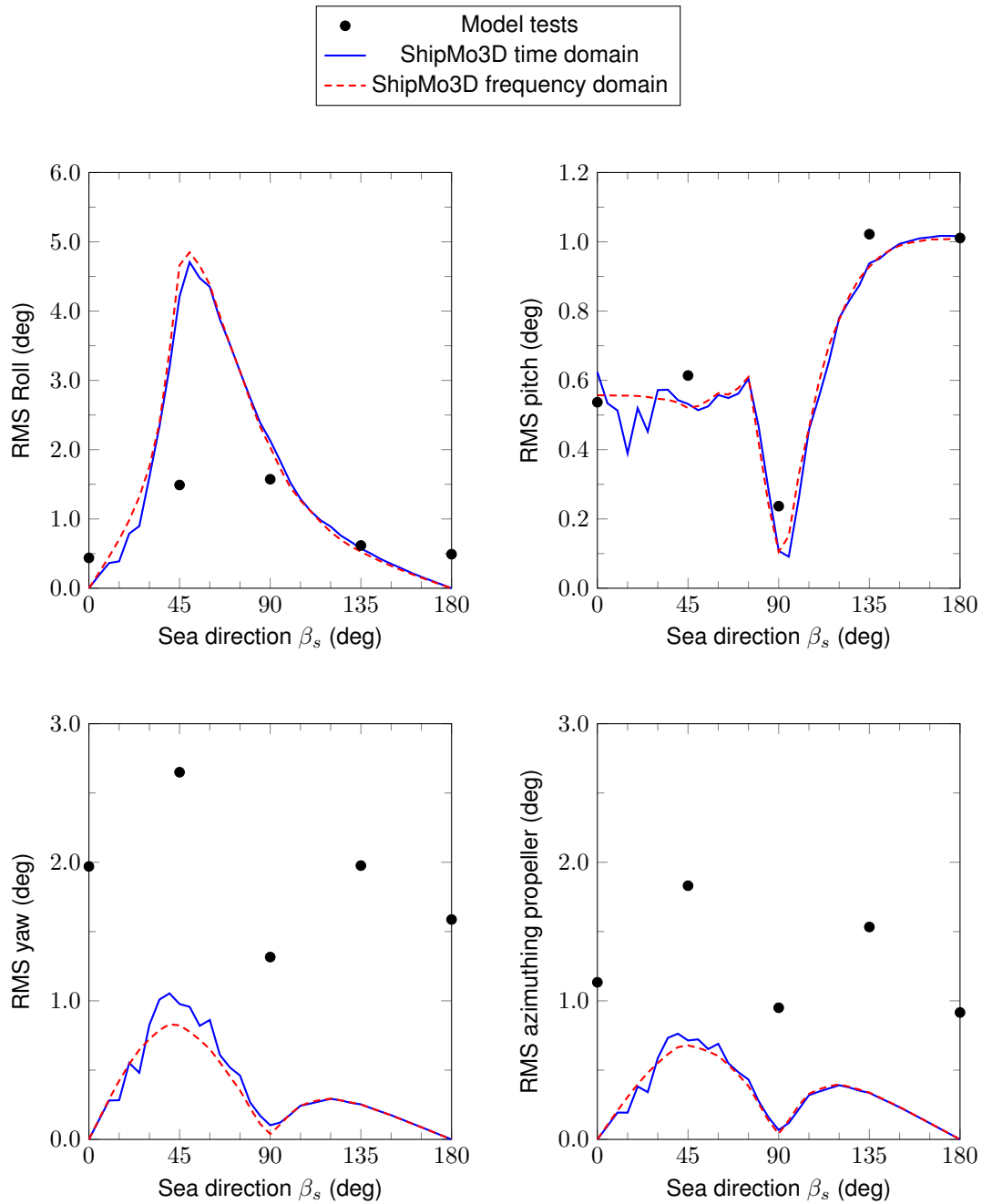


Figure 45: R/V Melville motions in random seas, Sea State 4, ship speed $U = 12$ knots.

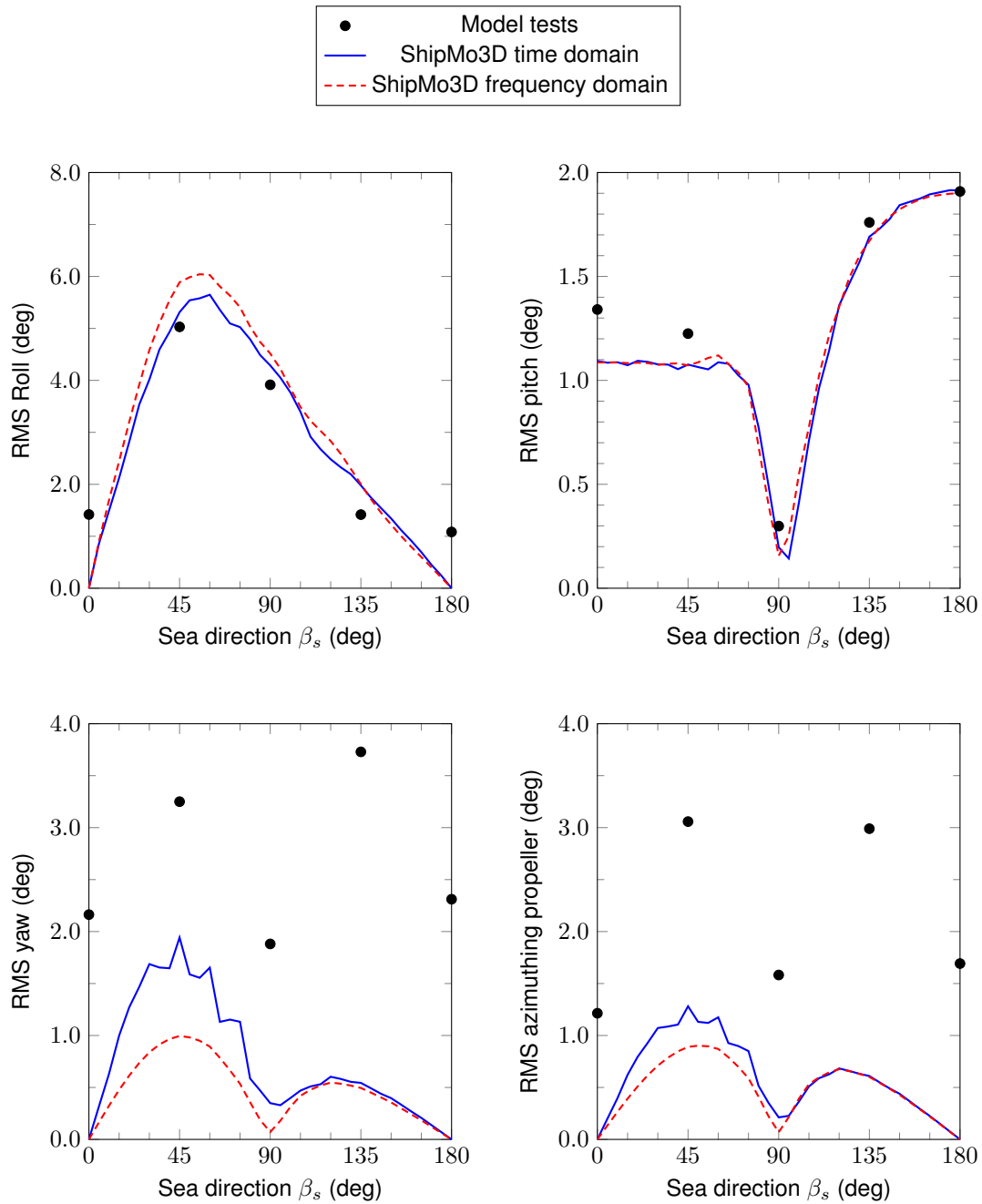


Figure 46: *R/V Melville motions in random seas, Sea State 5, ship speed $U = 8$ knots.*

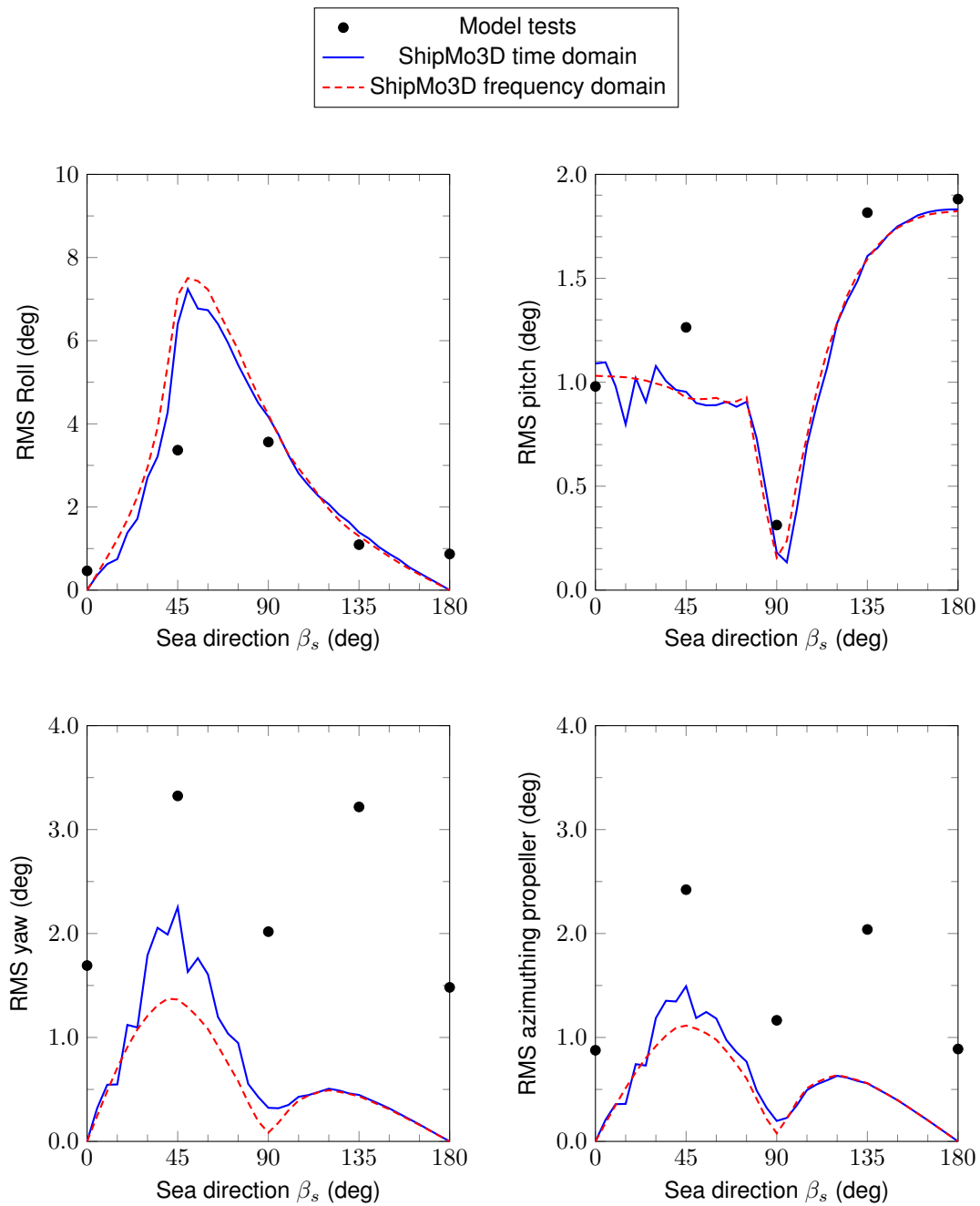


Figure 47: R/V Melville motions in random seas, Sea State 5, ship speed $U = 12$ knots.

7 Comparisons of Numerical Predictions and Experimental Results for Esso Osaka Turning Circles

Manoeuvring validation for ShipMo3D has been limited to full-scale trials data for the tanker Esso Osaka [17]. It has been the subject of many manoeuvring validation studies, as discussed by a specialist committee of the 2002 International Towing Tank Conference [36]. Table 31 gives particulars for the Esso Osaka. The ship includes a single rudder with a span of 13.85 m and chord length of 9.0 m, and a single propeller with a diameter of 9.1 m.

Table 31: Main particulars for the Esso Osaka during manoeuvring trials.

Length L (between perpendiculars)	325 m
Beam B	53 m
Midships draft T_{mid}	21.73 m
Trim by stern t_{stern}	0.0 m
Displacement Δ	319,400 tonnes
Longitudinal CG forward of midship	10.3 m

7.1 ShipMo3D Model of Esso Osaka

Figure 48 shows the ShipMo3D model of the Esso Osaka. Due to lack of available data, some of the input parameters for the Esso Osaka had to be estimated. Resistance coefficients were taken from the Series 60 hull with $C_B = 0.80$ [37], which has geometric properties very similar to the Esso Osaka. Based on data given in Reference [26], the wake fraction w_{prop} was estimated to be 0.352 and the thrust deduction coefficient t_{prop} was estimated to be 0.2. The variation of propeller thrust coefficient with advance ratio was based on a representative curve from Reference [26] with a minor correction factor such that a speed of 10 knots was obtained for a propeller speed of 51 RPM, as reported by Crane [17]. The rudder-propeller interaction coefficient was estimated to be 0.66 based on the ratio of the propeller diameter to the rudder span. The rudder flow straightening coefficient was estimated to be 0.4 based on data given in Reference [36]. Hull maneuvering coefficients were determined using experimental values presented in Reference [36], with Reference [6] giving details on conversion of the experimental values to ShipMo3D values.

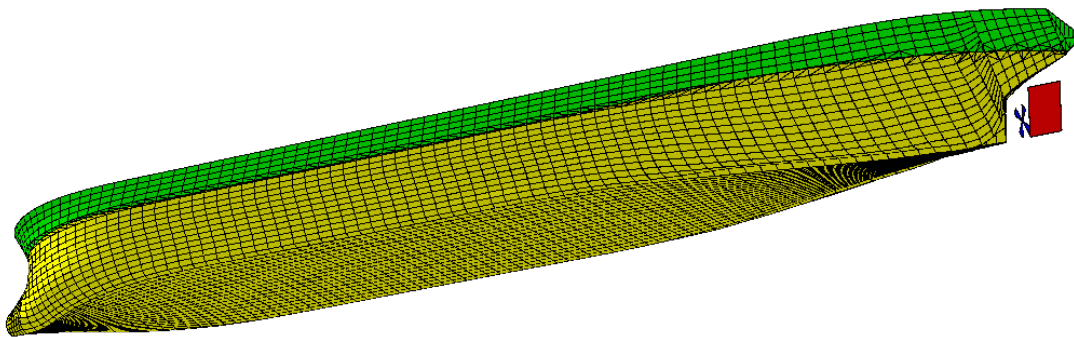


Figure 48: ShipMo3D model for Esso Osaka.

7.2 Comparisons of Numerical Predictions and Experimental Results for Esso Osaka Turning Circles

Table 32 and Figures 49 to 54 show results for turning circles at 10 knots and 7.7 knots. The results from sea trials given in Table 32 are nominal values based on the available sea trial data. Agreement between ShipMo3D predictions and trials results is generally good. For observed data, there is more scatter for the data at the lower initial speed of 7.7 knots. This increased scatter is likely due to the ship being more susceptible to environmental forces at the lower ship speed. The predicted turning circle parameters in Table 32 are within 16 percent of measured values. Note that a time of 1500 s was selected for comparing ship speed and heading rate in the latter part of the turn because the sea trial data appears to have greater scatter at later times.

It should be noted that the good agreement between the current predictions and trials data is due partly to the availability of experimentally determined hull maneuvering coefficients. Predictions in Reference [6] give poorer agreement when using hull maneuvering coefficients estimated using the regression approach of Inoue et al. [28]. However, the current predictions serve the purpose of validating ShipMo3D predictions using the best available input data.

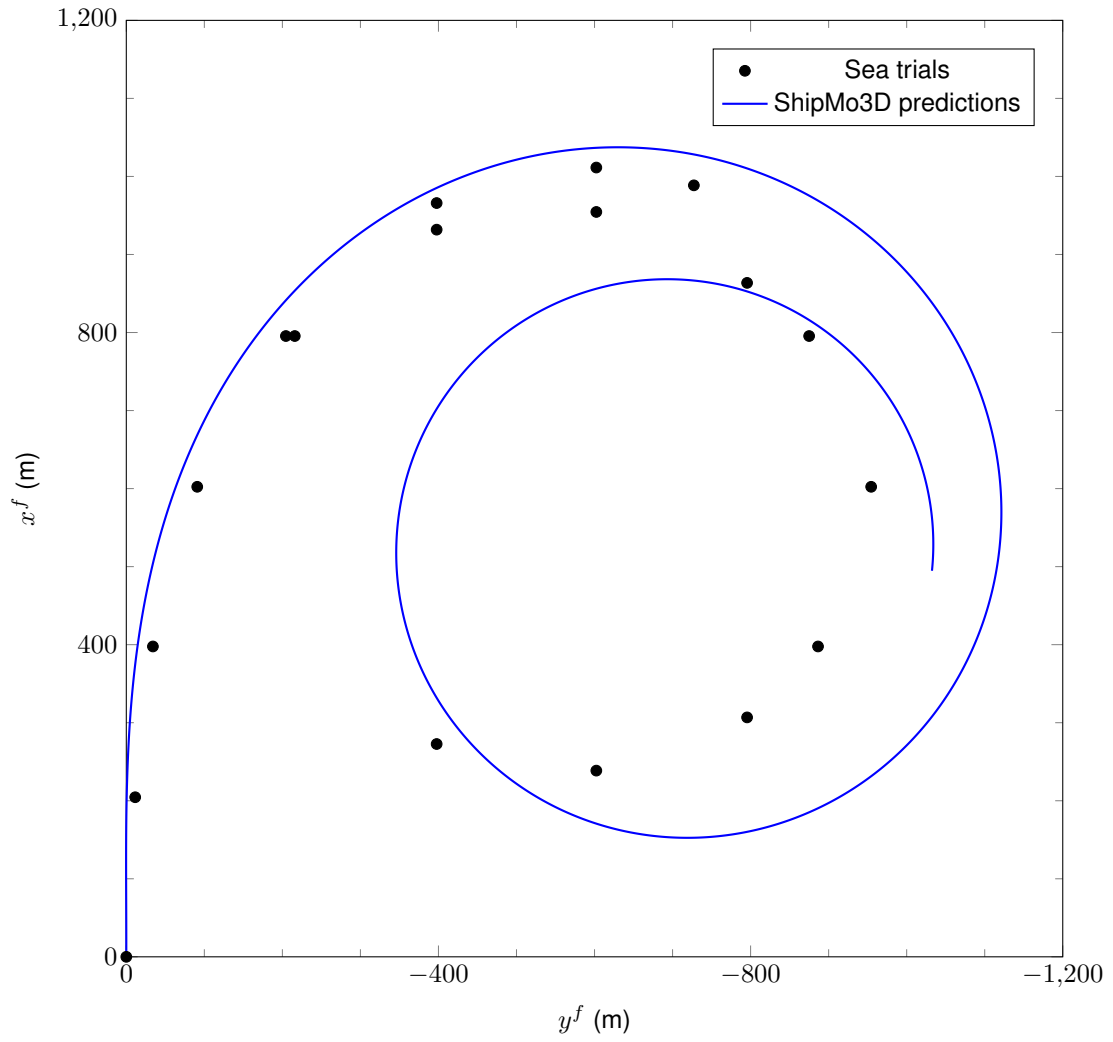


Figure 49: Esso Osaka trajectory during turning circle, initial speed of 10 knots.

Table 32: Turning circle parameters for Esso Osaka.

	Sea trials	ShipMo3D
Initial ship speed of 10 knots		
Tactical diameter	1011 m	1097 m
Speed V at 1500 s	3.3 knots	2.9 knots
Absolute heading rate $ \dot{\chi} $ at 1500 s	0.29 deg/s	0.25 deg/s
Initial ship speed of 7.7 knots		
Tactical diameter	1006 m	1122 m
Speed V at 1500 s	2.2 knots	2.5 knots
Absolute heading rate $ \dot{\chi} $ at 1500 s	0.18 deg/s	0.20 deg/s

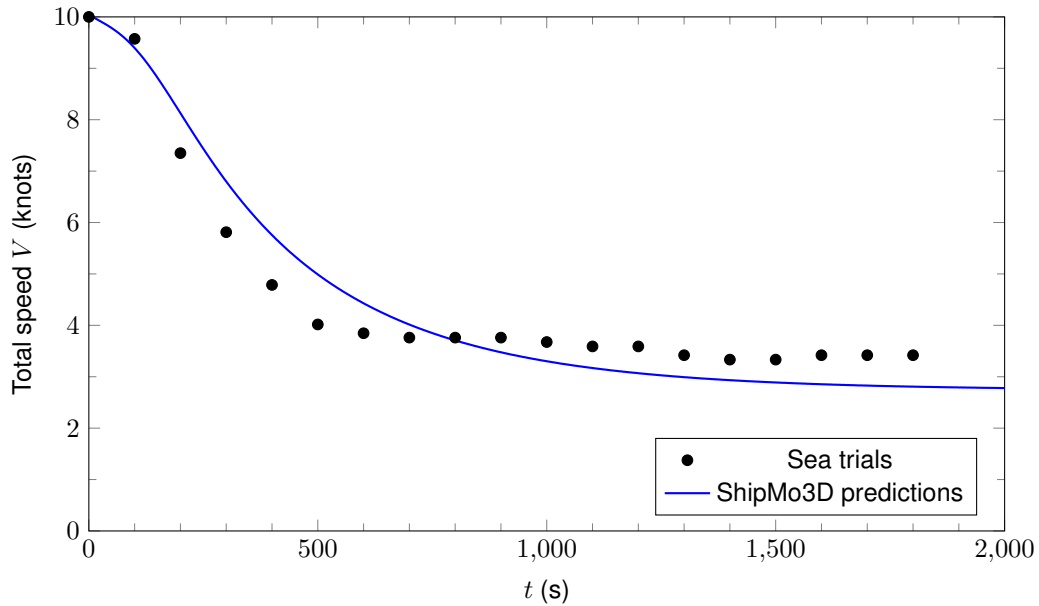


Figure 50: Esso Osaka total speed during turning circle, initial speed of 10 knots.

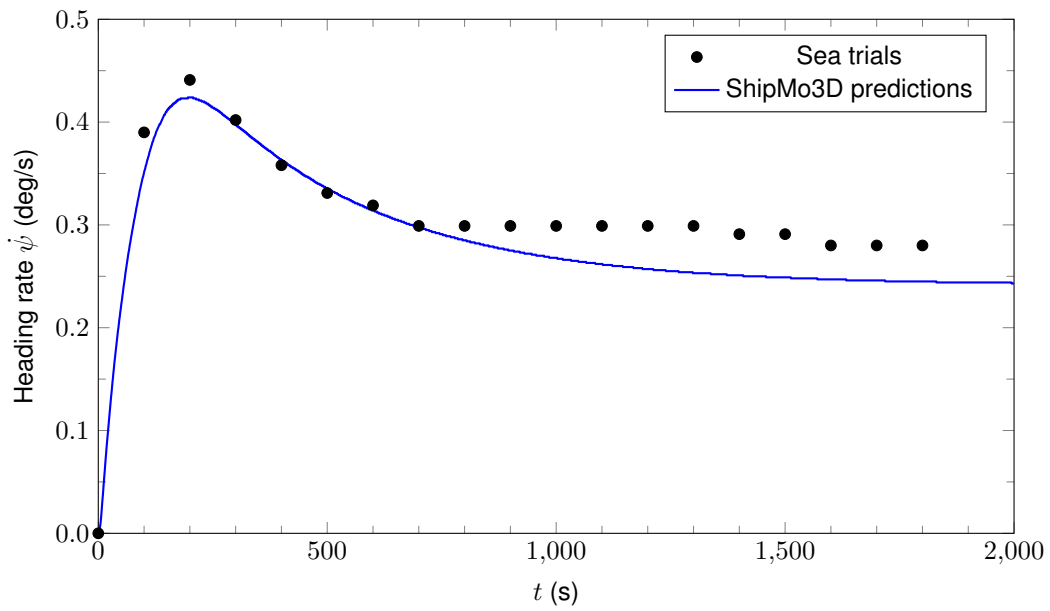


Figure 51: Esso Osaka heading rate during turning circle, initial speed of 10 knots.

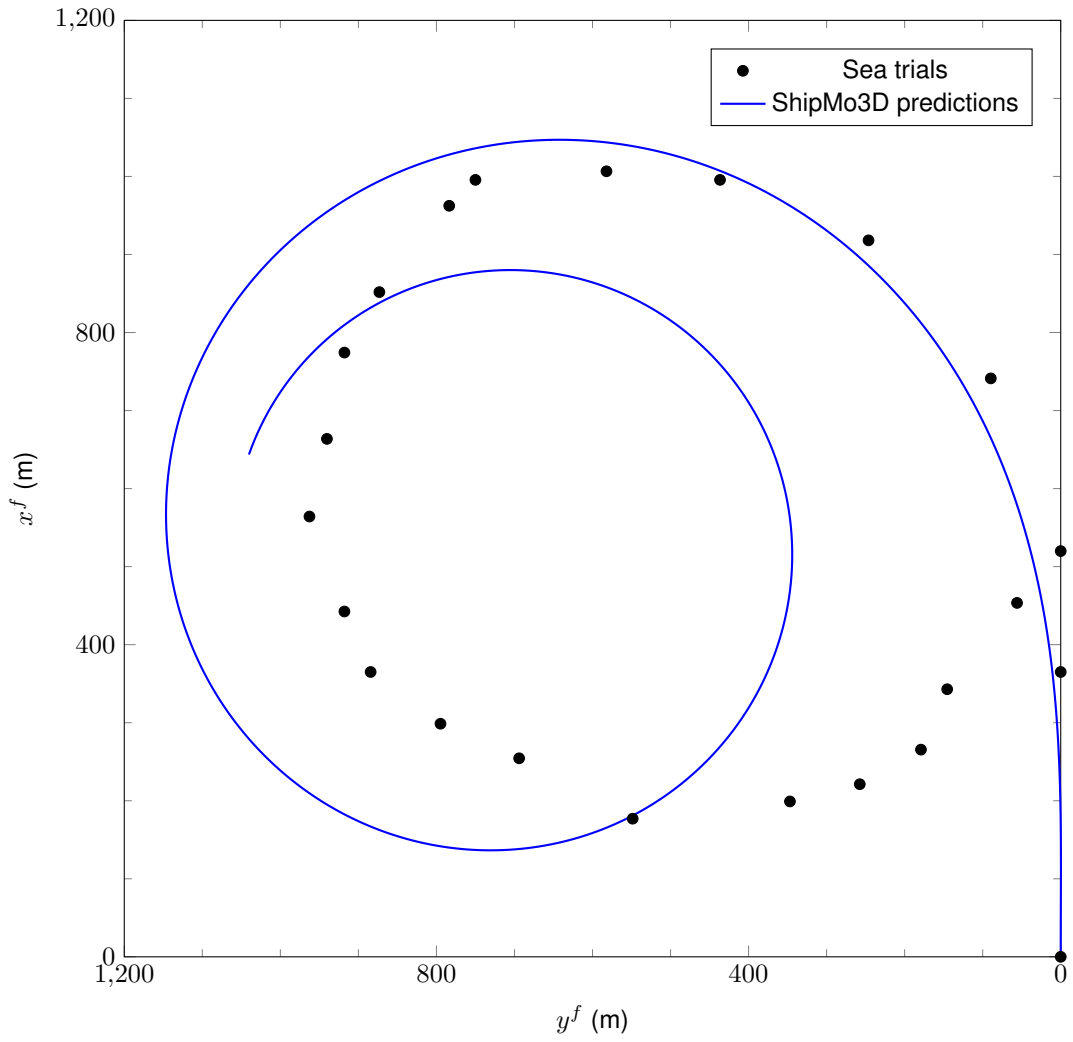


Figure 52: Esso Osaka trajectory during turning circle, initial speed of 7.7 knots.

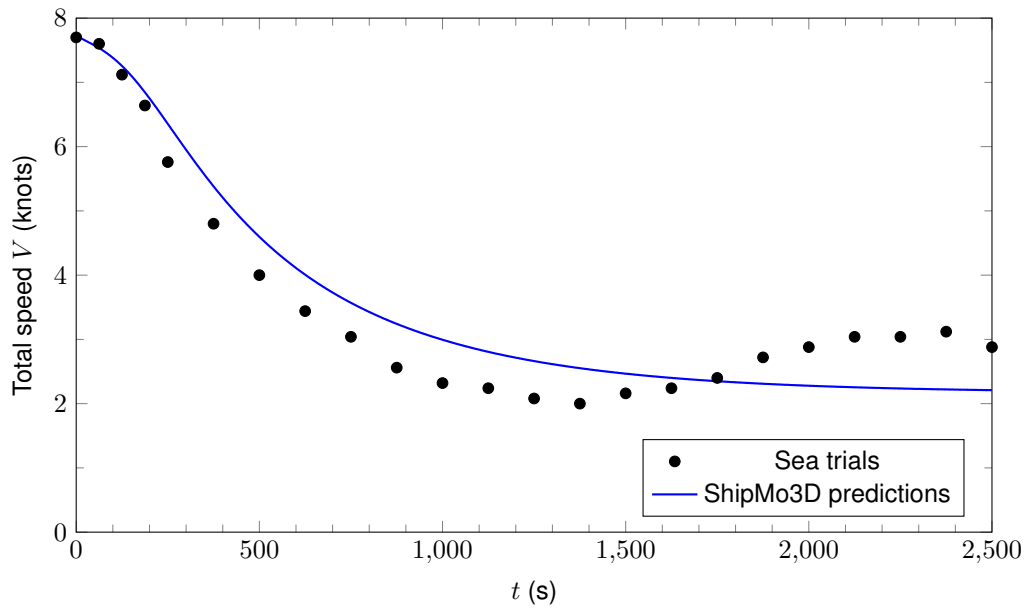


Figure 53: Esso Osaka total speed during turning circle, initial speed of 7.7 knots.

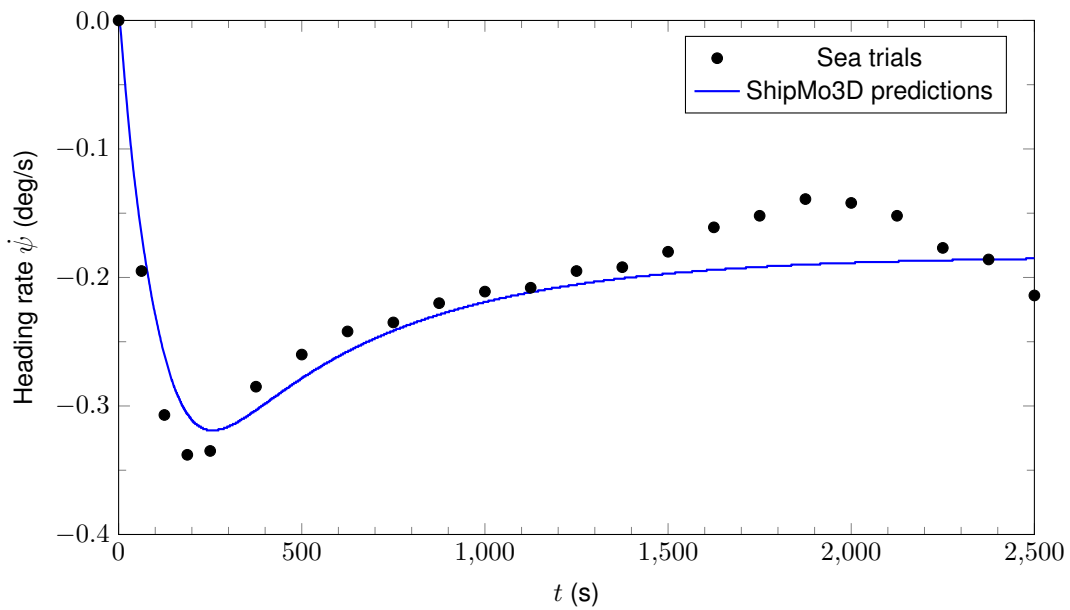


Figure 54: Esso Osaka heading rate during turning circle, initial speed of 7.7 knots.

8 Wave-induced Roll Motions of a Barge with Sloshing Tanks

ShipMo3D can model sloshing in tanks, which can occur when a ship is transporting liquid cargo or when flume tanks are used for roll stabilization. The tank sloshing modelling is based on Malenica et al. [38], with the ShipMo3D implementation described in Reference [39].

Roll motion predictions including sloshing have been validated using experimental data for a barge model tested by Molin et al. [40]. Table 33 gives the dimensions of the barge. Two sloshing tanks were placed on the deck of the barge, and Table 34 gives the dimensions for each tank. The tank dimensions in Table 34 are given using the ShipMo3D conventions for length and width, with tank length being along the ship longitudinal axis and tank width being along the ship lateral axis (Molin et al. use the opposite convention for tank length and width). Table 35 gives the inertial properties of the barge, which are required as inputs to ShipMo3D.

Table 33: Barge dimensions.

Length, L	3.0 m
Beam, B	1.0 m
Total depth	0.267 m
Draft, T	0.108 m

Table 34: Barge sloshing tank dimensions.

Length, L_{tank}	0.25 m
Width, w_{tank}	0.80 m
Total height, h_{tank}	0.267 m
Fluid height, h_{fluid}	0.19 m
Height above baseline, z_{bl}^{tank}	0.30 m

Table 35: Inertial properties of barge with two sloshing tanks with fluid height of 0.19 m.

	Mass	KG	r_{xx} (wrt own KG)
Barge	169 kg	0.240 m	0.414 m
Tanks	76 kg	0.395 m	0.237 m
Ballast masses	40 kg	0.280 m	0.35 m
Total	285 kg	0.287 m	0.372 m

8.1 ShipMo3D Model of Barge and Sloshing Tanks

Models of the barge including sloshing tanks were developed for validation. Roll motion predictions are sensitive to the modelling of viscous forces. Molin et al. indicate that the following roll damping equation can be used to model the observed experimental behaviour of the barge:

$$F_4^{hull-eddy} = -\frac{1}{2} \rho C_d B^4 L |\dot{\eta}_4| \dot{\eta}_4 \quad (6)$$

where $F_4^{hull-eddy}$ is the hull eddy damping force, C_d is the drag coefficient, and $\dot{\eta}_4$ is the ship roll velocity. ShipMo3D uses a similar approach but with different dimensional terms as follows (see Reference [4]):

$$F_4^{hull-eddy} = -\frac{1}{4} \rho C_{eddy}^{hull} \int_{S_{hull}} n_4^2 \sqrt{y^2 + z^2} dS |\dot{\eta}_4| \dot{\eta}_4 \quad (7)$$

Molin et al. assign the drag coefficient C_d a value of 0.2 based on experimental observations. Analysis of the hull geometry gives an associated value of 8.6 for the ShipMo3D input coefficient C_{eddy}^{hull} .

8.2 Validation Results for Barge with Sloshing Tanks

Figure 55 compares predicted frequency domain and experimental roll RAOs for the barge in a seaway modelled by a JONSWAP spectrum with significant wave height H_s of 0.066 m, peak wave period T_p of 1.6 s, and peak enhancement factor γ of 2.0. The experiments were conducted in finite water depth of 3 m, while the ShipMo3D predictions are in water of infinite depth; thus, the data comparison is given for encounter frequencies of 3 rad/s and greater, for which the assumption of deep water is applicable (water depth/wavelength > 0.5). The numerical predictions compare favourably with the experimental data. The water in the sloshing tanks is 27 percent of the total mass and is located high relative to the total centre of gravity; thus, sloshing likely has a large influence on the total roll motion.

Additional ShipMo3D predictions were made in regular waves of steepness $H/\lambda = 0.0165$, which is based on the significant wave height of 0.066 m and the peak wave period of

1.6 s for the random wave experiments. Figure 56 shows that the ShipMo3D time domain predictions give good agreement with the frequency domain predictions, suggesting correct implementation in the time domain.

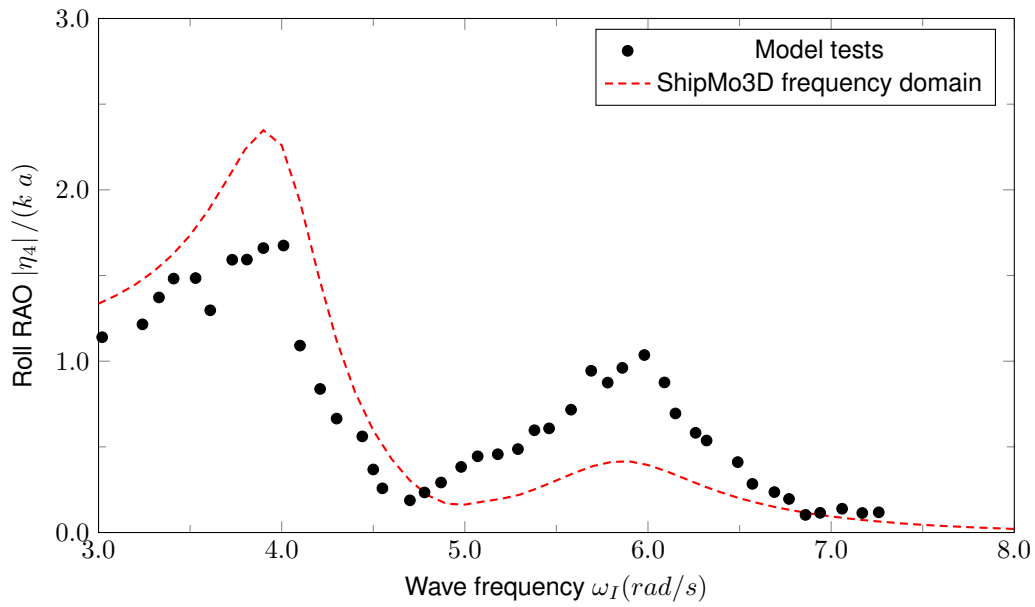


Figure 55: Barge with sloshing tanks roll RAOs in beam seas with JONSWAP spectrum, $H_s = 0.066$ m, $T_p = 1.6$ s, $\gamma = 2.0$.

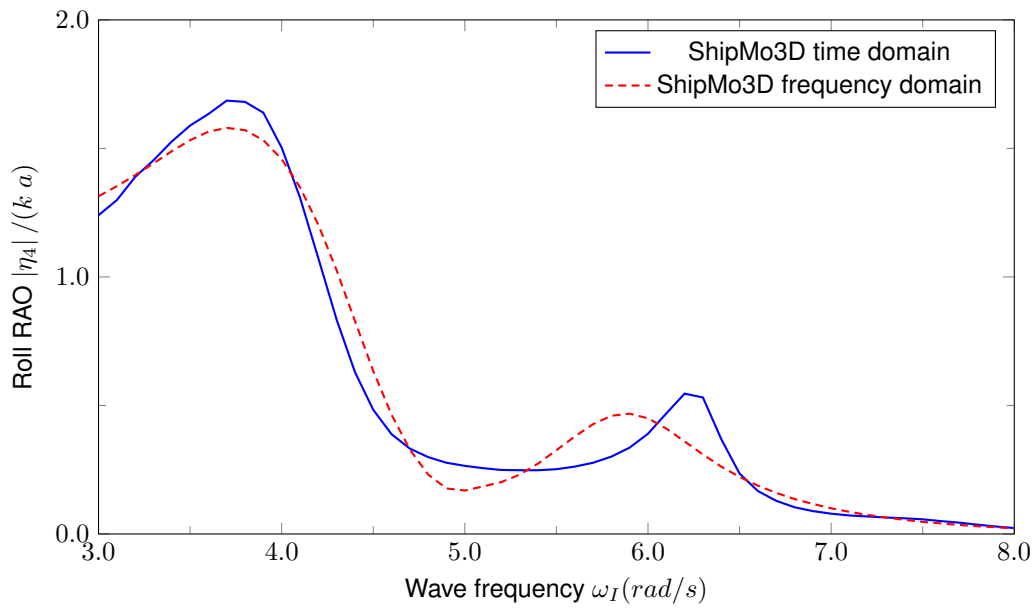


Figure 56: Barge with sloshing tanks roll RAOs in regular beam seas, wave steepness $H/\lambda = 0.0165$.

9 Verification for a Frigate with Stabilizer Fins for Roll Stabilization

Stabilizer fin modelling was verified through motion computations in the frequency and time domains for a generic frigate with and without stabilizer fins. The generic frigate is the standard ShipMo3D example, with particulars given in Table 36. Table 37 gives properties for the stabilizer fins added to the generic frigate, and Figure 57 shows the generic frigate with stabilizer fins.

Table 36: Main particulars for generic frigate.

Length L	120.0 m
Beam B	14.1 m
Midships draft T_{mid}	4.2 m
Trim by stern t_{stern}	0.0 m
Displacement Δ	3719 tonnes
Vertical centre of gravity \overline{KG}	6.0 m
Metacentric height \overline{GM}	1.4 m
Roll radius of gyration r_{xx}	4.8 m
Pitch radius of gyration r_{yy}	30.0 m
Natural roll period	9.0 s

Table 37: Stabilizer fin properties for generic frigate.

Station	10.0
Span s	2.0 m
Chord length c	1.0 m
Roll velocity gain	-3.0 deg/(deg/s)
Maximum deflection	35 deg
Maximum velocity	20 deg/s

Figures 58 and 59 show roll motions and stabilizer fin deflections for the generic frigate travelling at 10 knots in regular beam seas with a low wave steepness H/λ of 0.01. The results show expected reduction in roll motions by the stabilizer fins. Predictions in the time and frequency domains show close agreement.

Figures 60 and 61 show roll motions and stabilizer fin deflections for the generic frigate travelling at 10 knots at various headings in Sea State 5, which is modelled by unidirectional waves with significant wave height of 3.25 m and peak wave period of 9.7 s. The stabilizer fins provide generally reduced roll motions, as expected. Predictions in the frequency and time

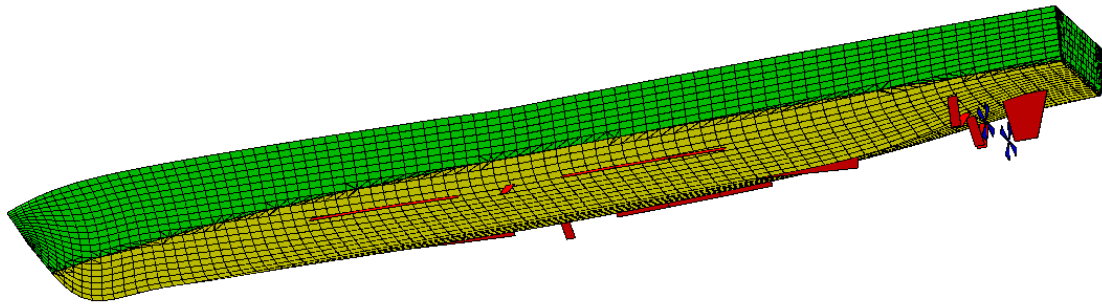


Figure 57: *ShipMo3D model of generic frigate with stabilizer fins.*

domains are in general agreement, with differences likely due to more detailed modelling of appendage forces for time domain predictions. The smaller stabilizer fin deflections in the time domain Figure 61 are consistent with the smaller roll predictions in Figure 60.

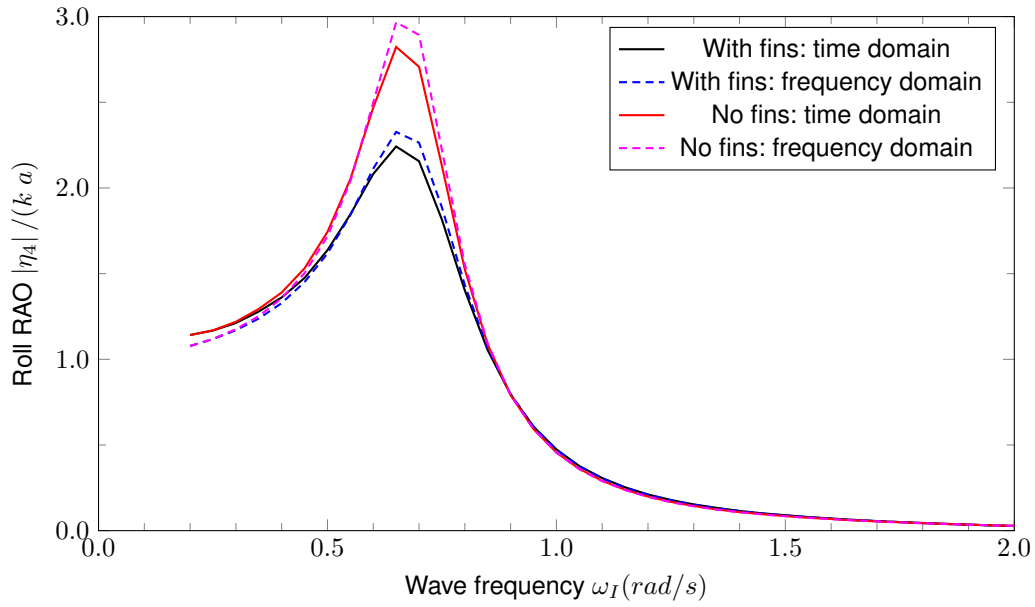


Figure 58: Roll amplitude versus wave frequency, generic frigate at 10 knots in regular waves, beam seas with steepness H/λ of 0.01.

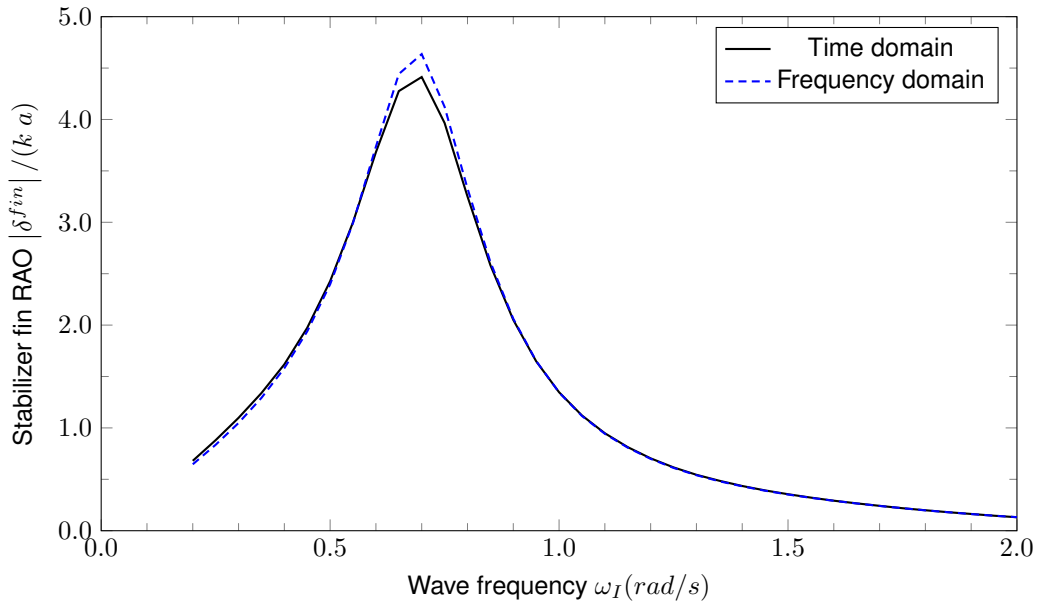


Figure 59: Stabilizer fin deflection RAO versus wave frequency, generic frigate at 10 knots in regular waves, beam seas with steepness H/λ of 0.01.

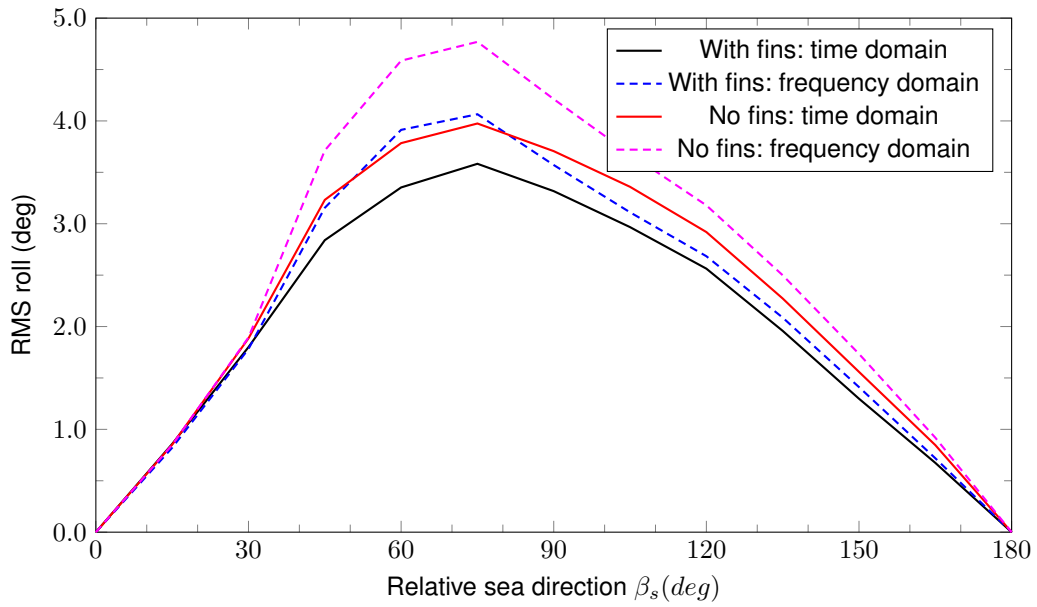


Figure 60: RMS roll versus relative sea direction, generic frigate at 10 knots in Sea State 5.

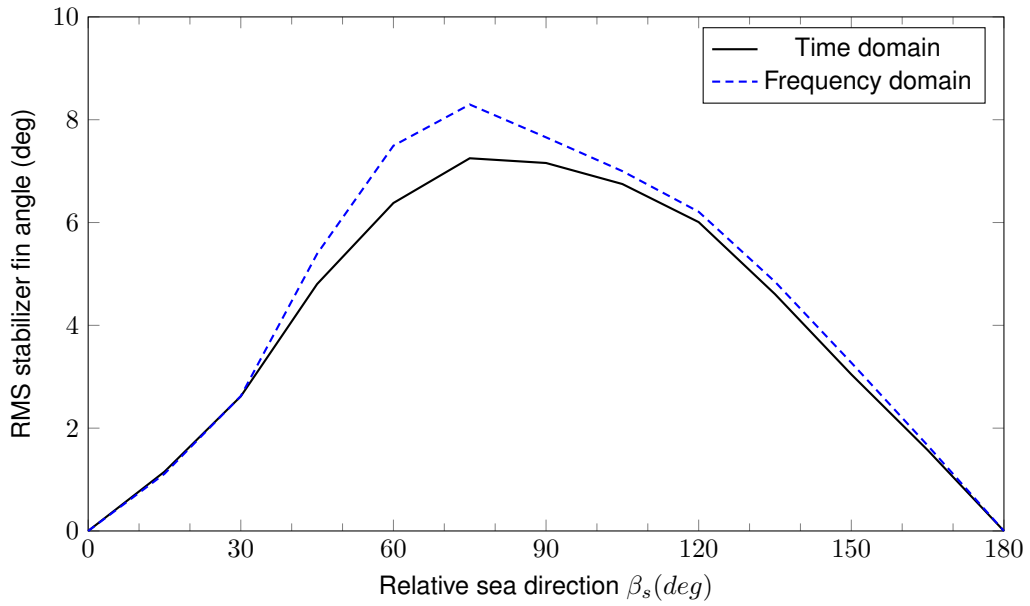


Figure 61: RMS stabilizer fin deflection versus sea direction, generic frigate at 10 knots in Sea State 5.

10 Verification for a Frigate with a U-tube Tank for Roll Stabilization

U-tube tank modelling was verified through motion computations in the frequency and time domains for a generic frigate with and without a U-tube tank. The generic frigate is the standard ShipMo3D example, with particulars given in Table 36. Table 38 gives properties for the U-tube tank added to the generic frigate, and Figure 62 shows a diagram of the U-tube tank in the generic frigate.

Table 38: Properties of example U-tube tank for generic frigate.

Fluid density (fresh water), ρ_{tank}	1000 kg/m ³
Station (AP at station 20)	10
Length L_{tank}	7.0 m
Duct width w_d	8.0 m
Reservoir width w_r	2.0 m
Height of bottom above baseline z_{bl}^{tank}	3.0 m
Total height h_t	6.0 m
Duct height h_d	0.6 m
Fluid height h_{fluid}	3.3 m
Fluid mass m_{tank}	126 tonnes
Tank fluid frequency ω_{tau}	0.706 rad/s
Maximum fluid angle τ_{max}	28.4°
Effective change in metacentric height $\Delta \overline{GM}^{tank}$	-0.189 m

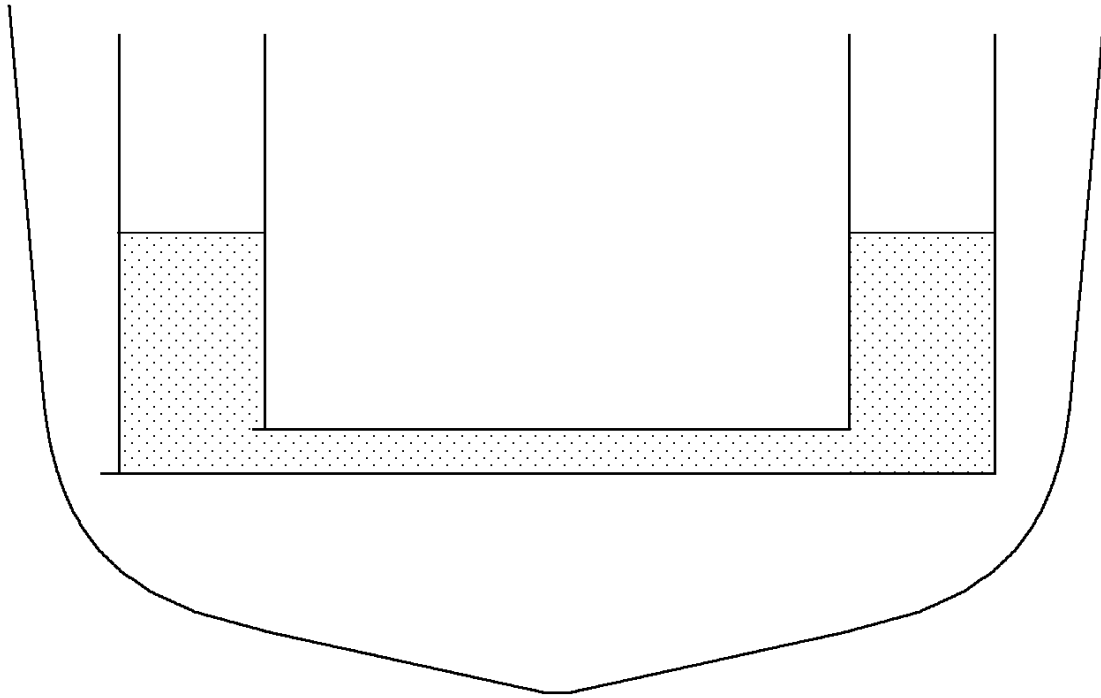


Figure 62: Example U-tube tank for generic frigate.

Figures 63 and 64 show ship roll motions and U-tube tank fluid displacements for the generic frigate at 10 knots in regular beam seas with wave steepness H/λ of 0.01. The numerical results show effective reduction of roll motions by the U-tube tank. Predictions in the frequency and time domains give excellent agreement. At low frequency, the U-tube fluid displacement approaches zero. This behaviour was investigated further by examining the U-tube tank model as described in Reference [41]. It was determined that ship sway acceleration and ship roll displacement effectively can cancel each other for excitation of the U-tube tank displacement at low wave frequencies in beam seas.

Note that the low frequency roll motions and U-tube tank displacements in Figures 63 and 64 are significantly lower than for the ShipMo3D Version 3 results presented in Reference [9]. The inclusion of wave excitation maneuvering forces in ShipMo3D Version 4.2 causes the differences with the Version 3 results, with the Version 4.2 results considered more realistic.

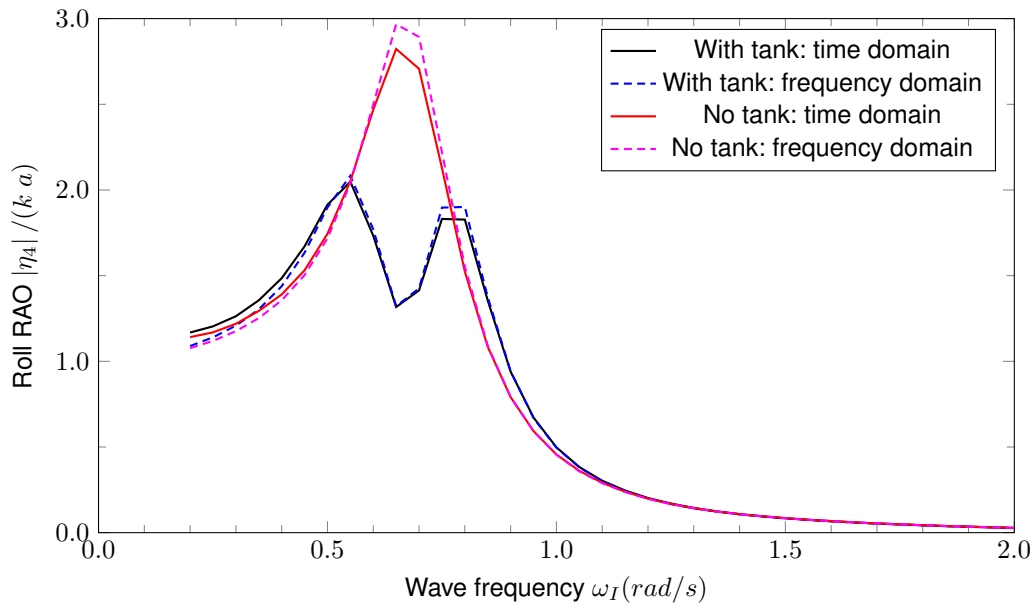


Figure 63: Roll amplitude versus wave frequency, generic frigate at 10 knots in regular waves, beam seas with steepness H/λ of 0.01.

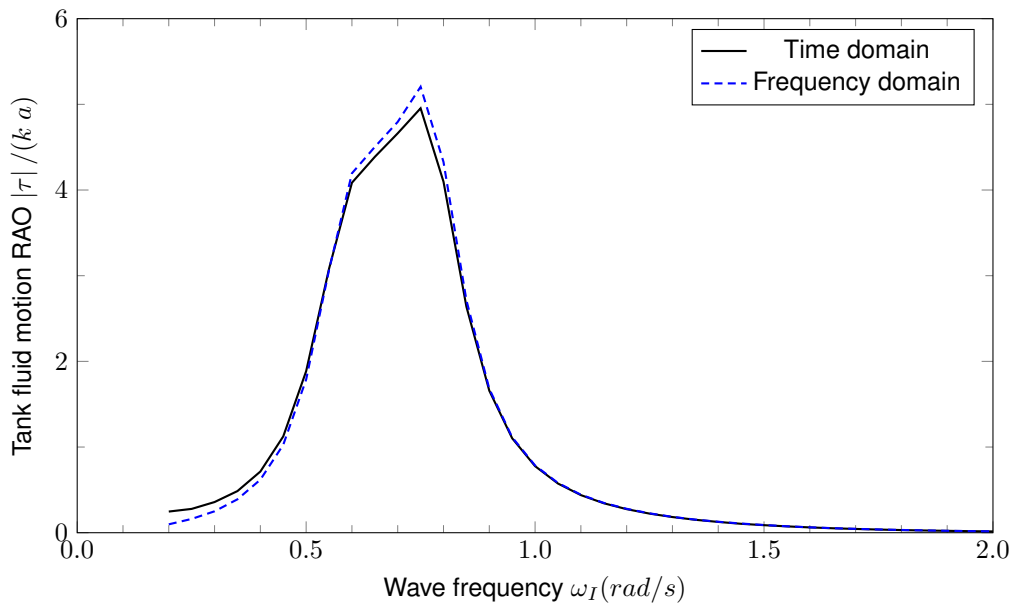


Figure 64: U-tube tank fluid displacement amplitude versus wave frequency, generic frigate at 10 knots in regular waves, beam seas with steepness H/λ of 0.01.

Figures 65 and 66 shows roll and U-tube tank fluid displacements for the generic frigate at 10 knots in Sea State 5. The U-tube tank provides reductions in roll motions, as expected. Time domain predictions give similar results to frequency domain predictions.

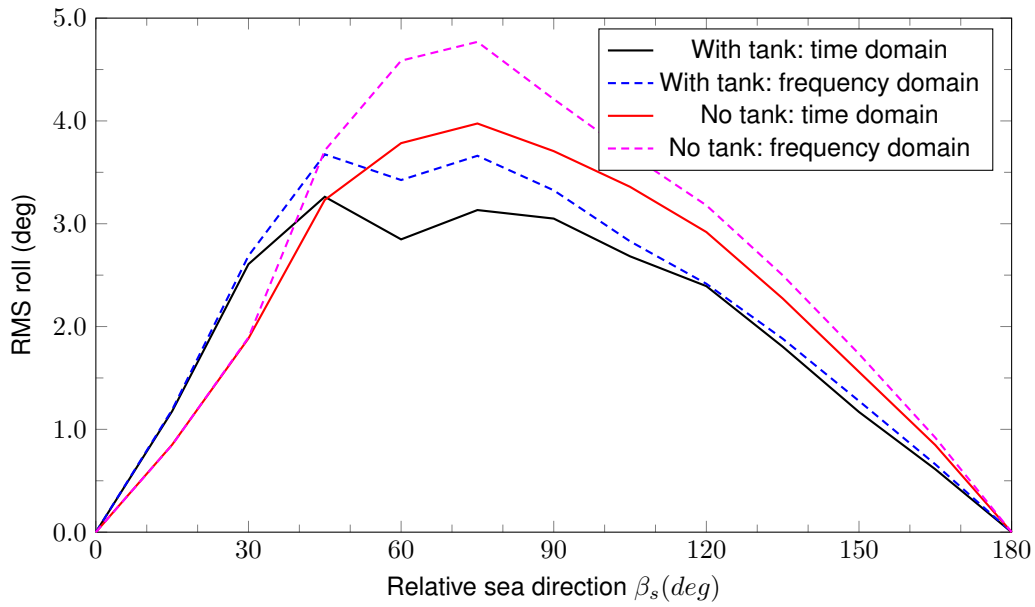


Figure 65: RMS roll versus relative sea direction, generic frigate at 10 knots in Sea State 5.

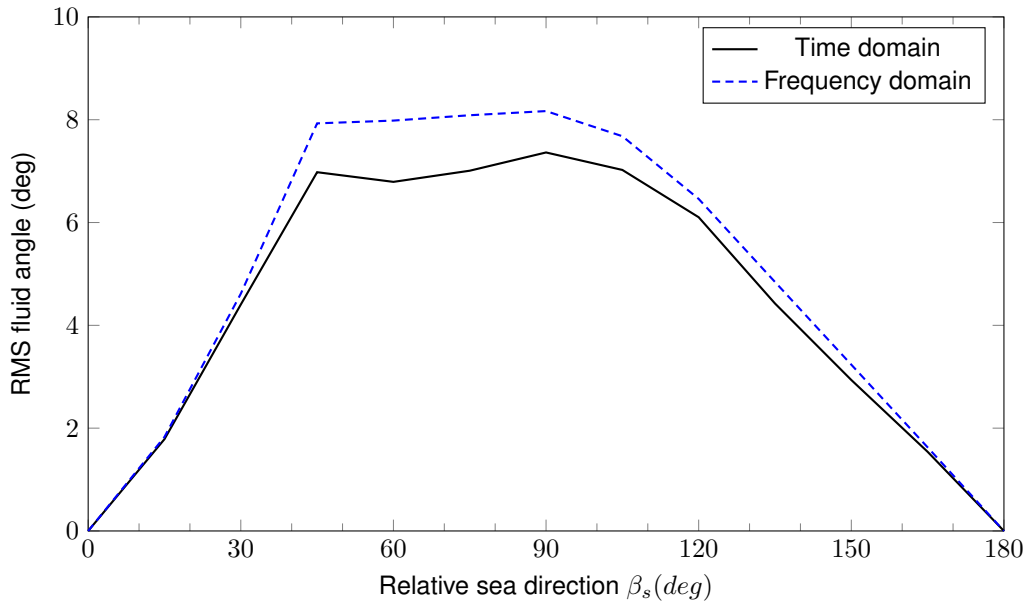


Figure 66: RMS U-tube tank fluid displacement angle versus sea direction, generic frigate at 10 knots in Sea State 5.

11 Verification of SM3DSeakeepSeawayFromRaos Motions in Random Seas Determined using Precomputed RAOs

The application SM3DSeakeepSeawayFromRaos can predict seakeeping in a seaway defined in earth-fixed axis using previously computed motion response amplitude operators (RAOs). SM3DSeakeepSeawayFromRaos is intended to give results very similar to SM3DSeakeepSeaway; however, SM3DSeakeepSeawayFromRaos runs much faster because it doesn't have to compute ship motion RAOs. SM3DSeakeepSeawayFromRaos can be very useful when many different combinations of ship speed and heading in a seaway need to be evaluated quickly, such as when providing operator guidance onboard a ship.

Figure 67 gives heave and roll motions for the generate frigate introduced in Section 9 travelling at 10 knots in Sea State 5 with short-crested seas. The heave from the two applications are identical. The small differences in roll motion from the two applications are expected and are caused by differences in the roll motion amplitudes used to evaluate the nonlinear roll damping.

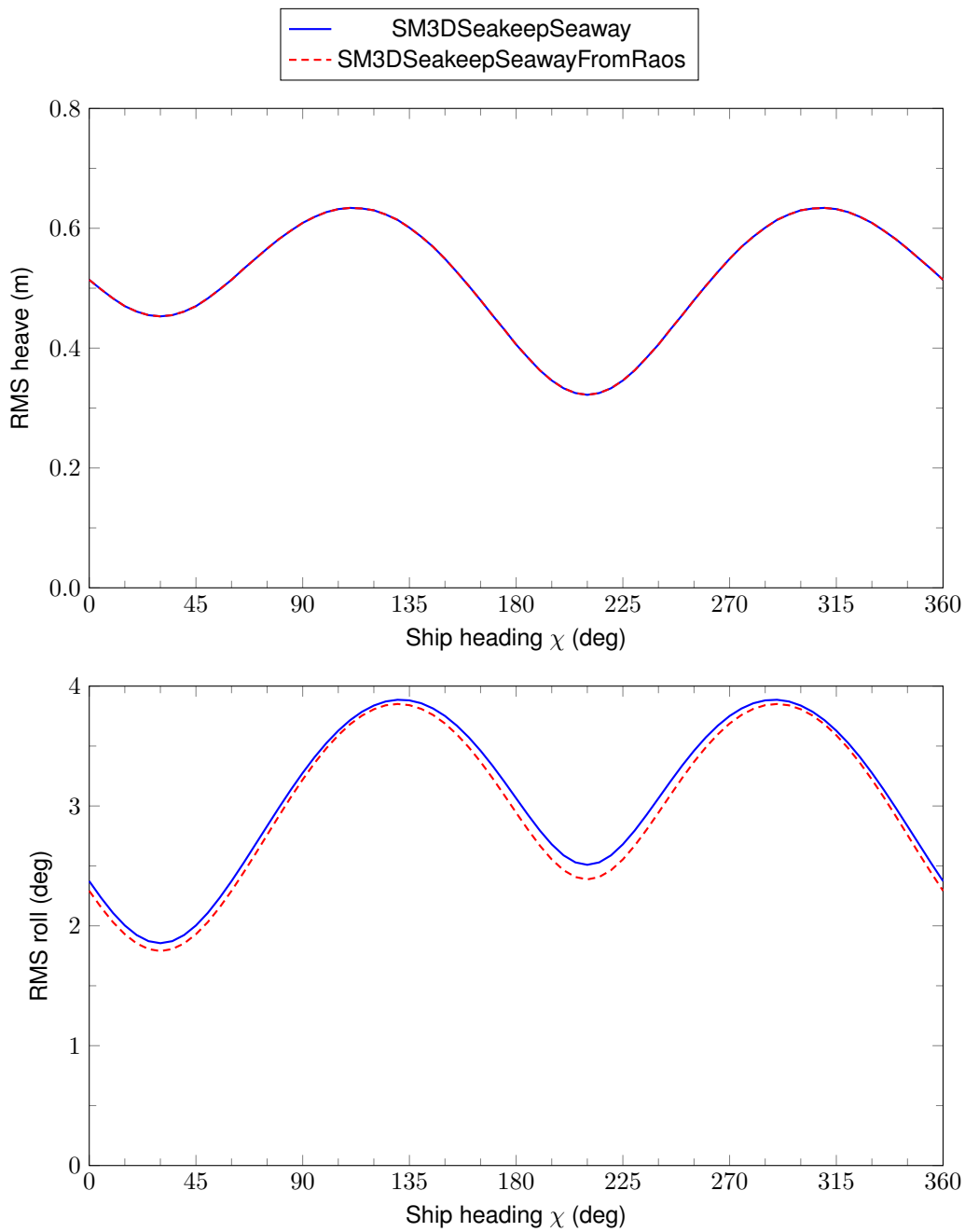


Figure 67: Frequency domain predictions of RMS heave and roll for generic frigate at 10 knots in Sea State 5, short-crested Bretschneider spectrum, mean wave heading 30 degrees, cosine-squared spreading angle 90 degrees.

12 Verification of SM3DTimeSeriesFromRaos Motions in Random Seas

The application SM3DTimeSeriesFromRaos computes ship motions in the time domain based on pre-computed ship motion RAOs. Motions for the generic frigate were computed using SM3DFreeMo and SM3DTimeSeriesFromRaos. The seaway was long-crested with heading (from) of 0 degrees, with a Bretschneider spectrum having a significant wave height H_s of 3.25 m and peak wave period T_p of 9.7 s. The ship was travelling at 20 knots at a heading of 30 degrees. To reduce transient force effects at the beginning of the time domain simulation with SM3DFreeMo, seaway component amplitudes were increased from 0 to full amplitude during the first 20 seconds. Figure 68 shows excellent agreement between the motions computed by SM3DFreeMo and SM3DTimeSeriesFromRaos.

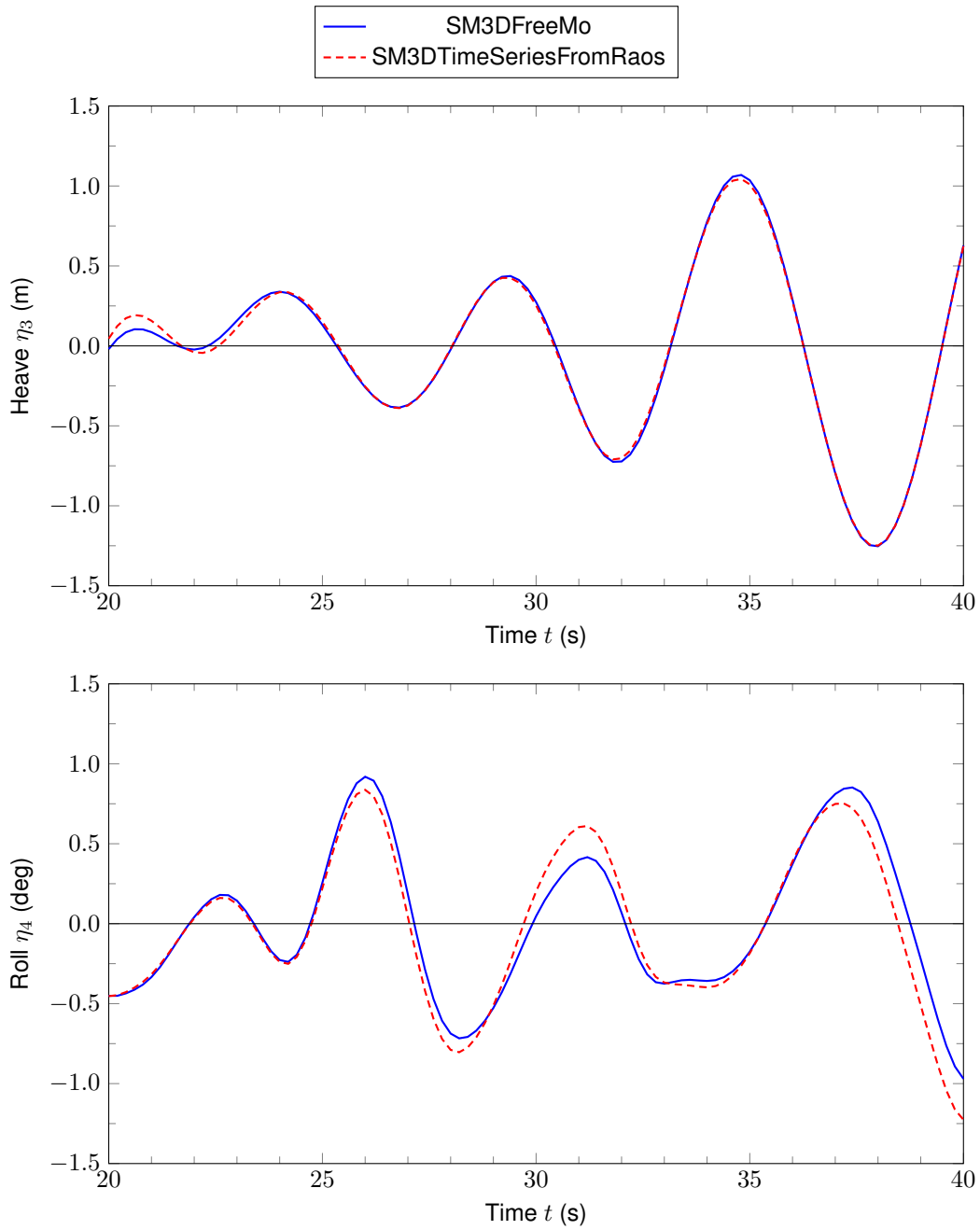


Figure 68: Heave and roll time series for generic frigate at 20 knots in Sea State 5, ship heading 30 degrees, unidirectional Bretschneider spectrum with waves from 0 degrees.

13 Conclusions

Verification and validation have been completed for ShipMo3D Version 4.2. The completed work confirms that the software is working as expected. Most of the verification and validation work has focussed on ships travelling with quasi-steady speed and heading in moderate seaways. As expected, roll motions are generally more challenging to predict than other modes due to the complex nature of roll damping. Predicted motion accuracy is dependent on mode, with typical RMS motion accuracy in random seas ranging from 10 percent for heave to 30 percent for roll.

Validation of manoeuvring has been limited to the tanker Esso Osaka performing turning circles in calm water. Validation of manoeuvring for other ships will be the focus of future work.

The most noticeable differences between ShipMo3D Version 4.2 and the earlier results of Version 3.0 [9] are caused by the addition of wave excitation manoeuvring forces [22] in Version 4.2. The influence of these force terms is greatest for ships travelling at higher speeds in oblique seas at lower wave frequencies.

This page intentionally left blank.

References

- [1] McTaggart, K. (2002), Three Dimensional Ship Hydrodynamic Coefficients Using the Zero Forward Speed Green Function, (Technical Memorandum, DRDC Atlantic TM 2002-059) Defence R&D Canada – Atlantic.
- [2] McTaggart, K. (2003), Modelling and Simulation of Seaways in Deep Water for Simulation of Ship Motions, (Technical Memorandum, DRDC Atlantic TM 2003-190) Defence R&D Canada – Atlantic.
- [3] McTaggart, K. (2003), Hydrodynamic Forces and Motions in the Time Domain for an Unappended Ship Hull, (Technical Memorandum, DRDC Atlantic TM 2003-104) Defence R&D Canada – Atlantic.
- [4] McTaggart, K. (2004), Appendage and Viscous Forces for Ship Motions in Waves, (Technical Memorandum, DRDC Atlantic TM 2004-227) Defence R&D Canada – Atlantic.
- [5] McTaggart, K. (2005), Simulation of Hydrodynamic Forces and Motions for a Freely Maneuvering Ship in a Seaway, (Technical Memorandum, DRDC Atlantic TM 2005-071) Defence R&D Canada – Atlantic.
- [6] McTaggart, K. (2008), Improved Maneuvering Forces and Autopilot Modelling for the ShipMo3D Ship Motion Library, (Technical Memorandum, DRDC Atlantic TM 2008-162) Defence R&D Canada – Atlantic.
- [7] McTaggart, K. (2007), Validation of ShipMo3D Version 1.0 User Applications for Simulation of Ship Motions, (Technical Memorandum, DRDC Atlantic TM 2007-173) Defence R&D Canada – Atlantic.
- [8] McTaggart, K. (2010), Validation of ShipMo3D Version 2.0 User Applications for Simulation of Ship Motions, (Technical Memorandum, DRDC Atlantic TM 2010-133) Defence R&D Canada – Atlantic.
- [9] McTaggart, K. (2012), Validation of ShipMo3D Version 3.0 User Applications for Simulation of Ship Motions, (Technical Memorandum, DRDC Atlantic TM 2011-306) Defence R&D Canada – Atlantic.
- [10] McTaggart, K. (under review), ShipMo3D Version 4.2 User Manual for Creating Ship Models, (Reference Document, D20-0924-04156) Defence Research and Development Canada.
- [11] McTaggart, K. (under review), ShipMo3D Version 4.2 User Manual for Computing Ship Motions in the Time and Frequency Domains, (Reference Document, D20-0924-04154) Defence Research and Development Canada.
- [12] Lloyd, A. and Crossland, P. (1990), Motions of a Steered Model Warship in Oblique Waves, *Transactions, Royal Institution of Naval Architects*, 132, 79–98.

- [13] McTaggart, K., Datta, I., Stirling, A., Gibson, S., and Glen, I. (1997), Motions and Loads of a Hydroelastic Frigate Model in Severe Seas, *Transactions, Society of Naval Architects and Marine Engineers*, Vol. 105.
- [14] Stredulinsky, D., Pegg, N., and Gilroy, L. (2000), Motion and Wave Load Predictions and Measurements on HMCS NIPIGON, *Transactions, Royal Institution of Naval Architects*, Vol. 142.
- [15] Minnick, L., Hanyok, L., Tomaszek, H., Melendez, M., Turner, C., Park, J., Belenky, V., and Bassler, C. (2012), Model-Scale Experiment of the Seakeeping Performance for R/V Melville, Model 5720, (Hydromechanics Department Report NSWCCD-50-TR-2012/035) Naval Surface Warfare Center Carderock Division.
- [16] McTaggart, K. and Marly, J.-F. (2015), Seakeeping of a Research Vessel with Azimuthing Propellers, In *34th International Conference on Ocean, Offshore and Arctic Engineering—OMAE 2015*, St. John's, Newfoundland.
- [17] Crane, C., Jr. (1979), Maneuvering Trials of the 278,000 DWT Esso Osaka in Shallow and Deep Water, *Transactions, Society of Naval Architects and Marine Engineers*, Vol. 87.
- [18] McTaggart, K. (2015), Ship Radiation and Diffraction Forces at Moderate Forward Speed, In *World Maritime Technology Conference*, Providence, Rhode Island.
- [19] American Society of Civil Engineers (1961), Wind Forces on Structures, *Transactions*, 126, Part II, 1124–1198.
- [20] Sarpkaya, T. and O'Keefe, J. L. (1996), Oscillating Flow About Two and Three-Dimensional Bilge Keels, *Transactions of the ASME, Journal of Offshore Mechanics and Arctic Engineering*, 118, 1–6.
- [21] Himeno, Y. (1981), Prediction of Ship Roll Damping – State of the Art, (Report 239) Department of Naval Architecture and Marine Engineering, University of Michigan.
- [22] McTaggart, K. (2019), Rapid Simulation of Ship Motions during Maneuvering in Operational Wave Conditions, In *Society of Naval Architects and Marine Engineers Maritime Convention*, Tacoma.
- [23] Bertram, V. (2012), *Practical Ship Hydrodynamics*, 2nd ed, Oxford: Butterworth-Heinemann.
- [24] Söder, C. J., Rosén, A., and Huss, M. (2019), Ikeda Revisited, *Journal of Marine Science and Technology*, 24, 306–316.
- [25] Holtrop, J. and Mennen, G. (1982), An Approximate Power Prediction Method, *International Shipbuilding Progress*, 29(335), 166–170.

- [26] van Manen, J. and van Oossanen, P. (1988), Principles of Naval Architecture, Volume II, Ch. 6, Propulsion, Society of Naval Architects and Marine Engineers.
- [27] Lewandowski, E. M. (2004), The Dynamics of Marine Craft - Maneuvering and Seakeeping, Vol. 22 of *Advanced Series on Ocean Engineering*, River Edge, New Jersey: World Scientific.
- [28] Inoue, S., Hirano, M., and Kijima, K. (1981), Hydrodynamic Derivatives on Ship Manoeuvring, *International Shipbuilding Progress*, 28(321), 112–125.
- [29] McTaggart, K. (2011), Robust Computation of Ship Hydrodynamic Coefficients at Moderate Forward Speed, In *Twenty-Third Canadian Congress of Applied Mechanics*, Vancouver, Canada.
- [30] Huang, Z. and Hsiung, C. (1993), An Improved 3-D Panel Method to Compute mj-Terms for Ship Motion, In *Proceedings of the Second Canadian Marine Dynamics Conference*, Vancouver.
- [31] Chen, X. and Malenica, S. (1998), Interaction Effects of Local Steady Flow on Wave Diffraction-Radiation at Low Forward Speed, *International Journal of Offshore and Polar Engineering*, 8(2), 102–109.
- [32] Huijsmans, R., van 't Veer, R., and Kashiwagi, M. (2010), Ship Motion Predictions: A Comparison Between a CFD Based Method, a Panel Method and Measurements, In *29th International Conference on Ocean, Offshore and Arctic Engineering—OMAE 2010*, Shanghai.
- [33] Jensen, J. J. (2001), Load and Global Response of Ships, Ocean Engineering Series, Elsevier.
- [34] McTaggart, K. and Stredulinsky, D. (2001), Comparisons of Motions for HMCS NIPIGON with Numerical Predictions, (DREA ECR 2001-156) Defence Research Establishment Atlantic.
- [35] Islam, M., Veitch, B., Akinturk, A., Bose, N., and Liu, P. (2007), Experiments with Podded Propulsors in Static Azimuthing Conditions, In *Proceedings of the Eighth Canadian Marine Hydromechanics and Structures Conference*, St. John's, Newfoundland.
- [36] The Specialist Committee on Esso Osaka (2002), Final Recommendations to the 23rd ITTC, In *23rd International Towing Tank Conference*, Vol. II, pp. 573–609, The Hague.
- [37] Todd, F. (1953), Some Further Experiments on Single-Screw Merchant Ship Forms—Series 60, *Transactions, Society of Naval Architects and Marine Engineers*, 61, 516–589.

- [38] Malenica, S., Zalar, M., and Chen, X. (2003), Dynamic Coupling of Seakeeping and Sloshing, In *Thirteenth International Offshore and Polar Engineering Conference*, Honolulu, Hawaii.
- [39] McTaggart, K. (2012), Modelling of Sloshing in Free Surface Tanks for ShipMo3D Ship Motion Predictions, (External Client Report, DRDC Atlantic ECR 2011-084) Defence R&D Canada – Atlantic.
- [40] Molin, B., Remy, F., Rigaud, S., and de Jouette, C. (2002), LNG-FPSO's: Frequency Domain, Coupled Analysis of Support and Liquid Cargo Motions, In *International Maritime Association of the Mediterranean Conference*, Rethymnon, Greece.
- [41] McTaggart, K. (2012), Modelling of U-tube Tanks for ShipMo3D Ship Motion Predictions, (External Client Report, DRDC Atlantic ECR 2011-300) Defence R&D Canada – Atlantic.

List of Symbols/Abbreviations/Acronyms/Initialisms

AP	aft perpendicular
a	wave amplitude
B	ship beam
C_B	ship block coefficient
C_d	hull viscous roll damping coefficient from barge experiments
C_d^{osc}	drag coefficient of plate in oscillatory flow
C_{eddy}^{hull}	ShipMo3D viscous hull roll damping coefficient
CG	centre of gravity
c	chord length
CPF	Canadian Patrol Frigate
$F_4^{hull-eddy}$	hull roll damping moment due to eddy effects
g	gravitational acceleration
\overline{GM}	metacentric height
\overline{GM}_{fluid}	metacentric height, including fluid effects
H	wave height
H_s	significant wave height
h_t	tank total height
\overline{KC}	Keulegan-Carpenter number
\overline{KG}	vertical centre of gravity relative to baseline
k	wavenumber
$k_{\delta j}^D$	autopilot derivative gain for mode j
$k_{\delta j}^I$	autopilot integral gain for mode j
$k_{\delta j}^P$	autopilot proportional gain for mode j
L	ship length between perpendiculars
L_{oa}	overall length
L_{tank}	tank length along ship longitudinal axis
m_{tank}	tank fluid mass
PID	proportional-integral-derivative
RAO	response amplitude operator
RMS	root-mean-square
r_{BK}	local radius bilge keel from ship centre of gravity
r_{xx}, r_{yy}, r_{zz}	radii of gyration in roll, pitch, and yaw
S_{hull}	hull surface
s	span
T_{mid}	draft at midships
T_p	peak wave period
T_z	zero-crossing period
T_4	roll natural period
t	time
t_{stern}	trim by stern
U	forward ship speed
V	total ship speed in horizontal plane

w_d	tank duct width
w_r	tank reservoir width
x^f, y^f	horizontal plane coordinates in earth-fixed axes
z_{bl}^{tank}	height of tank bottom above ship baseline
β_s	relative sea direction (180° for head seas)
γ	peak enhancement factor for JONSWAP spectrum
γ^r	rudder flow straightening constant
$\Delta \overline{GM}^{tank}$	effective change in ship metacentric height due to tank
δ^{fin}	stabilizer fin deflection angle
δ^{rudder}	rudder deflection angle
δ_{max}^{rudder}	maximum rudder deflection angle
$\dot{\delta}^{rudder}$	rudder deflection velocity
$\dot{\delta}_{max}^{rudder}$	maximum rudder deflection velocity
$\ddot{\delta}^{rudder}$	rudder deflection acceleration
δ_C^{rudder}	command rudder angle
ζ_δ	rudder control damping coefficient
η_j	motion displacement in translating earth axes for mode j
η_j^f	motion displacement in earth-fixed axes for mode j
η_{Cj}^f	command motion displacement in earth-fixed axes for mode j
$\dot{\eta}_j^f$	motion velocity in earth-fixed axes for mode j
ρ	water density (for water external to hull)
ρ_{tank}	tank fluid density
τ	tank fluid displacement angle
τ_{max}	tank maximum fluid displacement angle
τ_{max}^{rudder}	autopilot integration duration
$\hat{\phi}$	roll amplitude
χ	ship heading (0° for north)
$\dot{\chi}$	heading rate
ω_I	incident wave frequency
ω_δ	rudder control natural frequency
ω_τ	tank fluid motion natural frequency
Δ	ship mass displacement

DOCUMENT CONTROL DATA

*Security markings for the title, authors, abstract and keywords must be entered when the document is sensitive

1. ORIGINATOR (Name and address of the organization preparing the document. A DRDC Centre sponsoring a contractor's report, or a tasking agency, is entered in Section 8.) DRDC – Atlantic Research Centre PO Box 1012, Dartmouth NS B2Y 3Z7, Canada			2a. SECURITY MARKING (Overall security marking of the document, including supplemental markings if applicable.) CAN UNCLASSIFIED	
			2b. CONTROLLED GOODS NON-CONTROLLED GOODS DMC A	
3. TITLE (The document title and sub-title as indicated on the title page.) Validation of ShipMo3D Version 4.2 User Applications for Simulation of Ship Motions				
4. AUTHORS (Last name, followed by initials – ranks, titles, etc. not to be used. Use semi-colon as delimiter) McTaggart, K.				
5. DATE OF PUBLICATION (Month and year of publication of document.) January 2021		6a. NO. OF PAGES (Total pages, including Annexes, excluding DCD, covering and verso pages.) 104		6b. NO. OF REFS (Total cited in document.) 41
7. DOCUMENT CATEGORY (e.g., Scientific Report, Contract Report, Scientific Letter) Scientific Report				
8. SPONSORING CENTRE (The name and address of the department project or laboratory sponsoring the research and development.) DRDC – Atlantic Research Centre PO Box 1012, Dartmouth NS B2Y 3Z7, Canada				
9a. PROJECT OR GRANT NO. (If appropriate, the applicable research and development project or grant number under which the document was written. Please specify whether project or grant.) 41aa			9b. CONTRACT NO. (If appropriate, the applicable contract number under which the document was written.)	
10a. DRDC DOCUMENT NUMBER DRDC-RDDC-2021-R008			10b. OTHER DOCUMENT NO(s). (Any other numbers which may be assigned this document either by the originator or by the sponsor.)	
11a. FUTURE DISTRIBUTION WITHIN CANADA (Approval for further dissemination of the document. Security classification must also be considered.) Public release				
11b. FUTURE DISTRIBUTION OUTSIDE CANADA (Approval for further dissemination of the document. Security classification must also be considered.) None				

12. KEYWORDS, DESCRIPTORS or IDENTIFIERS (Use semi-colon as a delimiter.)

frequency domain; manoeuvring; seakeeping; ship motions; simulation; time domain; validation; waves

13. ABSTRACT/RÉSUMÉ (When available in the document, the French version of the abstract must be included here.)

ShipMo3D is an object-oriented library with associated user applications for predicting ship motions in calm water and in waves. This Scientific Report describes the validation of ShipMo3D Version 4.2 user applications with data from model tests and full-scale trials. Version 4.2 of ShipMo3D introduces several new capabilities developed since Version 3. Irregular frequencies for hull radiation and diffraction computations are eliminated using a lid method. Autopilot modelling now includes a track keeping capability. A new tracking spring capability can be used to model forces from various stationary or translating entities, including a mooring system, a towing tank carriage, or a ship replenishment system. New wave excitation maneuvering forces significantly influence lateral plane motions at lower encounter frequencies. Seakeeping predictions were validated using model tests and sea trials for a steered warship, a frigate, a destroyer, and a research vessel with azimuthing propellers. Predicted root-mean-squared (RMS) heave, roll, and pitch motions in random seas are typically within 10 to 30 percent of measured values, with heave motions being the most accurate and roll motions being the least accurate. Manoeuvring validation was performed for the tanker Esso Osaka performing turning circles. Validation of sloshing predictions was performed using data for a barge model with two sloshing tanks. In the absence of validation data, verification studies were performed for seakeeping for vessels with active stabilizer fins and U-tube tanks.

ShipMo3D est une bibliothèque orientée objet avec applications utilisateur connexes pour la prévision des mouvements de navires en eaux calmes et dans les vagues. Le présent rapport scientifique fournit une description de la validation des applications utilisateur de la version 4.2 de ShipMo3D avec des données provenant d'essais de modèles et d'essais à grand déploiement. La version 4.2 de ShipMo3D présente plusieurs nouvelles capacités mises au point depuis la version 3. Les fréquences irrégulières pour le calcul du rayonnement et de la diffraction de la coque sont éliminées grâce à une méthode dite « lid ». La modélisation du pilote automatique comporte à présent une capacité de suivi. On peut utiliser une nouvelle capacité de suivi pour la modélisation des forces de diverses entités stationnaires ou en translation, notamment un système d'amarrage, un réservoir de remorquage ou un système de ravitaillement de navire. Les nouvelles forces de manœuvre d'excitation des vagues influencent de manière significative les mouvements sur le plan latéral à des fréquences de rencontre plus basses. Les prévisions de la tenue en mer ont été validées à l'aide des essais sur modèle et en mer d'un navire de guerre commandé, d'une frégate, d'un destroyer et d'un navire de recherche à hélices orientables en azimuth. Les mouvements de tangage, de roulis et de houle prévus dans des mers aléatoires sont généralement compris entre 10 et 30 % des valeurs mesurées, les mouvements de tangage étant les plus précis et ceux de roulis les moins précis. On a procédé à la validation des manœuvres du pétrolier Esso Osaka effectuant des cercles de giration. La validation des prévisions du ballonnement a été effectuée à l'aide des données d'un modèle de barge avec deux citernes antiroulis. En l'absence de données de validation, on a mené des études de vérification de la tenue en mer de navires à ailerons stabilisateurs actifs et de citernes à tube en U.